## Title

THE MOMENTS, SPINS,, AND HYPERFINE STRUCTURES OF THE RADIOACTIVE ISOTOPES: I133(21-hr), Nd141(2.5-hr), Eu152(l3-yr), and Bi21O(5-day)



## Author

Alpert, Seymour S.

## Publication Date

1961-09-06

UCRL-9850
UC-34 Physics
TID-4500(16th Ed.)

UNIVERSITY OF CALIFORNIA

Lawrence Radiation Laboratory
Berkeley, California

Contract No. W-7405-eng-48

# THE MOMENTS, SPINS, AND HYPERFINE STRUCTURES OF THE RADIOACTIVE ISOTOPES: $I^{133}$ (21-hr), $Nd^{141}$ (2.5-hr), $Eu^{152}$ (13-yr), AND $Bi^{210}$ (5-day)

Seymour S. Alpert

(Thesis)

September 6, 1961

Printed in USA. Price $2.25. Available from the
Office of Technical Services
U. S. Department of Commerce
Washington 25, D.C.

## DISCLAIMER

# THE MOMENTS, SPINS, AND HYPERFINE STRUCTURES OF THE RADIOACTIVE ISOTOPES: $I^{133}$ (21-hr), $Nd^{141}$ (2.5-hr), $Eu^{152}$ (13-yr), AND $Bi^{210}$ (5-day)

Contents

# THE MOMENTS, SPINS, AND HYPERFINE STRUCTURES OF THE RADIOACTIVE ISOTOPES: $I^{133}$ (21-hr), $Nd^{141}$ (2.5-hr), $Eu^{152}$ (13-yr), AND $Bi^{210}$ (5-day)

Seymour S. Alpert

Lawrence Radiation Laboratory
University of California
Berkeley, California

September 6, 1961

## ABSTRACT

The atomic beam "flop-in" technique has been used to measure the nuclear constants of several radioactive species. The resulting values for the nuclear spin, I; the magnetic dipole interaction constant, a; and the electric quadrupole interaction constant, b, are tabulated below:

| Isotope | $\tau_{1/2}$ | I | a (Mc) | b (Mc) |
|---|---|---|---|---|
| $I^{133}$ | 21 hr | (7/2) | 597.0 ± 1.0 | 385.2 ± 7.4 |
| $Bi^{210}$ | 5 days | (1) | ±21.78 ± 0.03 | ±112.38 ± 0.03 |
| $Po^{210}$ | 138.4 d | 0 | | |
| $Nd^{141}$ | 2.5 hr | 3/2 | | |
| $Eu^{152}$ | 13 yr | (3) | ±9.345 ± 0.004 | ∓1.930 ± 0.117 |

Those results which appear within parentheses in the table above have been measured elsewhere; they are included above because they have been directly verified in this work and are fundamental to the measurement of the other nuclear constants.

The values of several hyperfine-structure separations were also directly measured or calculated. These nuclear constants are indicated by the symbol $\Delta\nu_{F,F'}$ where the subscripts indicate the total angular momentum involved.

| Isotope and half life | $\Delta\nu_{F, F'}$ (Mc) |
|---|---|
| $Bi^{210}$ (RaE) (5.0 days) | $\Delta\nu_{5/2, 3/2} = 194.93 \pm 0.09$ |
| | $\Delta\nu_{3/2, 1/2} = 220.19 \pm 0.08$ |
| $Eu^{152}$ (13 yr) | $\Delta\nu_{13/2, 11/2} = 59.848 \pm 0.060$ |
| | $\Delta\nu_{11/2, 9/2} = 51.246 \pm 0.022$ |
| | $\Delta\nu_{9/2, 7/2} = 42.343 \pm 0.025$ |
| | $\Delta\nu_{7/2, 5/2} = 33.191 \pm 0.032$ |
| $I^{133}$ (21 hr) | $\Delta\nu_{5, 4} = 3260.1 \pm 7.3$ (calc) |
| | $\Delta\nu_{4, 3} = 2277.9 \pm 4.6$ (calc) |
| | $\Delta\nu_{3, 2} = 1515.9 \pm 6.1$ (calc) |
| $Nd^{141}$ (2.5 hr) | $\Delta\nu_{11/2, 9/2} \geq 1630$ |

The values of the nuclear magnetic dipole moment, $\mu$, and the nuclear electric quadrupole moment, Q, were deduced from the experimental data where possible. These results are tabulated as follows:

| Isotope and half life | $\mu$ (nuclear magnetons) | Q(barns) |
|---|---|---|
| $I^{133}$ (21 hr) | $2.821 \pm .005$ | $-0.27 \pm .01$ |
| $Bi^{210}$(RaE) (5.0 days) | $\mp 0.0442 \pm .001$ | $\pm 0.13 \pm .01$ |
| $Eu^{152}$(13 yr) | $\pm 1.912 \pm .003$ | |

The theory, techniques, and apparatus are described, and the results for each isotope are discussed.

# I. INTRODUCTION

The atomic-beam technique is primarily concerned with the measurement of nuclear properties such as spin, the hyperfine interaction constants, and the nuclear moments. One of the main advantages of the technique is that it deals with a collision-free beam of atoms which are widely separated in terms of interatomic distances; in this manner the complications due to chemical forces or crystalline fields are avoided.

As this is a resonance technique, another important advantage is realized in the high precision of the measurements performed. Such precision is limited by the line widths of the observed resonances. By careful design and proper technique the line widths can often be minimized, with concomitant improvement in accuracy.

When applied to radioactive species, the atomic-beam technique is provided with a convenient means of detection as well as identification by half-life or characteristic radiation.

In recent years it has become the program of the atomic-beam group at the University of California and the Lawrence Radiation Laboratory to measure the nuclear constants of those radioactive species that are amenable to beam production. The long-range goal of such a program is to provide sufficient data, along with other laboratories doing similar work, to provide for the further development and modification of the various nuclear models now in existence. This paper presents some results in keeping with this over-all goal.

# II. GENERAL THEORY

## A. The Total Atomic Hamiltonian

A general expression for the Hamiltonian of the free atom can be written as

$$\mathcal{H}_{\text{total}} = \mathcal{H}_{\text{nuclear}} + \mathcal{H}_{\text{electronic}} + \mathcal{H}_{\text{hfs}} + \mathcal{H}_{\text{mag}} . \qquad (1)$$

Of the terms that occur in Eq. (1) we are concerned primarily with the last three. The first term, which we include for completeness, represents the internal energy of the atomic nucleus. The form of the nuclear Hamiltonian is directly dependent on the nature of nuclear forces and has been the subject of many books and papers. It suffices to say that this large and complex topic is not the subject of this thesis, and since we are presumably always dealing with the nuclear ground state, the first term in Eq. (1) will not be considered further.

The second term in Eq. (1) is representative of electron-electron interaction and will presently be given. Traditionally investigation of the effects of the second term in Eq. (1) has been the subject of optical spectroscopy. The magnitude of the eigenenergy separations of the $\mathcal{H}_{\text{electronic}}$ term are generally on the order of electron volts.

The third term of Eq. (1), $\mathcal{H}_{\text{hfs}}$, gives the interaction of the nucleus with the atomic electrons. It is this term of the total Hamiltonian that accounts for the hyperfine structure which was originally discovered by the methods of optical spectroscopy but which, because of the small energies (on the order of $10^{-5}$ electron volts), has become the subject of radio-frequency techniques.

The last term of the Hamiltonian (1) represents the energy of interaction of the nucleus and the atomic electrons with an externally applied magnetic field. It is by means of this term that we can experimentally perturb the energy eigenvalues of the total atomic Hamiltonian and thus determine the values of the constants that appear in this Hamiltonian. This last term was partially observed experimentally by Zeeman,[1] who first demonstrated the interaction of the atomic electrons with the external magnetic field.

1. Electron-Electron Interaction

The nonrelativistic electronic Hamiltonian is given by the expression[2]

$$\mathcal{H}_{\text{electronic}} = \sum_{i=1}^{N} \left( \frac{\vec{p}_i^{\,2}}{2m} - \frac{Ze^2}{r_i} + \xi(r_i)\, \vec{l}_i \cdot \vec{s}_i \right) + \sum_{i>j=1}^{N} \frac{e^2}{r_{ij}} . \tag{2}$$

Here the summation runs from 1 to N, which is the total number of electrons present. The first term in Eq. (2) represents the kinetic energy of the electrons. The second term represents the attractive force on the ith electron exerted by the nucleus of charge Ze; here $r_i$ is the distance from the nucleus to the ith electron. The third term in Eq. (2) gives the interaction of the electronic spin, $\vec{s}_i$, with the electronic angular momentum, $\vec{l}_i$; the preceding coefficients, $\xi(r_i)$, are a function of $r_i$ only. The last term in Eq. (2) represents the electrostatic repulsion between the electrons in the atom; $r_{ij}$ is the separation between the ith and jth electrons; the summation in the last term is actually a double summation giving the interaction of any one electron with all other electrons only once.

The Hamiltonian of Eq. (2) explains successfully the main features of optical spectroscopy. Unfortunately it is generally too complex to permit an exact solution. The usual approach to the solution of the Hamiltonian (2) is outlined by Condon and Shortley.[2] This technique consists of separating the electronic Hamiltonian (2) into two parts,

$$\mathcal{H}_{\text{electronic}} = \mathcal{H}_0 + \mathcal{H}_{\text{pert}}, \tag{3}$$

where

$$\mathcal{H}_0 = \sum_{i=1}^{N} \frac{\vec{p}_i^{\,2}}{2m} + U(r_i) \tag{3a}$$

and

$$\mathcal{H}_{\text{pert}} = \sum_{i=1}^{N} \left( \xi(r_i)\, \vec{l}_i \cdot \vec{s}_i - \frac{Ze^2}{r_i} - U(r_i) \right) + \sum_{i>j=1}^{N} e^2/r_{ij} . \tag{3b}$$

Here the expression appearing in Eq. (3a) is spherically symmetric, with $U(r_i)$ being a spherically symmetric potential fulfilling the boundary conditions

$$U(r) \rightarrow -\frac{Ze^2}{r} + \frac{(N-1)}{a} e^2 \quad \text{for } r \rightarrow 0 \tag{4a}$$

and

$$U(r) \rightarrow -\frac{(Z-N+1)}{r} e^2 = -\frac{e^2}{r} \quad \text{for } r \rightarrow \infty . \tag{4b}$$

The boundary conditions of Eqs. (4a) and (4b) are those which would be seen by an electron when near the nucleus and when at a great distance from it where it is screened by the N-1 other electrons. These boundary conditions are derived from elementary electromagnetic theory; the "a" appearing in Eq. (4a) is the harmonic mean of the radii of the shells of all other electrons except the one for which the boundary conditions (4a) and (4b) are visualized.

There are two general approaches to the solution of Eqs. (3) with the boundary conditions (4). The first approach was first formulated by L. H. Thomas[3] and E. Fermi.[4] This consists of assuming that the central potential $U(r_i)$ varies slowly enough in an electron wave length so that many electrons may be localized within a volume over which the potential changes by a small fraction of itself. Under this assumption the methods of statistical mechanics can be used. A differential equation for the potential $U(r_i)$ can thus be found in the form[5]

$$\frac{1}{r^2} \frac{d}{dr} \left[ r^2 \frac{d}{dr} (-U) \right] = \frac{4e^2 [-2m U]^{3/2}}{3\pi \hbar^3} . \tag{5}$$

This equation has been numerically solved by Bush and Caldwell.[6] The solution of Eq. (5) can be introduced into Eq. (3a), which then can be solved for the eigenfunctions which can in turn be used to evaluate the part of the Hamiltonian that appears in Eq. (3b) and is considered as a perturbation.

The second approach to the solution of Eq. (3) consists of first assuming a reasonable form for the central potential U(r). The total Hamiltonian is then solved for each electron in its own central field

and the resulting wave equation made consistent with the effects of the other electrons of the system by a method of successive approximations. This gives a product of single electron functions (Hartree) or an anti-symmetrized product of such functions (Hartree-Fock). These eigen-solutions of Eq. (3a) are then used to evaluate the noncentral Hamiltonian (3b). These two approaches to the solution of Eq. (2) are the chief theoretical problem of optical spectroscopy.

It is interesting to note several features of Eq. (2). If one considers only the first two terms of the Hamiltonian, the eigen-solutions are indexed by the quantum numbers n and $\ell$, which are the principal and orbital quantum numbers, respectively. Any set of n and $\ell$ is said to constitute an electronic configuration. Such configurations are highly degenerate. The spin-orbit and electrostatic interaction terms, i.e., the third and fourth terms of Eq. (2), remove the degeneracy of the first two terms, the good quantum number always being J, the total angular momentum quantum number. If, as for most atoms, the relation

$$\sum_{i>j=1}^{N} e^2/r_{ij} \gg \sum_{i=1}^{N} \xi(r_i)\, \vec{\ell}_i \cdot \vec{s}_i \qquad (6)$$

holds, then the electrostatic interaction has the major effect in removing the degeneracy of a given configuration. The electrostatic interaction when included with the first two terms of the Hamiltonian (2) has eigensolutions which are further indexed by the quantum numbers L and S, where L is the total orbital angular momentum quantum number and S is the total spin angular momentum quantum number. This is the case of Russell-Saunders coupling where $\vec{L} = \sum_i \vec{\ell}_i$ and $\vec{S} = \sum_i \vec{s}_i$, the small letters indicating the appropriate vector quantity of the individual electrons. The set n, $\ell$, L, and S defines a term. If the spin-orbit interaction is now considered there is a further splitting of each term into levels which are designated by the set n, $\ell$, L, S, and J.

In the heavier atoms, the condition (6) does not hold; the spin-orbit interaction assumes the same order of magnitude of the electrostatic repulsion term. In such a case L and S are no longer individually conserved. If condition (6) is reversed, so that the electrostatic repulsion term is much less than the magnitude of the spin-orbit term, the $\vec{\ell}_i$ and $\vec{s}_i$ of each electron couple tightly to form a $\vec{j}_i$ such that $\vec{J} = \sum_i \vec{j}_i$. This is known as j-j coupling. In such a situation, the electrostatic repulsion interaction acts as a perturbation that splits the J levels.

In this discussion of the optical Hamiltonian, no mention was made of the interactions of the types

$$\sum_{i>j=1}^{N} a_{ij}\ \vec{s}_i \cdot \vec{\ell}_j, \quad \sum_{i>j=1}^{N} b_{ij}\ \vec{\ell}_i \cdot \vec{\ell}_j, \text{ and } \sum_{i>j=1}^{N} c_{ij}\ \vec{s}_i \cdot \vec{s}_j. \tag{7}$$

In general such interactions are small and need only be considered when it becomes obvious that the Hamiltonian (2) is inadequate to describe the spectroscopic facts.

2. Hyperfine Interaction

That part of the total Hamiltonian (1) which we have labeled as $\mathcal{H}_{hfs}$ is basic to the atomic beam method of radio-frequency spectroscopy. There have been many theoretical treatments of this hyperfine-structure interaction. Ours follows that by Schwartz.[7] It seems desirable, before applying the methods of Schwartz, to first show that the hyperfine interaction can be written as

$$\mathcal{H}_{hfs} = \sum_k \sum_q (-)^q\ T_q^k(e)\ T_{-q}^k(n), \tag{8}$$

where the spherical tensor element $T_q^k(e)$ is a function of the electron coordinates alone and $T_{-q}^k(n)$ is a function of the nuclear coordinates alone.

First let us consider the electrostatic interaction between a finite nucleus and its surrounding electrons, as shown in Fig. 1.

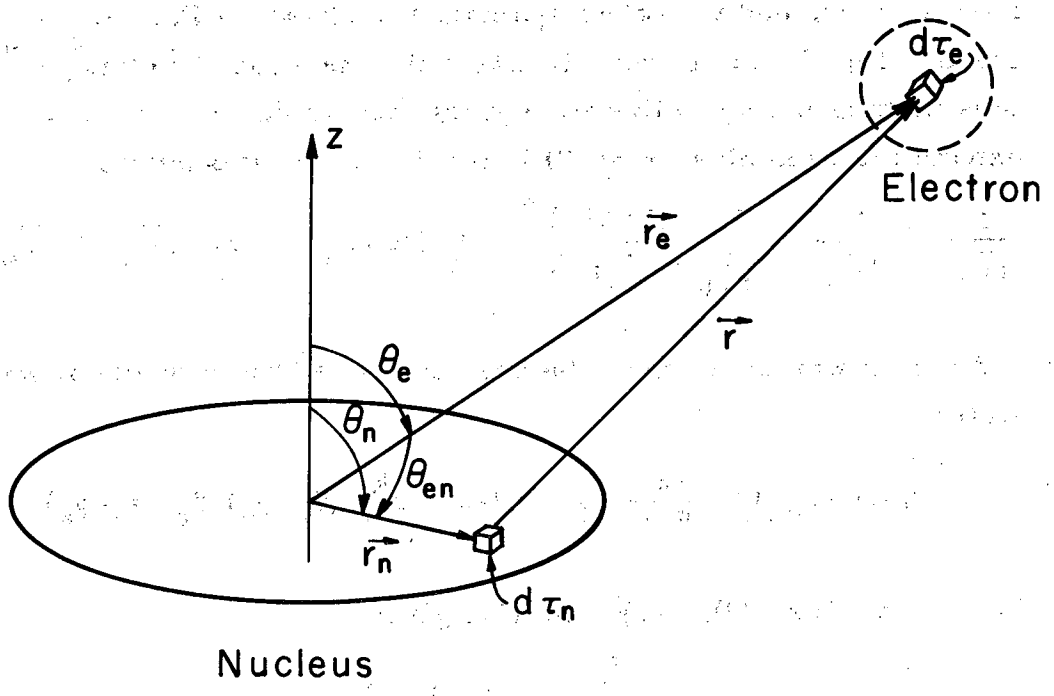


Fig. 1. This schematic diagram defines quantities used in Eqs. (9), (10), and (11).

The classical interaction may be written as

$$\mathcal{H}_{\text{electrostatic}} = \int_{\tau_e} \int_{\tau_n} \frac{\rho_e(\vec{r}_e)\, \rho_n(\vec{r}_n)}{|\vec{r}|}\, d\tau_e\, d\tau_n, \tag{9}$$

where $\rho_e$ and $\rho_n$ are the electron and nuclear charge densities, respectively, and the other symbols are shown in Fig. 1. As it now stands, Eq. (9) is not readily integrable because $|\vec{r}| = |\vec{r}_e - \vec{r}_n|$, thus making it impossible to separate the variables. One can first expand the denominator of (9) into a Legendre expansion,

$$\frac{1}{|\vec{r}|} = \frac{1}{|\vec{r}_e|} \sum_{k=0}^{\infty} \left( \frac{|\vec{r}_n|}{|\vec{r}_e|} \right)^k P_k(\cos\theta_{en}) \quad \text{for } |\vec{r}_n| < |\vec{r}_e|, \tag{10}$$

and then make use of the spherical-tensor addition theorem which states

$$P_k(\cos\theta_{en}) = \frac{4\pi}{2k+1} \sum_{q=-k}^{k} (-1)^q\, Y^k_{-q}(\theta_n, \phi_n)\, Y^k_q(\theta_e, \phi_e). \tag{11}$$

Combining Eqs. (9), (10), and (11) gives

$$\mathcal{H}_{\text{electrostatic}} = \sum_{q=-k}^{k} (-1)^q\, Q^k_q\, F^k_{-q}, \tag{12}$$

where

$$Q^k_q = \sqrt{\frac{4\pi}{2k+1}} \int_{\tau_n} \rho_n\, r_n^{-k}\, Y^k_q(\theta_n, \phi_n) \tag{13}$$

and

$$F^k_q = \sqrt{\frac{4\pi}{2k+1}} \int_{\tau_e} \rho_e\, r_e^{-(k+1)}\, Y^k_q(\theta_e, \phi_e) \tag{14}$$

In Eqs. (13) and (14) we use the usual convention that $|\vec{r}_n| \equiv r_n$ and $|\vec{r}_e| \equiv r_e$. Thus we have shown that the electrostatic part of the hyperfine interaction is a product of spherical tensors, as suggested in Eq. (8). It remains to be shown also that the magnetic interaction can be represented as a product of spherical tensors. This demonstration is simplified by the substitution, which has been justified by Ramsey,[8] to the effect

$$\rho_e \rightarrow \vec{\nabla}_e \cdot \vec{m}_e \quad \text{and} \quad \rho_m \rightarrow -\vec{\nabla}_n \cdot \vec{m}_n , \tag{15}$$

where $\vec{m}_e$ and $\vec{m}_n$ are the magnetization density vectors.

It follows, therefore, on the substitution of Eq. (15) into (13) and (14), that a similar relation to (12) exists for magnetic interaction also. Hence, we have shown that it is reasonable for Eq. (8) to hold.

In order to express the expectation values of the hyperfine-structure Hamiltonian of Eq. (8) in states indexed by the quantum numbers I, J, F, and $M_F$ we follow the methods of Schwartz.[7] The F referred to in the preceding sentence is related to the total atomic angular momentum, $\vec{F} = \vec{I} + \vec{J}$, and $M_F$ is the projection of $\vec{F}$ along the axis of quantization. First we rewrite Eq. (8) in a slightly contracted form,

$$\mathcal{H}_{hfs} = \sum_k \underline{\underline{T}}^k(e) \cdot \underline{\underline{T}}^k(n) . \tag{16}$$

Here $\underline{\underline{T}}^k(e)$ and $\underline{\underline{T}}^k(n)$ are spherical tensors of order k which are functions of the electron and nuclear coordinates, respectively. The symbol $\underline{\underline{\ }}$ is used to indicate that we are dealing with a tensor *per se*, not with a tensor element. What we wish to evaluate is

$$W_{F, M_F} = \left\langle IJFM_F \middle| \mathcal{H}_{hfs} \middle| IJFM_F \right\rangle =$$

$$\left\langle IJFM_F \middle| \sum_k \underline{\underline{T}}^k(e) \cdot \underline{\underline{T}}^k(n) \middle| IJFM_F \right\rangle . \tag{17}$$

We will consider each term of the series of Eq. (17) separately; i.e.,

$$W_{F,M_F}(k) = \left\langle IJFM_F \left| \underline{T^k(e)} \cdot \underline{T^k(n)} \right| IJFM_F \right\rangle . \tag{18}$$

Application of a theorem due to Racah[9] gives

$$W_{F,M_F}(k) = (-)^{I+J-F} \begin{Bmatrix} F & J & I \\ k & I & J \end{Bmatrix} \left\langle I \left\| \underline{T^k(n)} \right\| I \right\rangle \left\langle J \left\| \underline{T^k(e)} \right\| J \right\rangle . \tag{19}$$

The symbol in the braces is the Wigner 6-j symbol and is defined in Appendix A. The last two factors in Eq. (19) are reduced matrix elements of the spherical tensors of rank k, and are independent of any magnetic quantum numbers. Perusal of Eq. (19) shows the complete independence of the expectation value of $\mathcal{H}_{hfs}$ from the total magnetic quantum number, $M_F$. Thus the expectation value can better be written as $W_F(k)$. We now let

$$W_F(k) = A_k M(I, J; F; k) \tag{20}$$

with the normalization that

$$M(I, J; I+J; k) = 1. \tag{21}$$

Hence,

$$W_{F=I+J}(k) = A_k = (-)^{2I+2J} \begin{Bmatrix} I+J & J & I \\ k & I & J \end{Bmatrix} \left\langle I \left\| \underline{T^k(n)} \right\| I \right\rangle \left\langle J \left\| \underline{T^k(e)} \right\| J \right\rangle . \tag{22}$$

The 6-j symbol of Eq. (22) is evaluated in Appendix A. This gives

$$A_k = \frac{(2J)!\,(2I)! \left\langle J \left\| \underline{T^k(e)} \right\| J \right\rangle \left\langle I \left\| \underline{T^k(n)} \right\| I \right\rangle}{[\,(2J-k)!\,(2J+k+1)!\,(2I-k)!\,(2I+k+1)!\,]^{1/2}} . \tag{23}$$

Schwartz[7] shows this to be equivalent to

$$A_k = \left\langle II \left| T^k(n) \right| II \right\rangle \left\langle JJ \left| T^k(e) \right| JJ \right\rangle . \tag{24}$$

A general expression for M(I, J; F; k) appears in Appendix A. Below appear the values for k = 1 (dipole) and k = 2 (quadrupole):

k = 1 (dipole):

$$M(I, J; F; 1) = \frac{K}{2IJ} \; ; \tag{25}$$

k = 2 (quadrupole):

$$M(I, J; F; 2) = \frac{6[K(K+1) - \frac{4}{3} I(I+1) J(J+1)]}{2I(I-1)\, 2J(J-1)}$$

where $K = 2\vec{I} \cdot \vec{J} = F(F+1) - I(I+1) - J(J+1)$. The constants $A_k$ are related to the commonly used magnetic dipole interaction constant a and electric quadrupole interaction constant b by

$$A_1 = IJa \qquad \text{and} \qquad A_2 = 1/4\ b. \tag{26}$$

Thus the first two terms of the expectation value of $\mathcal{H}_{hfs}$, which is the eigenenergy of this Hamiltonian, are

$$W_F = ah\vec{I} \cdot \vec{J} + bh \frac{3(\vec{I} \cdot \vec{J})^2 + 3/2(\vec{I} \cdot \vec{J}) - I(I+1) J(J+1)}{2IJ(2I-1)(2J-1)} \; , \tag{27}$$

where $\vec{I} \cdot \vec{J}$ is not here an operator but is a symbol meaning $1/2[\, F(F+1) - I(I+1) - J(J+1)]$. In the isotopes studied in this thesis, there was no need to introduce the existence of interactions for which $k > 2$. If such interactions existed they were too small to be observed.

Judd has stated that there are four triangular conditions for the nonvanishing of the 6-j symbol;[10] these conditions are symbolically given as

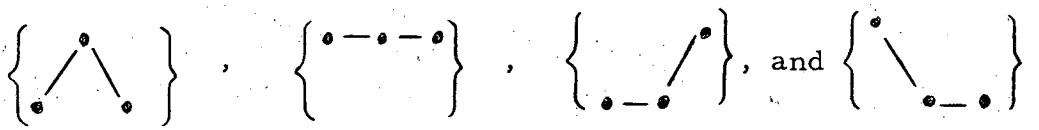 (28)

The meaning of these symbols is this: any of the elements a, b, and c appearing where the heavy dots are in the symbolic relation (28) are subject to the triangular conditions

$$\begin{aligned} |a + b| &\geq c \geq |a - b|, \\ |a + c| &\geq b \geq |a - c|, \\ |b + c| &\geq a \geq |b - c|. \end{aligned} \tag{29}$$

Thus we see from Eq. (19) and the symbolic relation (28) that the triads (I, J, F), (I, I, k), and (J, J, k) must satisfy the triangular conditions (29). The first triad just repeats the statement that the only allowed values of F are between $|I - J|$ and $|I + J|$. The second two triads govern the termination of the series (17). The series ends at a value of k given by $k = 2I$ or $k = 2J$, whichever is smaller.

## 3. Magnetic Interaction

The last term in the total Hamiltonian (1) gives the interaction of the externally applied magnetic field with both the electronic and nuclear moments. This interaction is of the form

$$\mathcal{H}_{mag} = -g_J \mu_0 \vec{J} \cdot \vec{H} - g_I \mu_0 \vec{I} \cdot \vec{H} \ , \tag{30}$$

where $g_J$ and $g_I$ are constants known as the electronic and nuclear g factors, respectively; $\mu_0$ is the Bohr magneton; $\vec{J}$ is the total electronic angular momentum; $\vec{I}$ is the nuclear spin; and $\vec{H}$ is the externally applied magnetic field.

In the limit where $\mathcal{H}_{mag}$ is much smaller than any other term in the total interaction Hamiltonian, the energy eigenvalues of $\mathcal{H}_{mag}$ are given by the diagonal matrix elements in the $IJFM_F$-representation. We shall consider the first term of Eq. (30) first. The Wigner-Eckart theorem[11] gives

$$\left\langle IJFM_F \left| J_z \right| IJFM_F \right\rangle = (-1)^{F-M_F} \begin{pmatrix} F & 1 & F \\ -M_F & 0 & M_F \end{pmatrix} \left\langle IJF \| J \| IJF \right\rangle . \tag{31}$$

Here the symbol contained in the large parenthesis is the Wigner 3-j symbol and is defined in Appendix B. The last factor in Eq. (31) is a reduced matrix element. Edmonds[12] gives

$$\begin{pmatrix} F & 1 & F \\ -M_F & 0 & M \end{pmatrix} = (-1)^{F-M_F} \frac{M_F}{[(2F+1)(F+1)F]^{1/2}} \tag{32}$$

and

$$\left\langle IJF \middle\| J \middle\| IJF \right\rangle = \frac{F(F+1) + J(J+1) - I(I+1)}{2[F(F+1)]^{1/2}} \cdot (2F+1)^{1/2}. \tag{33}$$

Combining Eqs. (31), (32), and (33) gives

$$\left\langle IJFM_F \middle| J_z \middle| IJFM_F \right\rangle = (-1)^{2(F-M_F)} M_F \frac{F(F+1) + J(J+1) - I(I+1)}{2F(F+1)}. \tag{34}$$

Since $F-M_F$ is integral, we have

$$(-1)^{2(F-M_F)} = 1,$$

and Eq. (34) becomes

$$\left\langle IJFM_F \middle| J_z \middle| IJFM_F \right\rangle = M_F \frac{F(F+1) + J(J+1) - I(I+1)}{2F(F+1)}. \tag{35}$$

By letting $J \rightarrow I$ and $I \rightarrow J$ in Eq. (35), we get, by substitution,

$$\left\langle IJFM_F \middle| I_z \middle| IJFM_F \right\rangle = M_F \frac{F(F+1) + I(I+1) - J(J+1)}{2F(F+1)}.$$

Thus we get

$$\left\langle IJFM_F \middle| \mathcal{H}_{mag} \middle| IJFM_F \right\rangle = \tag{36}$$

$$-g_J \mu_0 H_z M_F [F(F+1) + J(J+1) - I(I+1)]/2F(F+1)$$

$$-g_I \mu_0 H_z M_F [F(F+1) + I(I+1) - J(J+1)]/2F(F+1).$$

This expression governs the separation between hyperfine magnetic sublevels of different $M_F$ for small values of the magnetic field. The second term of Eq. (36) is on the order of 1/2000 of the magnitude of the first, and is often neglected in low-field work, giving the separation in units of frequency between adjacent magnetic sublevels as

$$\nu_F \approx -g_J \frac{\mu_0}{h} H_z \frac{[F(F+1)+J(J+1)-I(I+1)]}{2F(F+1)}. \tag{37}$$

Since Expression (37) shows a dependency on I, it is used as a basis for the experimental determination of I, the nuclear spin, in weak-field experiments.

As the magnetic field intensity is increased, it becomes less justifiable to neglect off-diagonal matrix elements of the magnetic interaction Hamiltonian. These off-diagonal elements are not derived here but are taken from Ramsey,[8] and are of the form

$$\left\langle I, J, F, M_F \,\middle|\, I_z \,\middle|\, I, J, F+1, M_F \right\rangle = \left\{ \frac{(F+1-I+J)\,(F+1+I-J)\,(I+J+2+F)\,(I+J-F)\,[(F+1)^2-M_F^2]}{4(F+1)^2\,(2F+1)\,(2F+3)} \right\}^{1/2}$$

$$\left\langle I, J, F, M_F \,\middle|\, I_z \,\middle|\, I, J, F-1, M_F \right\rangle = \left\{ \frac{(F-I+J)\,(F+1-J)\,(I+J+1+F)\,(I+J+1-F)\,(F^2-M_F^2)}{4F^2(2F-1)\,(2F+2)} \right\}^{1/2}. \tag{38}$$

Since Eqs. (38) are invariant under interchange of I and J, it follows that the corresponding off-diagonal matrix elements of $J_z$ are equal to those used in Eqs. (38).

4. The Atomic-Beam Hamiltonian

The Hamiltonian we will be concerned with is

$$\mathcal{H} = \mathcal{H}_{hfs} + \mathcal{H}_{mag}. \tag{39}$$

For most cases this is an adequate Hamiltonian, but in those unusual cases in which the separation between the levels of the same J is comparable to the hyperfine separation, then perturbations on the multiplet from the levels of the same J exist and must be considered. In general, Eq. (39) must be diagonalized to fit the experimental data. This is the main theoretical problem of the atomic-beam technique.

## B. Generalized Nuclear Moments

A generalized definition of the magnetic and electric multipole moments may be made as the nuclear expectation value of the appropriate operator. The generalized magnetic multipole operator, $\mathcal{M}^k$, is given[13] as

$$\mathcal{M}^k = \mu_{nm} \sum_{i=1}^{A} \left[ \frac{2}{k+1} \, g_{\ell_i} \, \underset{\sim}{\ell}_i + \frac{1}{2} \, g_{s_i} \, \underset{\sim}{s}_i \right] \cdot \nabla \left[ r_i^k \, P_k(\theta_i) \right], \quad (40)$$

where $g_{\ell_i}$ is the orbital g factor of the ith nucleon; $g_\ell = 1$ for protons and $g_\ell = 0$ for neutrons; $g_{s_i}$ is the spin g factor for the ith nucleon such that $g_s = 5.587$ for protons and $g_s = -3.826$ for neutrons; $\underset{\sim}{\ell}_i$ and $\underset{\sim}{s}_i$ are the orbital angular momentum and the Pauli spin operator for the ith nucleon, respectively, and $P_k(\theta_i)$ is the Legendre polynomial of order k. The electric multipole operator, $\mathcal{Q}^k$, is similarly defined[13] by

$$\mathcal{Q}^k = e \sum_{i=1}^{A} g_{\ell_i} \, r_i^k \, P_k(\theta_i), \quad (41)$$

where e is the electron charge and the other symbols have already been defined.

It is interesting to note that the operator $\mathcal{M}^k$ has parity $(-1)^{k+1}$ while the operator $\mathcal{Q}^k$ has parity $(-1)^k$. On the assumption of a nuclear ground-state wave function of a definite parity, only even-parity multipoles have nonzero expectation values. It thus follows immediately that only nuclear magnetic multipole moments of odd order exist ($2^k$ with odd k), and that only nuclear electric multipole moments of even order exist ($2^k$ with even k).

### 1. Magnetic Dipole and Electric Quadrupole Moment

Taking k = 1 in Eq. (40), we get, for the magnetic dipole moment,

$$\begin{aligned} \mu &= \left\langle II \left| \mathcal{M}^{(1)} \right| II \right\rangle \\ &= \mu_{nm} \left\langle II \left| \sum_{i=1}^{A} \left\{ g_{\ell_i} \, \underset{\sim}{\ell}_i + \frac{1}{2} \, g_{s_i} \, \underset{\sim}{s}_i \right\} \cdot \hat{k} \right| II \right\rangle, \end{aligned} \quad (42)$$

where $\hat{k}$ is the unit vector along the axis of quantization.

Likewise, the electric quadrupole is given by

$$Q = \frac{2}{e} \left\langle II \left| \mathcal{Q}^{(2)} \right| II \right\rangle = 2 \left\langle II \left| \sum_{i=1}^{A} g_{\ell_i} r_i^2 (3 \cos^2\theta_i - 1) \right| II \right\rangle . \tag{43}$$

Both Eqs. (42) and (43) are evaluated for $M_I = I$.

Equations (42) and (43) exhibited above are seldom used for the direct evaluation of the magnetic dipole and electric quadrupole moments mainly because the nuclear wave function, $|II\rangle$, is rarely known.

2. Relations between Interaction Constants and Moments

The magnetic dipole interaction constant, a, and the electric quadrupole interaction constant, b, are related to the magnetic dipole moment and electric quadrupole moment, respectively.

For an s-electron, Fermi[14] derived the relation

$$a = -\frac{8\pi}{3} \frac{\mu_I}{I} g_J \frac{\mu_0}{h} \left| \psi(0) \right|^2 , \tag{44}$$

where the only new symbol is $\psi(0)$, the electronic wave function evaluated at the nucleus, i.e., $\vec{r}_n = 0$.

For a single non-s electron, one of several derivations gives[15]

$$a = \frac{2\mu_I \mu_0}{I h} \frac{\ell(\ell+1)}{j(j+1)} \left\langle \frac{1}{r^3} \right\rangle \mathcal{F} \tag{45}$$

and

$$b = -\frac{e^2 Q}{h} \frac{2\ell}{(2\ell+3)} \left\langle \frac{1}{r^3} \right\rangle \mathcal{R} \tag{46}$$

where $\mathcal{F}$ and $\mathcal{R}$ are relativistic correction factors which are generally close to unity and are tabulated by Kopfermann.[16] These equations are used in our calculation dealing with $I^{133}$, which has an electronic configuration of $5s^2 5p^5$; this case, in which we have an electron hole, $5p^{-1}$, is amenable to treatment by Eqs. (45) and (46).

For an atom having several non-s electrons, the magnetic dipole interaction constant must be determined from its defining operator relation,

$$ah\vec{I}\cdot\vec{J} = -\vec{\mu}_I\cdot\vec{H}_J, \tag{47}$$

where by $\vec{H}_J$ is meant that operator which represents the magnetic field produced at the nucleus of moment $\vec{\mu}_I$ by the electrons. This field is known to be of the form

$$\vec{H}_J = -2\mu_0 \sum_i \frac{1}{r_i^3}\left[\vec{\ell}_i - \vec{s}_i + \frac{3\vec{r}_i(\vec{r}_i\cdot\vec{s}_i)}{r_i^2}\right] \tag{48}$$

where $\vec{r}_i$ is the vector distance of the ith electron from the nucleus. Taking expectation values for Eq. (47) requires the use of the spherical tensor method of evaluation as proposed by Judd,[10] or else evaluation by finding the equivalent single-electron wave functions by the methods of Condon and Shortley.[2] Hubbs et al.[17] have chosen this latter approach and have found the following for a system of $n_\ell$ equivalent electrons of orbital angular momentum, $\ell$, coupled to the Hund's rule ground-state term, $^{2S+1}L_J$:

$$a = \frac{\mu_I\mu_0}{IJ(J+1)h}\left\langle\frac{1}{r^3}\right\rangle\left\{J(J+1) + L(L+1) - S(S+1)\right.$$
$$\pm \frac{2(2L - n_\ell^2)}{n_\ell^2(2L-1)(2\ell-1)(2\ell+3)}\left\{L(L+1)[J(J+1) + S(S+1) - L(L+1)]\right.$$
$$\left.\left. - \frac{3}{2}[J(J+1) - L(L+1) - S(S+1)][J(J+1) + L(L+1) - S(S+1)]\right]\right\}. \tag{49}$$

The positive sign above applies to all subshells that are less than half full and the negative sign to all subshells that are more than half full. Equation (49) is nonrelativistic.

The quadrupole interaction constant b is related to the nuclear quadrupole moment Q by

$$hb = -e^2 Q \left\langle \frac{1}{r^3} \right\rangle \left\langle SLJJ \left| \sum_i (3\cos^2\theta_i - 1) \right| SLJJ \right\rangle , \qquad (50)$$

where the summation is over all electrons.

The last expectation value appearing in Eq. (50) is that of the gradient of the electric field. Equation (50) can be evaluated[18] for the Hund's rule term as

$$hb = e^2 Q \left\langle \frac{1}{r^3} \right\rangle \left\{ \frac{3K(K+1) - 4L(L+1)\,J(J+1)}{2L(L-1)(J+1)(2J+3)} \times (\pm) \quad \frac{2L(2L-n_\ell^2)}{n_\ell(2\ell-1)(2\ell+3)} \right\} , \qquad (51)$$

where $K = S(S+1) - L(L+1) - J(J+1)$, and the appropriate sign is used as explained in the preceding paragraph.

In both Eqs. (49) and (51), some independent means must be used for an evaluation of the expectation value $\left\langle \frac{1}{r^3} \right\rangle$ if these equations are to be at all applicable. Very often such an estimate results directly from optical spectroscopic sources.

Experimental information concerning other isotopes of the element being studied can sometimes be used to advantage. Regardless of the number of electrons present in a system, the relations

$$a \propto g_I \quad \text{and} \quad b \propto Q$$

hold, and the factors of proportionality are dependent only on parameters relating to the electronic wave function, which should be the same for all isotopes of a given element. Thus we get the relations

$$\frac{a_1}{a_2} = \frac{g_1}{g_2} \quad \text{and} \quad \frac{b_1}{b_2} = \frac{Q_1}{Q_2} . \qquad (52)$$

Relations (52) are exact in the absence of hyperfine anomalies. The subscript 1 can be taken to refer to the isotope under investigation, while subscript 2 refers to the comparison isotope. Because the atomic-beam method can generally measure only the separation between energy levels and not the absolute energy ordering of such levels, there is an inherent difficulty involved in determining the signs of "a" and "b," although the relative signs may generally be determined. It is for this reason that Eq. (52) is usually used with absolute values of the quantities involved.

# III. METHODS AND APPARATUS

## A. General Properties of Atomic-Beam Apparatus

Two atomic-beam machines were used throughout this experiment. They are discussed in a very general fashion in a subsequent section of this paper. This section reviews the basis of the conventional atomic-beam technique.

Figure 2 is a schematic diagram of a typical atomic-beam "flop-in" machine. The magnets indicated by the letters A and B are inhomogeneous magnets, the field gradients of which are oriented in the fashion shown in Fig. 2. An atom having a nonzero electronic magnetic moment leaves a thermally heated oven, O, and is deflected in the strongly inhomogeneous magnetic-field region of the A magnet. It then passes into the homogeneous C field region, where it may or may not undergo a resonant transition from one of the quantized energy levels to another such level. If it does not undergo a transition it is further deflected as it enters the B region and is lost to the beam. Such a trajectory is indicated by (1) in Fig. 2. If, on the other hand, the atom in question undergoes a transition in the C field region such that its z component of the electronic magnetic moment is reversed when it enters the B region, then it is "refocused," i.e., it follows a trajectory (2) and strikes the detector D.

The focusing condition, $M_J \rightarrow -M_J$, can be better understood from Fig. 3, an energy-level diagram for $K^{39}$ which has $J = 1/2$ and $I = 3/2$. If an energy level is considered to be representative of the potential energy, W, of an atom, the force $\vec{F}$ on an atom is classically

$$\vec{F} = -\vec{\nabla} W = -\frac{\partial W}{\partial H_z}\,\vec{\nabla} H_z \,. \qquad (53)$$

Since the A and B magnets operate in the region of 10,000 gauss, the strong-field approximation to the energy levels of an atom in the magnetic field is very good. This approximation is

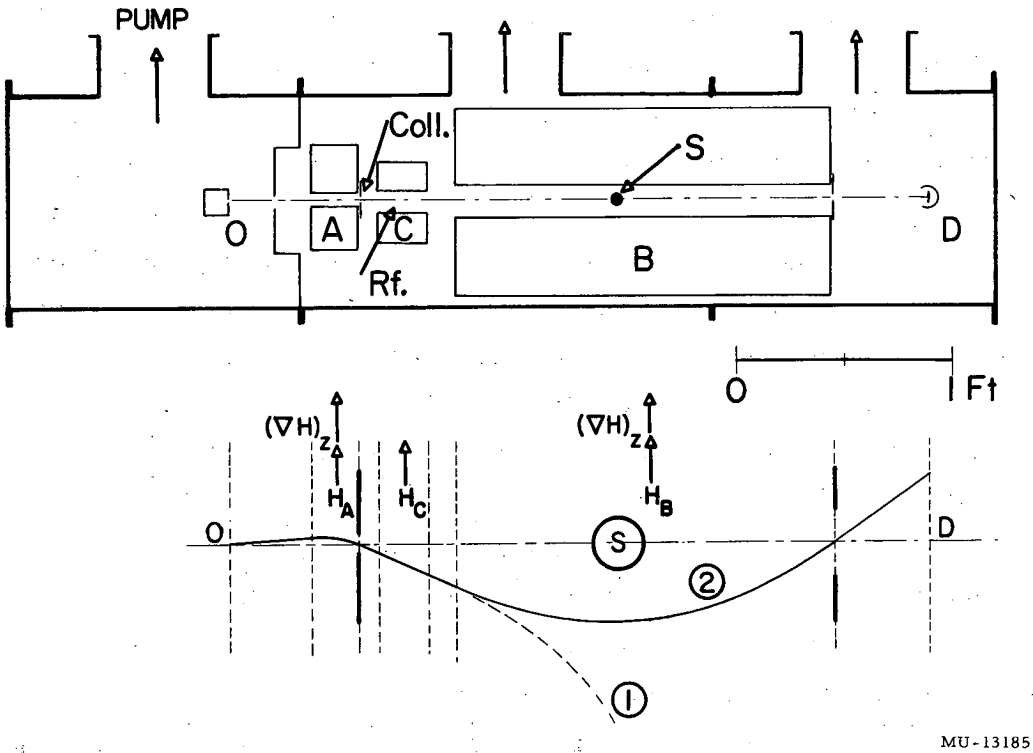


Fig. 2. Schematic arrangement and trajectory in an atomic-beam "flop-in" apparatus.

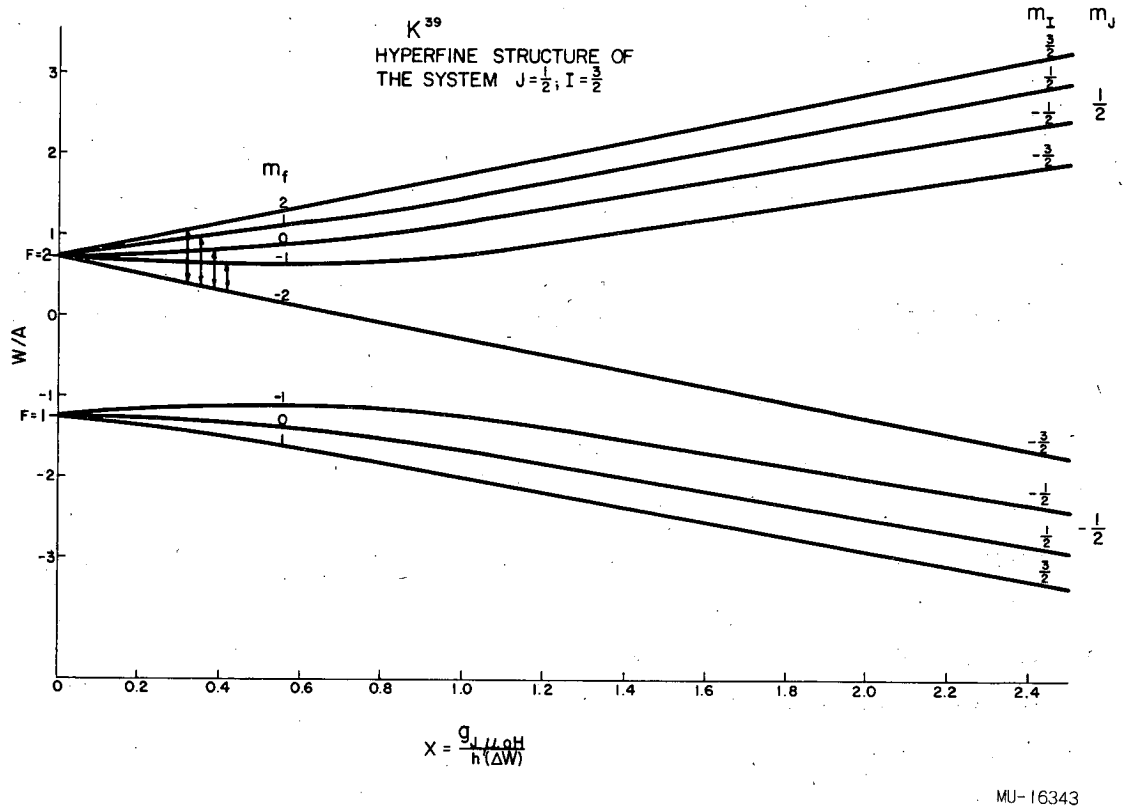


Fig. 3. Energy levels of the system I = 3/2, J = 1/2, in a magnetic field. Note dimensionless units. Above diagram applies to $K^{39}$ in a magnetic field.

$$W_{M_I, M_J} =$$

$$ahM_IM_J + \frac{bh}{4} \frac{3M_J^2 - J(J+1)}{J(2J-1)} \frac{3M_I^2 - I(I+1)}{I(2I-1)} - g_J \mu_0 H_z M_J - g_I \mu_0 H_z M_I \quad (54)$$

hence

$$\frac{\partial W_{M_I, M_J}}{\partial H_z} = -g_J \mu_0 M_J - g_I \mu_0 M_I \quad (55)$$

Since we have $g_J >> g_I$, to a good approximation we have

$$\frac{\partial W_{M_I, M_J}}{\partial H_z} \simeq -g_J \mu_0 M_J \quad (56)$$

Thus, referring back to Eq. (53), we see that the force on an atom is reversed by reversing the sign of $M_J$. In a balanced magnet system the opposite forces may be different in the A and B magnets, but the total deflection is equal and opposite without regard to the velocity of the atom.

In the resonance process, approximately one in $10^5$ atoms reaches the detector. The remaining atoms are lost to the beam and contribute to the machine background. The stopwire S in Fig. 2 serves to stop fast atoms which suffer little deflection in the A and B magnets and which might possibly reach the detector having undergone no resonant transition.

## B. Machine Description

As briefly mentioned in the previous section, two atomic-beam machines were used. The first machine, on which the work on $I^{133}$, $Bi^{210}$, and $Po^{210}$ was performed, will be called machine A, whereas the other machine, on which the work pertaining to $Nd^{141}$ and $Eu^{152}$ was performed will be called Machine B.

Both machines have been described in detail in the literature and hence little of the specific details need be given here. Machine A is photographed in Fig. 4 and is described in References 19 and 20. Machine B is photographed in Fig. 5 and is described in References 21 and 22.

The chief differences in the two machines is in their vacuum systems. Machine A has its vacuum contained inside the magnet coils and hence has the advantage that repairs to the external parts of the machine may be made without risk of exposure to radioactive contamination. For this reason Machine A is referred to as an "inside-out" machine. Machine B, on the other hand, contains all the working magnets inside a large manifold. This is a more conventional design.

Machine B has heavy lead shielding in the oven region of the apparatus, making it possible to handle samples of a high radioactive level, e.g., $Eu^{152}$. Machine B also has a buffer region between the oven chamber in Fig. 2 and the A-magnet region. This chamber allows a separation between the relatively high-pressure region ($10^{-5}$ or $10^{-6}$ mm Hg) surrounding an effusion oven and the low-pressure region ($10^{-6}$ or $10^{-7}$ mm Hg) of the body of the machine. It is hoped by this device to decrease scattering which might give rise to high machine background.

Machine A has the feature, which is not a common one, of having a long copper bar ($21 \times 2 \times 1/2$ in.) extending down the length of its B magnet. This copper bar is in thermal contact with a trap filled with liquid nitrogen. This cold bar extending down the long B magnet was incorporated into the machine to reduce pressure and concomitant scattering.

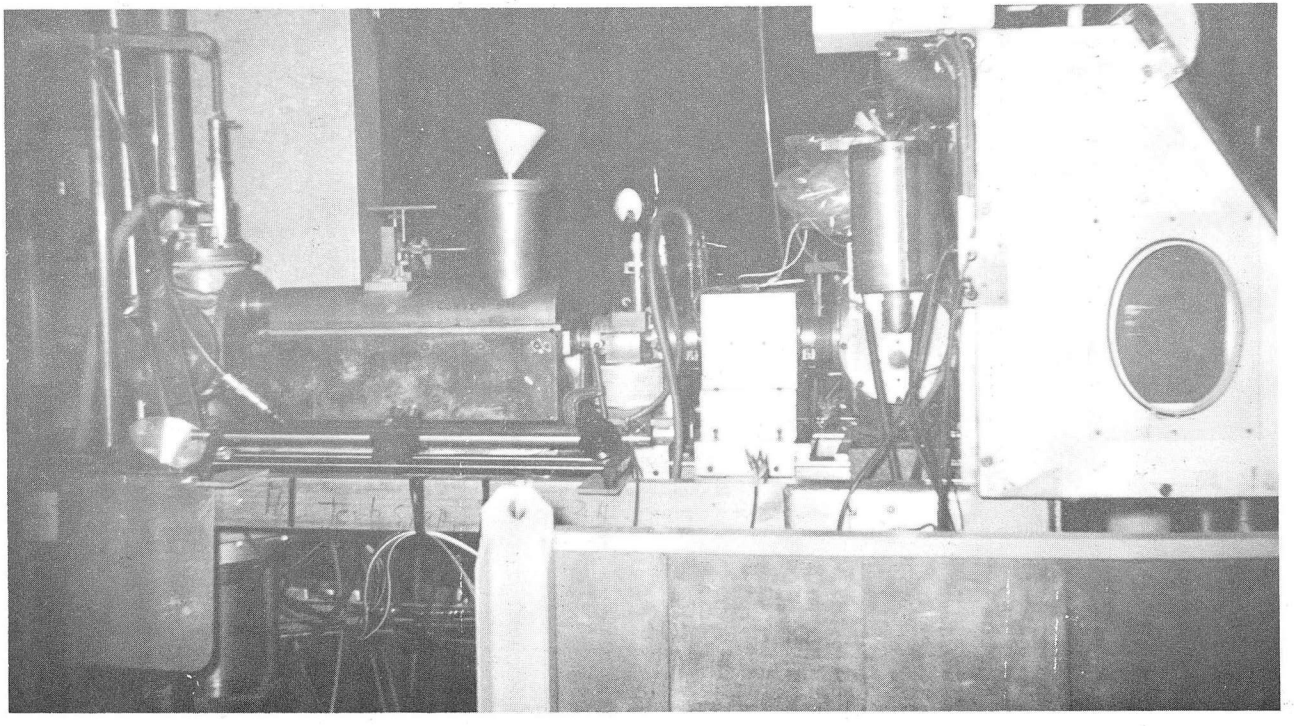

ZN-2213

Fig. 4. Atomic-beam machine A. This machine has vacuum system contained inside the magnets. "Cave" used for containing activity is at right. Plunger used to introduce "buttons" into the machine can be seen at the left. The magnets are clearly visible.

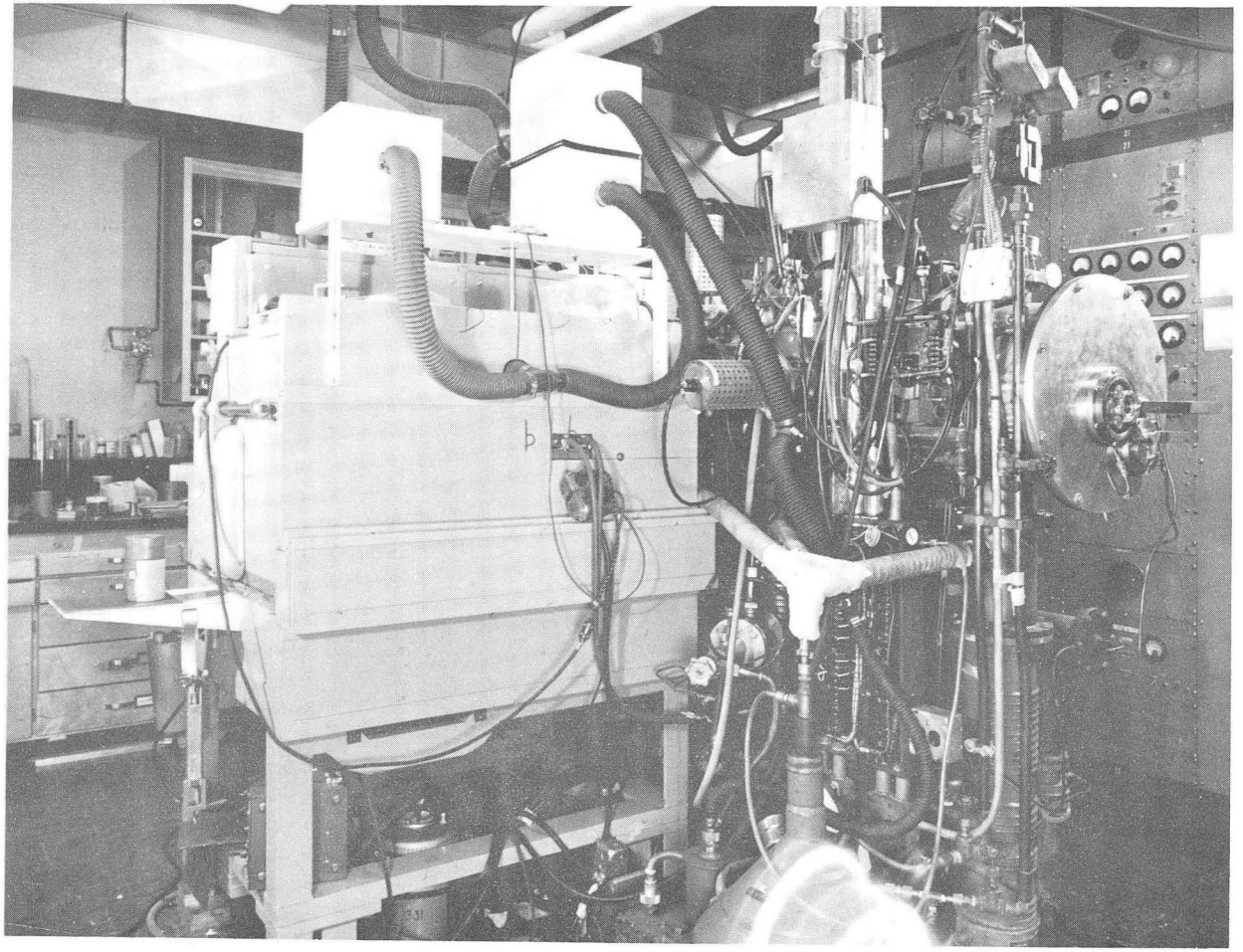

ZN-2591

Fig. 5. Atomic-beam machine B. On the left is the back of the cave used to contain activity. On right, outline of large vacuum manifold can be seen. At end of machine is rotating mechanism for positioning platinum foils.

## C. "Hairpin" and Selection Rules

The loop arrangement that carries the oscillating radio-frequency current into the C-field region is shown in Fig. 6. As can be seen from the figure, there are two possible orientations of the loop--or "hairpin," as it is often called. These two possible orientations, neglecting fringing effects, give rise to two selection rules on the transitions involved in the C-field region.

Consider the situation as shown at the left in Fig. 6. In this case we have an oscillating magnetic field parallel to the field of the C magnet. Let us write the general perturbing potential as $\vec{V}^{\,pert} = A \sin \omega t \; \hat{\rho}$, where $\hat{\rho}$ is a general unit vector in any direction, $\omega$ is the angular frequency of the incident rf radiation, A is the amplitude of this incident radiation, and t is the time. We are interested in that part of the general perturbation which is along the direction of the C field, i.e., $V_z^{pert} = A \sin \omega t \cos \theta$, where $\theta$ is the angle between the direction of the perturbing rf and the C-field direction. A general definition of the spherical tensors is given as

$$C_q^k = (-)^q \sqrt{\frac{(k-q)!}{(k+q)!}} \; P_k^q (\cos \theta) \, e^{iq\phi} , \tag{57}$$

where k is the order of the spherical tensor and q indexes the components of these tensors; $P_k^q$ are the associated Legendre polynomials. Making use of the definition (57), we see

$$V_z^{pert} = A \sin \omega t \; C_0^1 . \tag{58}$$

The matrix element of the perturbing potential (58) which connects two states is by the Wigner-Eckart theorem,[11]

$$\left\langle F'M'_F \middle| V_z^{pert} \middle| FM_F \right\rangle = A \sin \omega t \left\langle F'M'_F \middle| C_0^1 \middle| FM_F \right\rangle =$$

$$A \sin \omega t \times (-1)^{F'-M'_F} \begin{pmatrix} F' & 1 & F \\ -M'_F & 0 & M_F \end{pmatrix} \left\langle F' \middle|\middle| C^1 \middle|\middle| F \right\rangle . \tag{59}$$

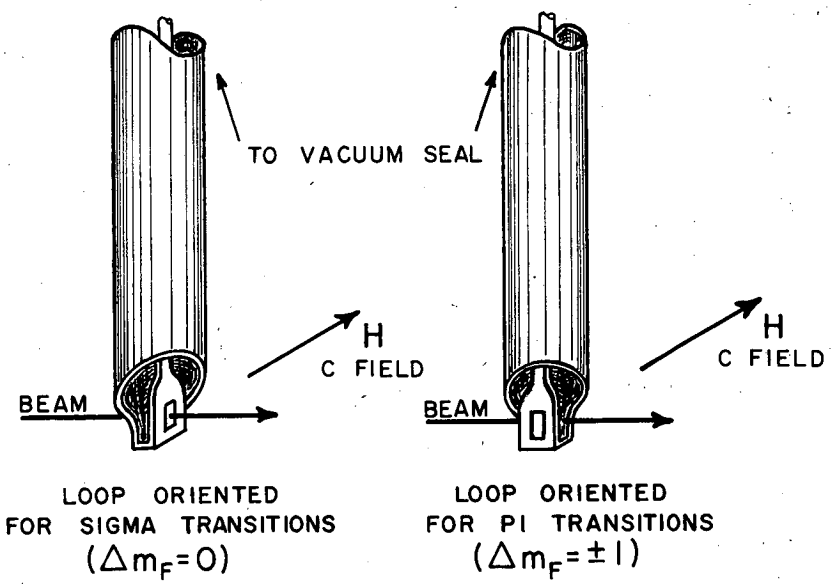


MU-18042

Fig. 6. Dual-purpose radio-frequency loop. Loop may be easily rotated from one position to the other.

For the nonvanishing of the Wigner 3-j symbol in Eq. (59) we must have the bottom row of three quantities algebraically add to zero. This immediately implies $\Delta M_F = 0$. This is one of the selection rules which we have set out to demonstrate. Transitions of this type are known as $\sigma$-type transitions.

Now let us consider the situation as shown on the right-hand side of Fig. 6. We are now interested in the part of the perturbation which is in the xy plane, $V^{pert}_{x,y} = A \sin \omega t(\cos \phi \pm i \sin \phi) \sin \theta$, where the quantity in parenthesis refers to the orientation of the perturbation in the xy plane, which is arbitrary. Referring back to Eq. (57), we see that we have

$$V^{pert}_{x,y} = \mp \sqrt{2}\, A \sin \omega t\, C^1_{\pm 1} \,. \tag{60}$$

The matrix element that connects two different states is

$$\left\langle F' M_{F'} \left| V^{pert}_{x,y} \right| F M_F \right\rangle = \mp \sqrt{2}\, A \sin \omega t \left\langle F' M'_F \left| C^1_{\pm 1} \right| F M_F \right\rangle =$$

$$\mp \sqrt{2}\, A \sin \omega t \begin{pmatrix} F' & 1 & F \\ -M_F & \pm 1 & M_F \end{pmatrix} \left\langle F' \left\| C^1 \right\| F \right\rangle . \tag{61}$$

This immediately implies $\Delta M_F = \pm 1$ for nonvanishing of the 3-j symbol of Eq. (61). Transitions of this type are indicated as $\pi$ transitions.

## D. Magnetic-Field Calibration

The magnetic field in the C-field region was calibrated and checked by observing the resonant transition frequency between the levels $(F = 2,\ M_F = -2 \leftrightarrow F = 2,\ M_F = -1)$ of $K^{39}$. To a much lesser extent the resonant transition frequency $(F = 4,\ M_F = -2 \leftrightarrow F = 4,\ M_F = -1)$ of $Cs^{133}$ was used as a basis for calibration.

The energy-level diagram for $K^{39}$ appears in Fig. 3. The possibility of the existence of multiple quantum transitions is indicated by small arrows connecting energy levels that fulfill the focusing condition of the atomic-beam "flop-in" apparatus. Such multiple quantum transitions, i.e., $\Delta M_F = \pm n\hbar$, $n = 2, 3, \cdots$, were never observed separately for the calibrating substance, although such transitions were observed for the experimental material, and in 5-day $Bi^{210}$ caused much confusion.

For $K^{39}$, $I = 3/2$ and $J = 1/2$. By a theorem discussed in a previous section, this limits the interaction between the nucleus and the atomic electrons to the magnetic-dipole type. There are no higher-order electric or magnetic interactions. The Hamiltonian for $K^{39}$ or for any $J = 1/2$ isotope can be readily diagonalized; the energy eigenfunctions are generally written in the form

$$W = -\frac{\Delta W}{2(2I \mp 1)} - g_I \mu_0 M_F H_z \pm \frac{\Delta W}{2}\left[1 + \frac{4M_F\chi}{2I+1} + \chi^2\right]^{1/2}, \tag{62}$$

where $\Delta W = \frac{ha(2I+1)}{2}$ and $\chi = \frac{(g_I - h_J)\mu_0 H_z}{\Delta W}$.

The sign of the square root is $\pm$, as $F = I \pm 1/2$. Equation (62) was first described by Breit and Rabi[23] in a slightly different form. The values of the electronic and nuclear constants used in connection with equation (62) are for $K^{39}$:

$$\begin{aligned} I &= 3/2, \; J = 1/2 \\ g_J &= -2.00228 \\ \Delta\nu &= 461.71971 \text{ Mc/sec} \\ \mu_{0/h} &= 1.399677 \text{ Mc/sec-gauss} \\ g_I &= +1.41945 \times 10^{-4} \quad \text{(referred to Bohr magneton)} \end{aligned} \tag{63}$$

Using the values of Eqs. (63) with Eq. (62), one can easily derive the relation between the resonant transition frequency and the magnetic field.

The potassium oven itself is a metal cylinder with an aperture on one side. When the oven is lowered into position either manually or by electric motor, the oven aperture comes into line with the machine

axis in front of the radioactive source oven. At the detector end of the machine, a hot tungsten strip ionizes the incident K beam. The $K^+$ ions are collected and their current measured.

## E. Radio-Frequency System

It is necessary to furnish a source of radio-frequency power to the loop arrangement discussed in a previous section. Since we are introducing a different radio-frequency signal for both the unknown isotope and the calibrating material, it is usually a more efficient system to use two oscillators and to switch between them correspondingly as our interest changes from the unknown isotope to the calibrating substance. Also because of the wide range of frequencies required (1.0 to 500.0 Mc) several oscillators were used at different times. Table I lists the rf equipment and the function of the main components.

## F. Radioactive Detection

Detection of an atomic beam generally is a difficult problem faced by one commencing an experiment. No universal detector exists as yet, and hence different schemes must be employed to detect an isotope; clearly, the properties of the isotope being studied will determine the method of detection.

With $K^{39}$, as mentioned in a previous section, detection was effected by means of hot-wire ionization off tungsten. That this was possible is a consequence of the relation between the work function of tungsten and the ionization potential of $K^{39}$, the value for the former quantity (4.49 ev) being greater than that of the latter (4.34 ev). It is unfortunately not generally possible to use hot-wire ionization for materials other than the alkalis. The value judgment appearing in the preceding sentence results from the relative ease and immediate results that one gets by using the hot-wire method.

Some attempts have been made to use mass-spectrographic techniques in conjunction with atomic-beam apparatus. Sandars has used this means of detection successfully on the stable isotopes of europium.[24] This method of detection has yet to be fully exploited, and will probably be employed to a greater extent in the future.

Table I. Radio-frequency system components

| Manufacturer, model, name | Frequency range Mc | Function |
|---|---|---|
| General Radio 805 oscillator | 0.016 to 50.0 | Provide primary source of rf power. |
| Tektronix 190A oscillator | 0.35 to 50.0 | |
| Hewlett-Packard 608A oscillator | 10.0 to 500.0 | |
| General Radio 1208B oscillator | 65.0 to 500.0 | |
| General Radio 1209B oscillator | 250.0 to 920.0 | |
| ifi 500 wide-band amplifier | 0.5 to 240.0 | Two-stage amplification of rf input. |
| ifi 510 wide-band amplifier | 0.5 to 240.0 | |
| Hewlett-Packard 524B frequency counter | 0.0 to 10.0 | Allows for counting frequency. |
| Hewlett-Packard 524A frequency converter unit | 10.0 to 100.0 | Extends range of frequency counter. |
| Hewlett-Packard 524B frequency converter unit | 100.0 to 220.0 | Further extends range of frequency counter. |
| Hewlett-Packard 540A transfer oscillator | 100.0 to 200.0 | Produces harmonic signal used for beating with rf greater than 220 Mc. Beats are then counted and multiplied by appropriate harmonic factor. |

Table I. (continued)

| Manufacturer, model name | Frequency range (Mc) | Function |
|---|---|---|
| Weston rf milliameter, model 425 | | Used to measure current in loop for frequencies below 100 Mc. |
| General Radio 874-LBA slotted line<br>General Radio 874-D50 50-cm adjustable stub | | Used for adjustment of effective length of cable connecting loop with oscillators. Very important at high frequencies > 200 Mc. |
| Federal Cable Co. 50-Ω cable<br>General Radio fittings | | Used for connecting various components. |

In the experimental work reported in this thesis radioactive detection of β rays has been used. This technique is a familiar one.

In machine A, brass or stainless steel "buttons" were coated with surfaces of silver, sulfur, or lampblack. A photograph of representative buttons as used in machine A is shown in Fig. 7. The choice of the surface material was empirical. It was found that a freshly coated sulfur surface efficiently collected atoms of $Bi^{210}$(RaE) and $Po^{210}$ and that a vacuum-evaporated surface of silver efficiently collected $I^{133}$ atoms. With the latter it was found essential that the silver surfaced buttons be stored under vacuum until used, since contact with air decidedly reduced the collection efficiency of the silver surface.

In machine B, platinum discs (0.001 × .495 in.) were used. Platinum is known to be a good collector for the rare earths; Cabezas,[25] using only platinum foils for collection purposes, investigated thirteen different rare earth isotopes. In machine A a test was made of the relative collection efficiencies for $Eu^{152}$ of platinum foil and a silver surface. The results of the test showed their collection efficiencies to be virtually the same. The platinum foil and holders for machine B are shown in Fig. 8.

After exposure the "buttons" or platinum foils are counted in small-volume continuous gas-flow β counters as shown in Fig. 9. Methane at very slightly greater than atmospheric pressure is used as the chamber gas. In the small-volume chamber a small loop of tungsten is maintained at 2500 to 2900 volts positive with respect to the housing. The small volume of the counter chamber makes possible a relatively low background counting rate, usually well below 10 counts per minute. The counting chamber is itself shielded in a lead container the walls of which are 1.75 in. thick.

The apparatus components used in the counting systems are indicated in Table II.

In addition to determining the activity deposited on a button during a run, the counting systems were used in decay studies to determine half lives for purposes of identification.

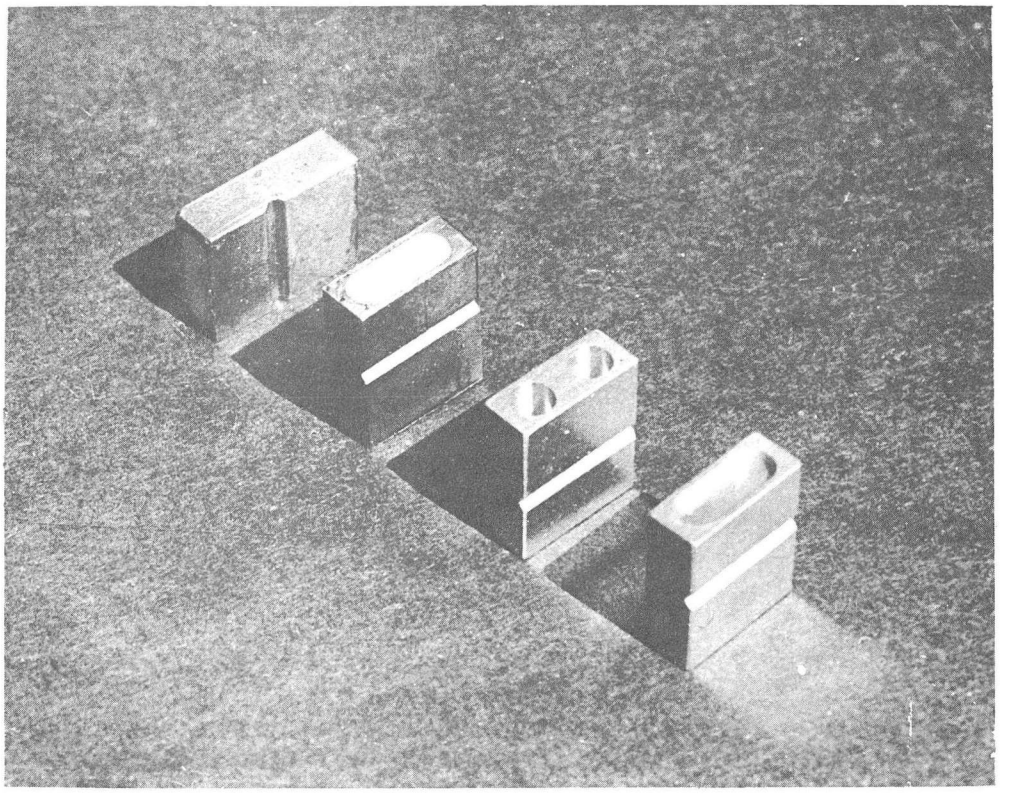

ZN-1732

Fig. 7. Buttons for use in atomic-beam machine A. The slot on the side of the button is used in conjunction with a spring–ball bearing arrangement for positioning purposes. Two holes in the button facilitate its removal from the apparatus with long-nose pliers.

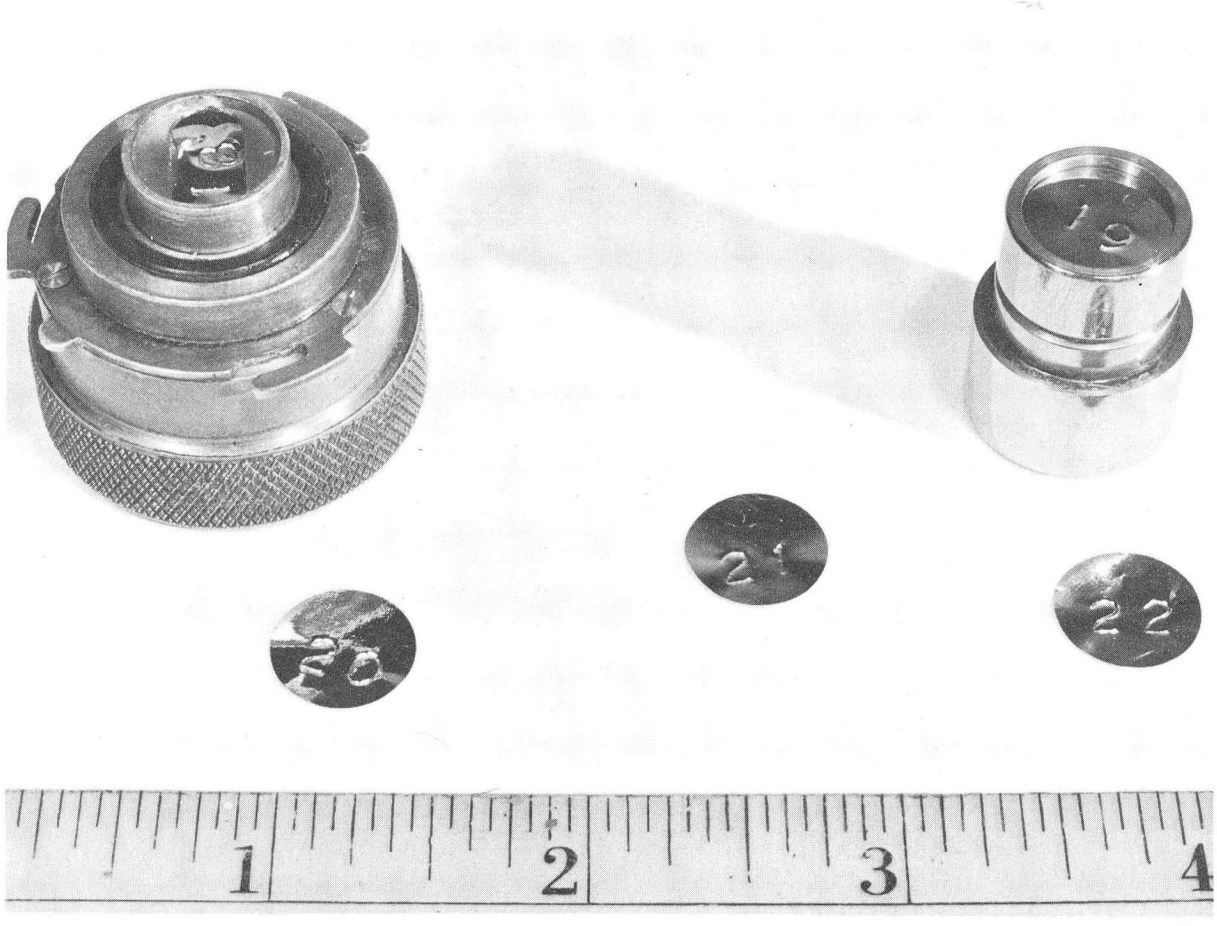


ZN-2936

Fig. 8. Platinum collection foils and associated holders. The holder at the upper left is used to introduce a foil into machine B after passing through a pumpout chamber; note the rubber O ring. The holder at upper right is used for introduction of the foil into the counting head, which is diagramatically shown in Fig. 9. In the foreground appear three representative foils. Numerals for identification purposes are stamped onto the platinum coils prior to a run.

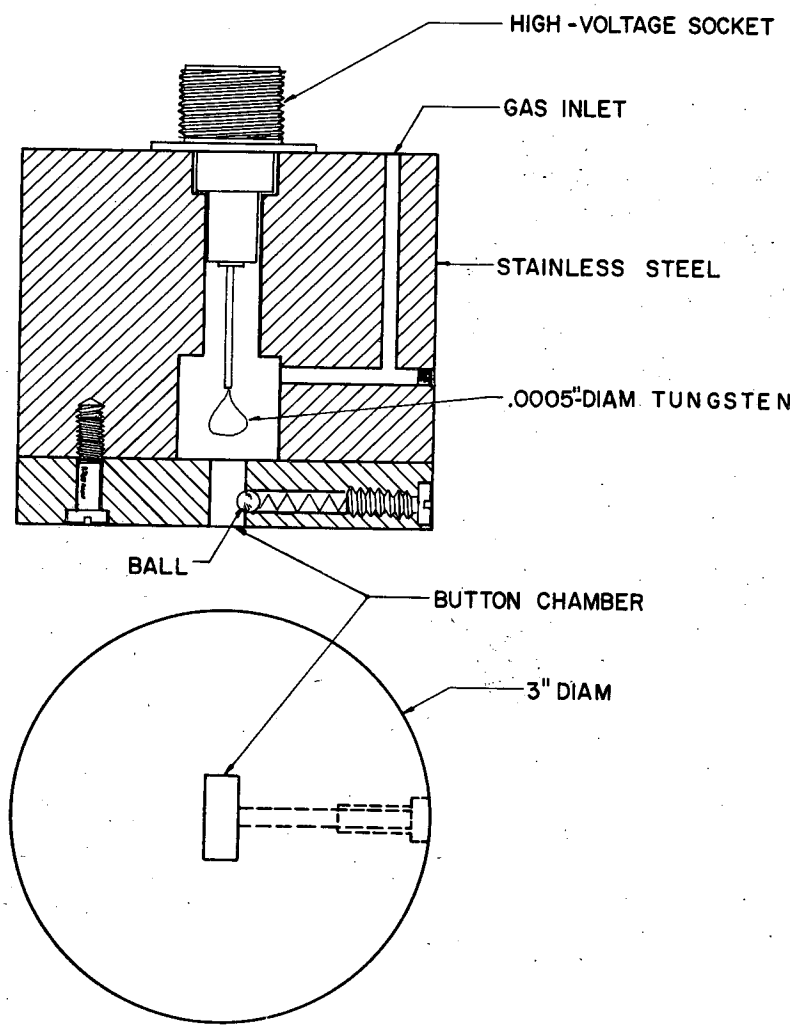


Fig. 9. Cross-sectional view of the counting head of the small-volume continuous-flow β counters.

Table II. Components making up counting system.

| Unit | Manufacturer | Function |
|---|---|---|
| ac voltage regulator | Sorenson and Co., Inc. Stamford, Conn. | Gives regulated 110-volt ac output to be used as input for other components. |
| Regulated high-voltage supply | Northeast Scientific Corp., Cambridge, Mass. | Maintains a 2.5- to 3.0-kv positive potential on tungsten loop of counting head. |
| Regulated power supply, Model 32 | Lambda Electronics Corp., Corona, N. Y. | Output is $B^+$ for decade scalers. |
| Low-level pre-amplifier, Type 122 | Tektronix, Inc., Portland, Oregon | Pulse amplification. |
| Decade scalers | UCLRL, Berkeley, Calif. | Count display. |
| "Pipper" | UCLRL circuitry in addition to printer sold by Presin Co., Santa Monica, Calif. | Automatic timer which prints out accumulated counts sequentially for any fixed time interval up to 20 minutes. |
| Timers | 1. Labline, Inc., Chicago, Ill.; 2. Precision Scientific Co., Chicago, Ill. | Measurement of time intervals. |

## G. Resumé of Experimental Method

The Hamiltonian with which we are concerned is

$$\mathcal{H} = ah\,\vec{I}\cdot\vec{J} + bh\,\frac{3(\vec{I}\cdot\vec{J})^2 + 3/2(\vec{I}\cdot\vec{J}) - I(I+1)J(J+1)}{2I(2I-1)J(2J-1)}$$

$$- g_J\mu_0\,\vec{J}\cdot\vec{H} - g_I\mu_0\,\vec{I}\cdot\vec{H}\,, \qquad (64)$$

where all the symbols have already been defined. For small values of H, i.e., for $-g_J\mu_0\,\vec{J}\cdot\vec{H} \ll a\,\vec{I}\cdot\vec{J}$, the separation in terms of frequency between adjacent magnetic sublevels of a given F is given (as shown earlier) by

$$\nu_F \approx -\,g_J\,\frac{\mu_0}{h}\,H_z\,\frac{[F(F+1) + J(J+1) - I(I+1)]}{2F(F+1)}\,. \qquad (37)$$

During the course of an experiment, transitions of the type $\Delta F = 0$, $\Delta m = \pm 1$ are first observed for different values of F at low applied magnetic fields where their field dependence is given by Eq. (37). The magnetic fields are increased and deviation from Eq. (37) is noted. This procedure is continued until Eq. (37) is no longer a valid means of approximation for the transition frequency. It then becomes necessary to determine the exact solution of the Hamiltonian (64). An IBM program has been written to solve the Hamiltonian as a function of magnetic field. The input data are the observed transition frequencies, the fields, and their uncertainties. The output is the best values of a and b obtained by the least-squares fit of Eq. (64) to the data. Provision is made within the program to permit $g_J$ to be an independent parameter if this is so desired; in this case the output is the best values of a, b, and $g_J$. With these values of a and b, a second IBM program is used to calculate transition frequencies at higher fields, and a search is made for new resonances. When they are found, the new data are treated as described above and the process continued until a and b are known sufficiently accurately to permit

a search to be made for the hyperfine transitions ($\Delta F = \pm 1$) at low fields. The fit of the Hamiltonian (64) to the data depends directly upon the choice of the sign of $g_I$. The data are processed for both choices of sign, and the "goodness of fit" is determined by the $\chi^2$ test of significance.[26] In this way, the sign of the nuclear moment can be determined if the precision of observation justifies. These programs have been described elsewhere.[27, 28]

# IV. BISMUTH-210

## A. Introduction

The beta spectrum of bismuth-210 has played an important role in the development of β-decay theory, for it is the only known case of a first-forbidden transition $\Delta I = 1$ (yes) with a nonallowed shape. At one time the spectrum shape was regarded as the only evidence for the existence of a pseudoscalar term in the β-decay interaction,[29] but subsequent theoretical work by Yamada[30] together with a measurement of the ground-state spin ($I = 1$) by Title[31] showed this was not in fact implied. There are two papers, by Plassmann and Langer[32] and by Wu,[33] that summarize the early history of the RaE spectrum.

In the past two or three years, and since the discovery of parity nonconservation in weak interactions, there has been a considerable revival of interest in bismuth-210[34-38] because both the shape of the spectrum and the degree of polarization of the emitted electrons are possible checks on time-reversal invariance. Perhaps the best discussion of this point is contained in the paper of Alikhanov et al., who measure the polarization of the decay electrons.[37] They point out that the degree of polarization fixes the range of a parameter X determined by the ratio of certain nuclear matrix elements and that this range is extremely sensitive to any violation of time-reversal invariance. They find little or no evidence for a violation, but point out that a direct calculation of X from the shell model would be a useful check on their conclusion. Such a calculation would involve a knowledge of the nuclear wave function. One independent check of the correctness of the wave function would be a comparison between experimental and calculated values of the nuclear moment of RaE.

There has been one prior attempt to measure the hyperfine structure of RaE -- that by Fred et al., who used the method of optical spectroscopy.[39] However, their apparatus was inadequate to resolve the hyperfine structure, and they assigned a nuclear magnetic moment of less than 0.1 that of the stable $Bi^{209}$. This appeared unreasonable

in view of the large moment of this latter isotope (4 nm), and they were led to assign an erroneous spin value (I = 0) to RaE. Some of the consequences of this assignment are traced in a paper by Lee-Whiting on the $\beta$ spectrum of RaE.[40]

The results presented in this thesis supplement a large body of information that exists now on the nuclear moments of the bismuth isotopes.[41] Blin-Stoyle and Parks have explained the large deviation of the moment of $Bi^{209}$ from the Schmidt value as being due to inter-configurational mixing,[42] but as far as we know, no systematic attempt has yet been made to explain the variation of moments between different bismuth isotopes.

## B. Additional Points of Theoretical Interest

The nuclear spin of $Bi^{210}$ is 1.[31] This value of the spin restricts the angular-dependent interactions between the nucleus and surrounding electrons to magnetic-dipole and electric-quadrupole interactions. These interactions give rise to a Hamiltonian of the form as shown in Eq. (64).

In the absence of an applied magnetic field, the total angular momentum, $\vec{F} = \vec{I} + \vec{J}$, is a constant of the motion. In a representation in which $F^2$ and $F_z$ are diagonal matrices, the operators $\vec{I}^2$, $\vec{J}^2$, and $\vec{I} \cdot \vec{J}$ are also diagonal. Therefore, the solution of Eq. (64) with $H_z = 0$ can be written as

$$(W/a)_F = C_1(F) + C_2(F)\, b/a, \tag{65}$$

where $C_1(F)$ and $C_2(F)$ are constants depending only upon F for a given I and J, and $(W/a)_F$ is the energy, in units of a, of the hyperfine level characterized by the quantum number, F. A plot of $(W/a)_F$ vs b/a is a straight line which, in general, has a different slope for each value of F. A plot of $(W/a)_F$ is shown in Fig. 10 for values of I and J appropriate to $Bi^{210}$ (i.e., 1 and 3/2, respectively). For vanishing quadrupole moment we have b = 0, and the hyperfine separations between levels of different F obey the well-known Landé interval rule. For values of b/a less than -2 or greater than 2/3, the levels are no

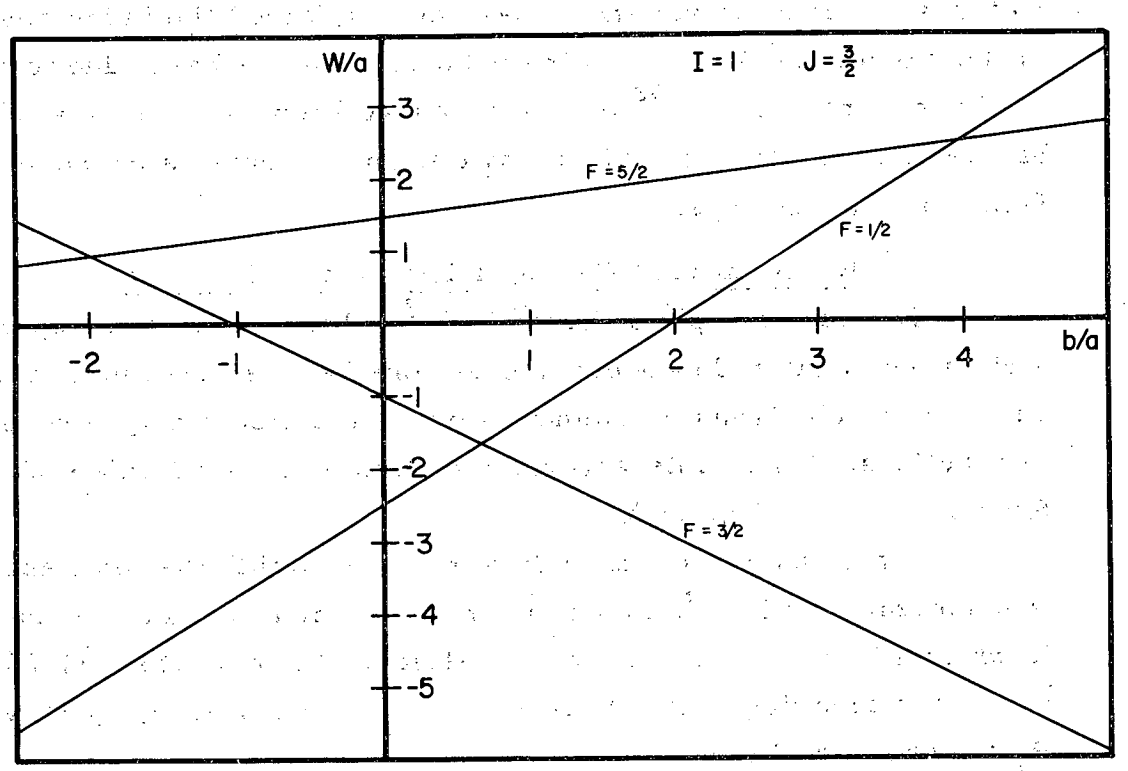


Fig. 10. Hyperfine-level separations (in units of W/a) in an isotope with I = 1 and J = 3/2 plotted as functions of b/a. Note that in the diagram, a has been assumed positive, whereas, in fact, the sign of a for RaE is not known.

longer in normal order, and an inversion is said to exist. Such is the case with $Bi^{210}$ where b/a = 5.160.

## C. Experimental Details

The general experimental method has already been discussed. Low field resonances were initially observed with the help of Eq. (37), which was very useful because the $g_J$ is known ($g_J = -1.6433 \pm .0002$).[43]

During the initial course of the experiment, the transitions labeled $\alpha$ and $\beta$ in the energy-level diagram of Fig. 11 were observed. These transitions are indexed by the quantum numbers

$$\alpha: \quad (F = 5/2,\ M_F = 1/2 \leftrightarrow F = 5/2,\ M_F = -1/2),$$

$$\beta: \quad (F = 3/2,\ M_F = 3/2 \leftrightarrow F = 3/2,\ M_F = 1/2).$$

The $\alpha$ transition was observed up to a field of 50 gauss and the $\beta$ to a field of 129 gauss, where the values of a and b were obtained sufficiently accurately to permit a search for the $\Delta F = \pm 1$ direct hyperfine transitions. All allowed direct hyperfine transitions have been observed at low field during the course of this experiment.

The active sample was produced by the reaction $Bi^{209}(n, \gamma)Bi^{210}$ in a high-flux reactor. Because of the low thermal-neutron-capture cross section of $Bi^{209}$ (0.02 barn), large samples of stable bismuth (5 g) were exposed for 15 to 20 days in a flux of $2 \times 10^{13}$ neutrons/$cm^2$ sec. The resulting specific activity of the samples was low, but with relatively long exposure and counting times (usually about 10 to 15 min), excellent resonances were obtained. A typical resonance is shown in Fig. 12. The active sample is evaporated from the oven shown in Fig. 13. Bismuth tends to evaporate as diamagnetic molecules, and before an atomic-beam deflection experiment upon it is possible, the molecules must be dissociated into atoms. The oven snout is heated at its tip by electron bombardment to a temperature of about 1500° C, at which point the bismuth molecules are well dissociated. The vapor pressure of the bismuth is maintained at a proper value by conduction of heat down the snout to the oven block; during operation the oven temperature was about 800° C. The snout and

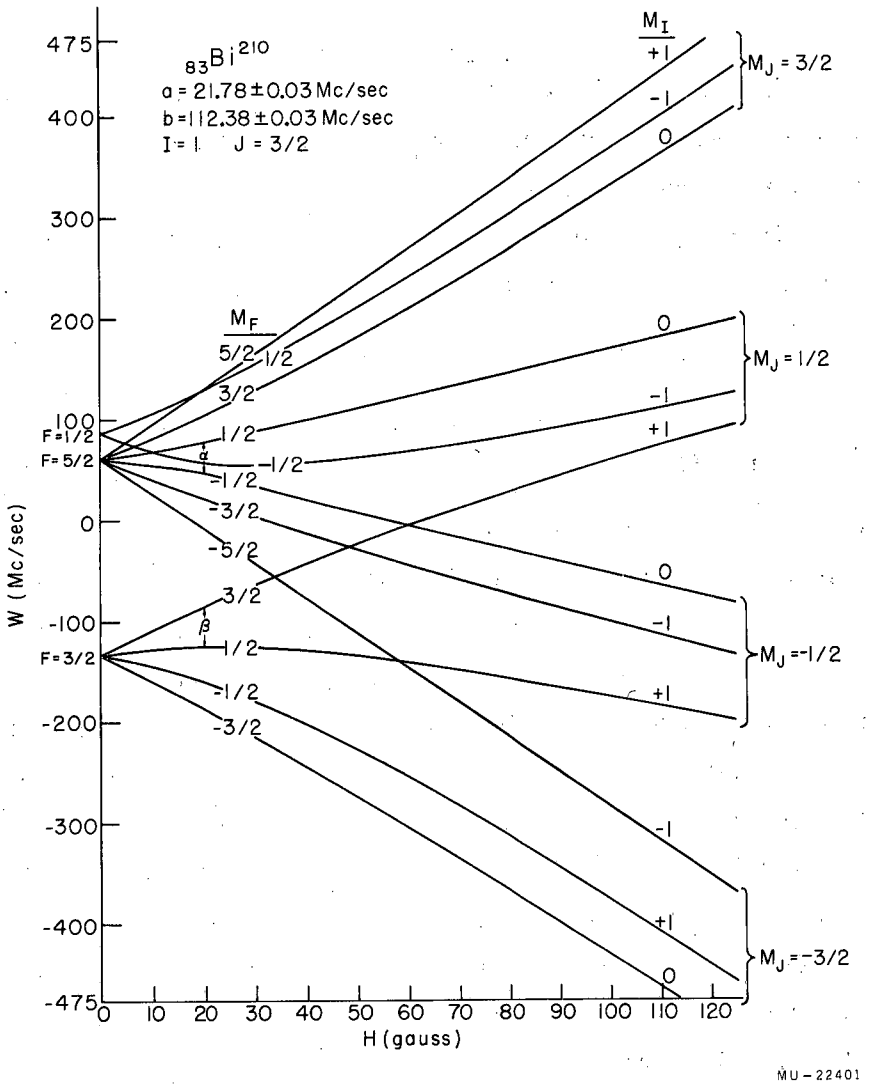


Fig. 11. Energy levels of RaE ($Bi^{210}$) plotted as a function of magnetic field. These were calculated with the aid of an IBM program; the sign of a has been assumed positive.

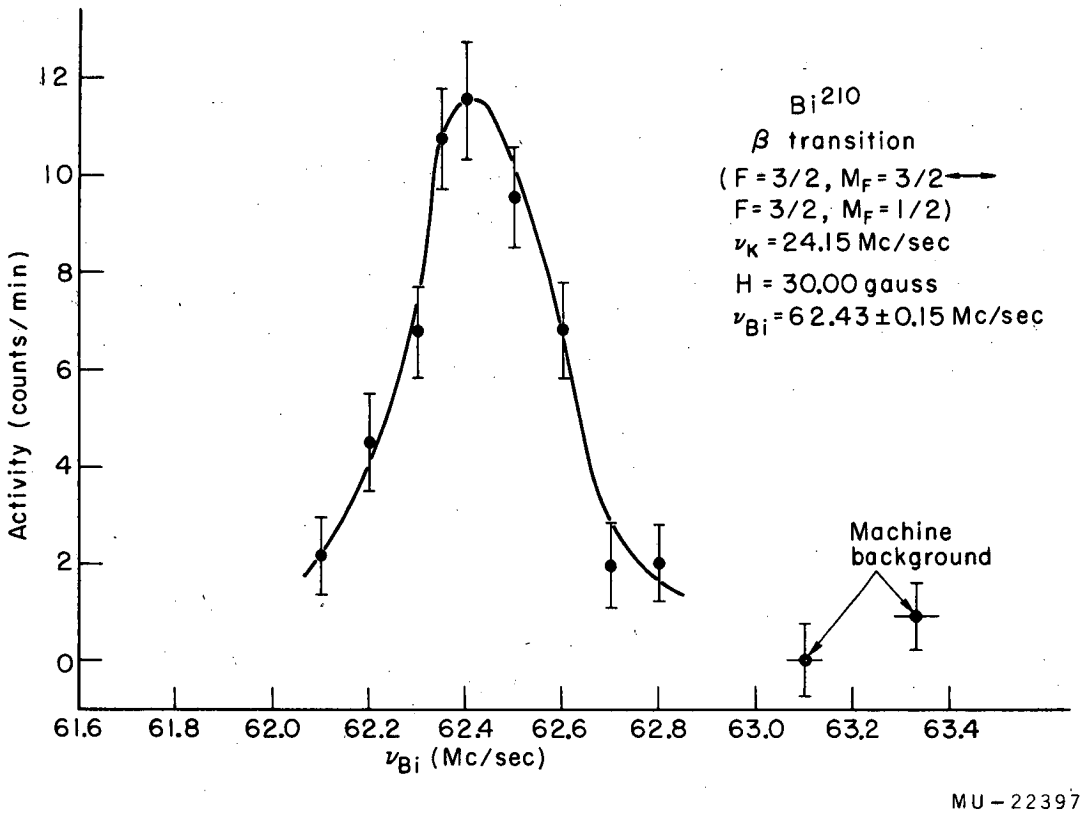


Fig. 12. A $Bi^{210}$ (RaE) resonance.

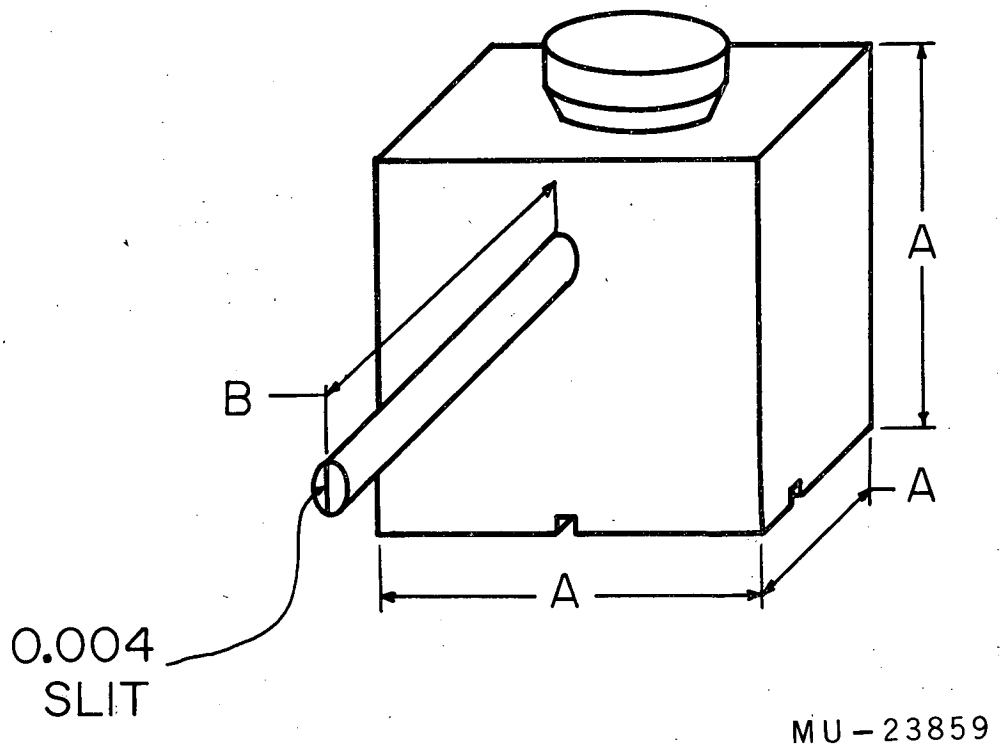


Fig. 13. Diagram of snouted oven; A is 5/8 in. and B is 1-1/16 in.

oven block are tantalum metal, and the exit slit at the end of the snout is 0.004 in. wide and 0.040 in. high. With this arrangement, a 70% dissociated beam of bismuth atoms was obtained.

The beam of $Bi^{210}$ was collected upon buttons as shown in Fig. 7. These buttons were coated with sulfur. The buttons were counted in small-volume continuous-flow methane $\beta$ counters, as discussed in a previous section. Before counting, the active surface was covered with a single layer of Scotch tape to prevent the counting of the $\alpha$ activity which is present in the beam and which arises from the decay of the $Bi^{210}$ daughter, $Po^{210}$, in going to $Pb^{206}$.

## D. Results

Table III contains a list of all single-quantum transitions observed during the course of this experiment. The last column in Table III contains the compounded uncertainty, $\Delta\nu_i$, in the position of the ith resonance center obtained from the relation

$$\Delta\nu_i = \left[ (\Delta f_i)^2 + \left( \frac{\partial f_i}{\partial H_i} \right)^2 (\Delta H_i)^2 \right]^{1/2} . \qquad (66)$$

Here $\Delta f_i$ is the estimated uncertainty in the position of the center of the ith resonance, $\frac{\partial f_i}{\partial H_i}$ is the rate at which the frequency of the ith resonance varies with magnetic field, and $\Delta H_i$ is the estimated uncertainty in the magnetic field; $\Delta H_i$ is estimated from the width of the calibrating isotope resonance. We have taken the uncertainty in both $Bi^{210}$ and the calibrating isotope resonances as one-fourth of their observed line widths.

In addition to the sixteen resonances given in Table III, three two-quantum resonances of the type ($F = 5/2$, $M_F = 1/2 \leftrightarrow F = 5/2$, $M_F = -3/2$) were observed. These are listed in Table IV. It is of interest to note that these transitions are observed at field values at which the differences in frequency between the contributing transitions are many line widths. For example, for the resonances observed at 30.00 gauss, the relevant frequency difference is about 160 line widths. No extraordinary amount of radio-frequency power was used to induce these transitions, which were observed accidentally at the same radio-frequency loop current (approx 70 ma) used to observe the single-quantum transitions.

Table III. Observed resonances in $Bi^{210}$

| Resonance type | Resonance frequency and uncertainty (Mc) | | Calibrating frequency[a] and uncertainty (Mc) | | Magnetic field and uncertainty (gauss) | | Compounded uncertainty (Mc) |
|---|---|---|---|---|---|---|---|
| α (5/2, 1/2 ⟷ 5/2, -1/2) | 54.299 | .075 | 24.150(K) | .030 | 30.000 | .032 | 0.110 |
| α | 103.699 | .050 | 44.209(K) | .039 | 49.998 | .036 | 0.104 |
| β(3/2, 3/2 ⟷ 3/2, 1/2) | 10.100 | .050 | 2.000(Cs) | .025 | 5.708 | .071 | 0.142 |
| β | 15.550 | .100 | 3.000(Cs) | .025 | 8.555 | .071 | 0.171 |
| β | 27.000 | .025 | 5.000(Cs) | .025 | 14.236 | .071 | 0.150 |
| β | 39.200 | .050 | 7.000(Cs) | .025 | 19.901 | .070 | 0.165 |
| β | 62.399 | .075 | 24.150(K) | .025 | 30.000 | .027 | 0.099 |
| β | 111.349 | .075 | 44.209(K) | .037 | 49.998 | .034 | 0.113 |
| β | 173.448 | .125 | 74.425(K) | .054 | 75.000 | .041 | 0.163 |
| β | 304.896 | .112 | 160.230(K) | .088 | 129.000 | .048 | 0.163 |
| $\nu_1$(5/2, 1/2 ⟷ 3/2, 1/2) | 194.798 | .037 | 0.704(K) | .025 | 1.000 | .035 | 0.038 |
| $\nu_1$ | 194.768 | .056 | 1.700(K) | .028 | 2.400 | .039 | 0.056 |
| $\nu_2$(3/2, -1/2 ⟷ 1/2, 1/2) | 223.022 | .094 | 0.704(K) | .029 | 1.000 | .041 | 0.149 |
| $\nu_2$ | 298.366 | .100 | 17.060(K) | .025 | 22.001 | .029 | 0.160 |
| $\nu_3$(3/2, 1/2 ⟷ 1/2, -1/2) | 217.247 | .094 | 0.704(K) | .031 | 1.000 | .043 | 0.151 |
| $\nu_3$ | 181.108 | .008 | 20.000(K) | .029 | 25.388 | .033 | 0.008 |

[a]Note that both cesium and potassium have been used as the calibrating element.

Table IV. Two-quantum transitions

| Magnetic field (gauss) | Observed frequency (Mc) | Calculated frequency[a] (Mc) |
|---|---|---|
| 14.24 | 20.050 ± .150 | 19.940 |
| 19.90 | 27.975 ± .075 | 27.960 |
| 30.00 | 42.400 ± .075 | 42.230 |

[a]Observed transitions are assumed to be identified by the quantum numbers ($F = 5/2,\ M_F = 1/2 \leftrightarrow F = 5/2,\ M_F = -3/2$).

The final values calculated for a and b on the basis of the results in Table III are

$$|a| = 21.78 \pm .03 \text{ Mc},$$
$$|b| = 112.38 \pm .03 \text{ Mc},$$

with $b/a = +5.160 \pm .007$. The uncertainties quoted are three times the mean-square uncertainties calculated on the basis of weights derived from Eq. (66), and are intended to allow for any unknown sources of systematic error. The values of $\chi^2$ (see Ref. 26) for the two possible choices of sign of $g_I$ are

$$\chi^2(g_I > 0) = 7.75,$$
$$\chi^2(g_I < 0) = 7.72.$$

The close agreement between these two values means that the experimental data cannot be used to determine the sign of the nuclear moment of $Bi^{210}$. There are two reasons for this failure: (a) the small size of the nuclear moment of $Bi^{210}$, and (b) inadequate resolution by the C magnet at high field values where the line width is appreciably increased by field inhomogeneities.

The data have also been reduced by taking $g_J$ as well as a and b as free parameters, with the result $g_J = -1.6431 \pm .0004$. This result agrees with that given in Ref. 43, and serves as an additional check on the consistency of the data.

Species identification is assured in several ways:

(a) Radioactive decay studies of the full beam intensity show a half life of $\tau_{1/2} = 4.8 \pm .5$ days, which is in agreement with the commonly accepted half life of $\tau_{1/2} = 5.0$ days. A decay plot appears in Fig. 14.

(b) Since bismuth appears in nature only as $Bi^{209}$, there is nothing else that can be made by an (n, γ) reaction. It is, of course, possible for (n, p) and (n, γ)(n, γ) reactions to occur, but they are held to be unlikely.

(c) The isotope under study is fitted by a Hamiltonian employing a $g_J$ which is known for bismuth.

## E. Magnetic Dipole Moment

The magnetic dipole moment of RaE can be calculated (neglecting a possible hyperfine anomaly) from Eq. (52), which is here rewritten in a slightly different form:

$$\left|\frac{\mu_1}{\mu_2}\right| = \left|\frac{a_1}{a_2}\right| \frac{I_1}{I_2} \quad . \tag{67}$$

By use of Eq. (67) together with a knowledge of μ, a, and I for the stable isotope $Bi^{209}$, it becomes an easy matter to calculate the nuclear moment of $Bi^{210}$. Using the value of the magnetic moment of $Bi^{209}$ as measured by Procter and Yu[44] [4.0400(5)nm] and corrected for diamagnetism by Walchli[45] [$\mu_{209} = 4.07970\ (81)$ nm], the spins $I_{209} = 9/2$, $I_{210} = 1$, $a_{209} = -446.97$ Mc,[43] and the experimentally determined value of $a_{210}$, we find

$|\mu_{210}| = 0.0438 \pm .0001$ nm (diamagnetically uncorrected),

$|\mu_{210}| = 0.0442 \pm .0001$ nm (diamagnetically corrected).

The sign of $\mu_{210}$ is not known, because the sign of $a_{210}$ has not been determined in this experiment.

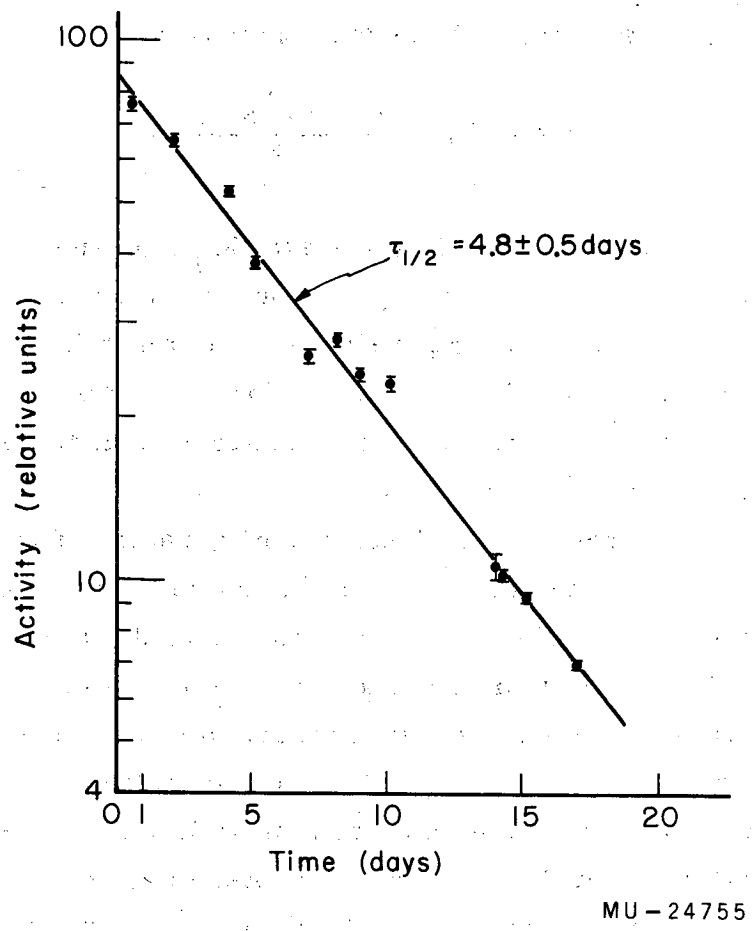


Fig. 14. Decay plot of full-beam sampling of $Bi^{210}$ (RaE).

## F. Electric Quadrupole Moment

The electric quadrupole interaction constant, b, is related to the quadrupole moment, Q, by the expression

$$hb = -e^2 Q \left\langle \frac{3\cos^2\theta - 1}{r^3} \right\rangle_{JJ} , \tag{50}$$

where the average is taken in the state $M_J = J$ and summed over all electrons. To evaluate this expression, we must know the electronic wave function. Since the $g_J$ value of bismuth is known to be $-1.6433 \pm .0002$,[43] and the $g_J$ values for pure LS or JJ coupling are -2 and -4/3, respectively, it is apparent that the electrons are in a state of intermediate coupling.

The electronic ground-state configuration of bismuth is $6s^2 6p^3$; in the LS scheme the three p electrons can couple to levels $^2D_{5/2}$, $^2P_{3/2}$, and $^4S_{3/2}$. The J value in the ground state is 3/2, and since J is a good quantum number, the intermediately coupled ground state can be expressed as a linear superposition of the three levels $^2D_{3/2}$, $^2P_{3/2}$, and $^4S_{3/2}$. The degree of level admixture can be determined by diagonalizing the 3-by-3 energy matrix in the LS energy scheme, treating the ratio of the electrostatic interaction energy to the spin-orbit coupling energy as a variable parameter, X, to be obtained by a fit to the experimental level scheme; for bismuth, Condon and Shortley find X = 0.295.[2] Once the energy matrix has been determined, it is easy to find the transformation matrix that determine the level admixture.

On the other hand, Inglis and Johnson have taken the transformation matrix and used it to obtain an expression for $g_J$ in intermediate coupling.[46] With $g_J = -1.6433$ and the method of Inglis and Johnson, Lindgren and Johansson have found X = 0.300,[41] which is in good agreement with the value obtained by Condon and Shortley. The intermediate coupled wave function in the JJ coupling scheme can be written as

$$\psi = C_1\psi_1 + C_2\psi_2 + C_3\psi_3, \tag{68}$$

where

$$\psi_1 = \left(\frac{3}{2}\ \frac{3}{2}\ \frac{3}{2}\right)_{3/2},\quad \psi_2 = \left(\frac{3}{2}\ \frac{3}{2}\ \frac{1}{2}\right)_{3/2},\ \text{and}\ \ \psi_3 = \left(\frac{3}{2}\ \frac{1}{2}\ \frac{1}{2}\right)_{3/2}.$$

Lindgren and Johansson[41] find

$$\left.\begin{aligned} C_1 &= -0.177 \\ C_2 &= \ \ 0.318 \\ C_3 &= \ \ 0.932 \end{aligned}\right\}. \tag{68'}$$

Schuler and Schmidt[47] have evaluated $\left\langle \frac{3\cos^2\theta - 1}{r^3} \right\rangle_{JJ}$ in intermediate coupling, and find

$$\left\langle \frac{3\cos^2\theta - 1}{r^3} \right\rangle_{JJ} = \frac{2}{5}\left[ (C_1^{\,2} - C_3^{\,2})\, R_r' + 2\sqrt{\frac{2}{5}}\ C_2(C_1 + C_3) S_r \right] \left\langle \frac{1}{r^3} \right\rangle, \tag{69}$$

where $R_r'$ and $S_r$ are relativistic correction factors tabulated by Kopfermann.[16]

Using calculations of Breit and Wills,[48] Lindgren and Johansson have shown[41]

$$ha = -g_I \mu_0^{\,2} \left[ \frac{16}{15}\ (1 + \frac{1}{5} C_2^{\,2})\, F' - \frac{16}{15}\ C_2^{\,2}\ F'' + \frac{4}{3}\sqrt{\frac{2}{5}}\ C_2(C_1 - C_3) G \right] \left\langle \frac{1}{r^3} \right\rangle, \tag{70}$$

where $F'$, $F''$, and $G$ are again relativistic correction factors tabulated by Kopfermann.[16] Combining Eqs. (50), (68'), (69), and (70), and using the values of $a$ and $g_I$ appropriate to $Bi^{209}$ to determine $\left\langle \frac{1}{r^3} \right\rangle$, Lindgren and Johansson[41] derived a general expression for the quadrupole moment of any isotope of bismuth,

$$\frac{Q}{b} = 1.14 \times 10^{-3}\ \text{barn}, \tag{71}$$

where b is in Mc. With this result we find

$$\left| Q(Bi^{210}) \right| = 0.13 \pm .01 \text{ barn}, \tag{72}$$

where we have assigned the uncertainty somewhat arbitrarily but taken it large enough to embrace any corrections due to polarization of the electron cloud[49] or possible uncertainties in the above calculational procedure. Title and Smith[43] have estimated the quadrupole moment of $Bi^{209}$ in a slightly different way. They obtain $\left\langle \frac{1}{r^3} \right\rangle$ from the fine-structure separations. Using their method, we find the same result as above (within the quoted uncertainty).

## G. Hyperfine Separations

The values of the hyperfine separations in RaE calculated from the above values of a and b and Eq. (65) are

$$\begin{aligned} \Delta\nu(5/2, 3/2) &= 194.93 \pm .09 \text{ Mc}, \\ \Delta\nu(3/2, 1/2) &= 220.19 \pm .08 \text{ Mc}. \end{aligned} \tag{73}$$

## H. Discussion of Bismuth-210

Bismuth-210 has 83 protons and 127 neutrons. The nuclear spins of $Bi^{203}$, $Bi^{205}$, and $Bi^{209}$ are all known to be 9/2,[41] a fact consistent with the odd proton's lying in the $h_{9/2}$ level. The state of the odd neutron is not known, but it could lie in one of the levels $g_{9/2}$, $i_{11/2}$, $g_{7/2}$ and couple with the proton to give a resultant spin of 1. In Table V we have listed the magnetic moments of $Bi^{210}$ calculated on the assumption that the proton and neutron parts of the core couple together in jj coupling.

Table V. Calculated magnetic moments of $Bi^{210}$ for different possible nuclear configurations

| Presumed configuration | | Calculated moment (nuclear magnetons) |
|---|---|---|
| $(\pi h_{9/2})$ | $(\nu g_{9/2})$ | 0.24 |
| $(\pi h_{9/2})$ | $(\nu i_{11/2})$ | -1.08 |
| $(\pi h_{9/2})$ | $(\nu g_{7/2})$ | 1.75 |

The magnetic moment for an odd-odd nucleus can be written[50]

$$\mu = \frac{1}{2}(g_p + g_n) I + (g_p - g_n) \frac{j_p(j_p+1) - j_n(j_n+1)}{I+1} \quad . \tag{74}$$

Here $g_p$ and $g_n$ are the g factors of the odd proton and neutron, $j_p$ and $j_n$ are their angular momenta, and I is the nuclear spin. For the proton part, we have used $g_p = 0.9066$, an effective value derived from the known magnetic moment of $Bi^{209}$; for the neutron part, we have taken the Schmidt value for $g_n$ in each case.

It appears that the most probable pure configuration if no mixing is assumed is $(\pi h_{9/2})(\nu g_{9/2})$. The experimental moment is so close to zero that we are not justified in presuming that it has the same sign as that calculated for the $(\pi h_{9/2})(\nu g_{9/2})$ configuration, i.e., that it is positive.

Newby and Konopinski, using pair-interaction considerations, deduce the nuclear ground-state wave function of RaE to be[51]

$$\psi(J=1) = 0.936 \left| h_{9/2}\, i_{11/2},\ J=1 \right\rangle + 0.134 \left| h_{9/2}\, g_{9/2},\ J=1 \right\rangle + 0.327 \left| f_{7/2}\, g_{9/2},\ J=1 \right\rangle \ , \tag{75}$$

which is consistent with an energy separation of 0.047 Mev between the J = 0 and J = 1 states, the latter state being the lower. Using this wave function, which has its major contribution from the term representing the $(\pi h_{9/2})(\nu i_{11/2})$ configuration, Newby and Konopinski have evaluated the nuclear moment as $\mu = 0.75$ nm. This value is not in good agreement with the experimentally determined value of $|\mu| = 0.0442$ nm, although it is possible that minor variation of the coefficients in Eq. (75) may improve the agreement.

Blin-Stoyle gives an expression for the quadrupole moment of an odd-odd nucleus based on the extreme single-particle model.[50] This expression appears below with the modification that we have replaced a Racah W coefficient with the appropriate 6-j symbol and taken into account the change in phase:

$$Q = \frac{(2I+1)!}{2j_p!}\left[\frac{(2j_p-2)!\ (2j_p+3)!}{(2I-2)!\ (2I+3)!}\right]^{1/2}(-1)^{-(2j_p+3I)} \times \begin{Bmatrix} j_p & I & j_n \\ I & j_p & 2 \end{Bmatrix} Q_{j_p}, \tag{76}$$

where $j_p$ and $j_n$ are the angular momenta of the odd proton and the odd neutron, respectively; $I$ is the total nuclear spin; and $Q_{j_p}$ is the quadrupole moment of a proton in the state $j_p$ according to the single-particle model. Blin-Stoyle gives an expression for $Q_{j_p}$ to be

$$Q_{j_p} = -\frac{2j_p - 1}{2(j_p + 1)}\left\langle r^2 \right\rangle, \tag{77}$$

where $\left\langle r^2 \right\rangle$ is the average squared distance of the proton in the nucleus. We will take

$$\left\langle r^2 \right\rangle = \frac{3R_0^2}{5} = \frac{3}{5} \times (1.4\times10^{-13})^2\ A^{2/3}. \tag{78}$$

Assuming the nuclear configuration $(\pi h_{9/2})(\nu g_{9/2})$ and combining Eqs. (76), (77), and (78), we get

$$Q(Bi^{210}) = +\ 0.08 \text{ barn}. \tag{79}$$

The value in Eq. (79) was arrived at by using compiled tables of the 6-j symbol by Rotenberg et al.[52] This is in reasonably good agreement in magnitude with the value calculated from the experimental data and given in Eq. (72).

## I. Signs of the Moments of $Bi^{210}$

As we have seen, an assumed nuclear configuration of $(\pi h_{9/2})(\nu g_{9/2})$ in conjunction with the single-particle model predicts for $Bi^{210}$ the following moments and signs:

$$\mu = +0.24 \text{ nm},$$
$$Q = +0.08 \text{ b}.$$

This shows reasonable agreement with the experimentally deduced magnitudes of these quantities, which are

$$|\mu| = 0.0442 \text{ nm},$$
$$|Q| = 0.13 \text{ b}.$$

The small magnitude of the magnetic dipole moment does not allow one to justifiably conclude any definite statements as to the sign of the dipole moment, since a negative value of $\mu$ agrees with the single-particle value almost as well as does a positive value.

Although the atomic-beam method does not absolutely fix the sign of the interaction constants, it does fix the relative sign of these constants. Also by means of Eq. (52) and the known data for $Bi^{209}$ we can make with relative certainty the following two statements:

1. The interaction constants a and b are both of the same sign,
2. The magnetic dipole moment and the magnetic dipole interaction constant are of opposite sign for all isotopes of bismuth.

Our reasoning in assigning the likely signs of the moments is as follows. Since the magnitudes of the electric quadrupole moments for both the experimentally deduced value and the value predicted by the single-particle model are in reasonable agreement, so too their signs are in agreement. This fact fixes b as positive. Since a must have the same sign as b, it too is positive. By Eq. (52), however, the magnetic dipole moment is of opposite sign to a and hence this moment is negative.

Such reasoning, of course, is not infallible, but is felt to have a certain degree of validity.

# V. POLONIUM-210

## A. Introduction

Previous parts of this thesis have discussed the hyperfine structure of $Bi^{210}$. Because of the decay reaction $Bi^{210} \xrightarrow[5.0\ day]{\beta^-} Po^{210}$, $Po^{210}$ exists in appreciable quantities in the bismuth target. $Po^{210}$ has 84 protons and 126 neutrons. As it is an even-even nucleus, one would expect the nuclear spin to be zero, as is the case for all even-even nuclei that have been observed; indeed, this is one of the experimental facts that historically first gave an impetus to the development of the nuclear shell model.

The purpose of this particular experiment is twofold:

(a) to verify the expected I = 0 for this even-even nucleus,

(b) to measure the $g_J$ factor to see if there is any pronounced deviation from the Russell-Saunders calculated value.

It is in keeping with these purposes that this experiment was undertaken.

## B. Theory

The case of a spin-zero nucleus is a simple one to describe, since the total interaction Hamiltonian (64) reduces to one term, i. e.,

$$\mathcal{H} = -g_J \mu_0 \vec{J} \cdot \vec{H} \ . \tag{80}$$

The eigenenergy solutions to Eq. (80) are

$$W_{M_J} = -g_J \mu_0 H_z M_J \ , \tag{81}$$

and the frequency separation between levels of adjacent $M_J$ values is

$$\nu = -g_J \frac{\mu_0}{h} H_z \ . \tag{82}$$

A diagram of the energy levels vs the magnetic field is extremely simple, being a group of equally spaced straight lines (Fig. 15). Since we have J = 2 for polonium, there are 2J + 1 or five such straight lines.

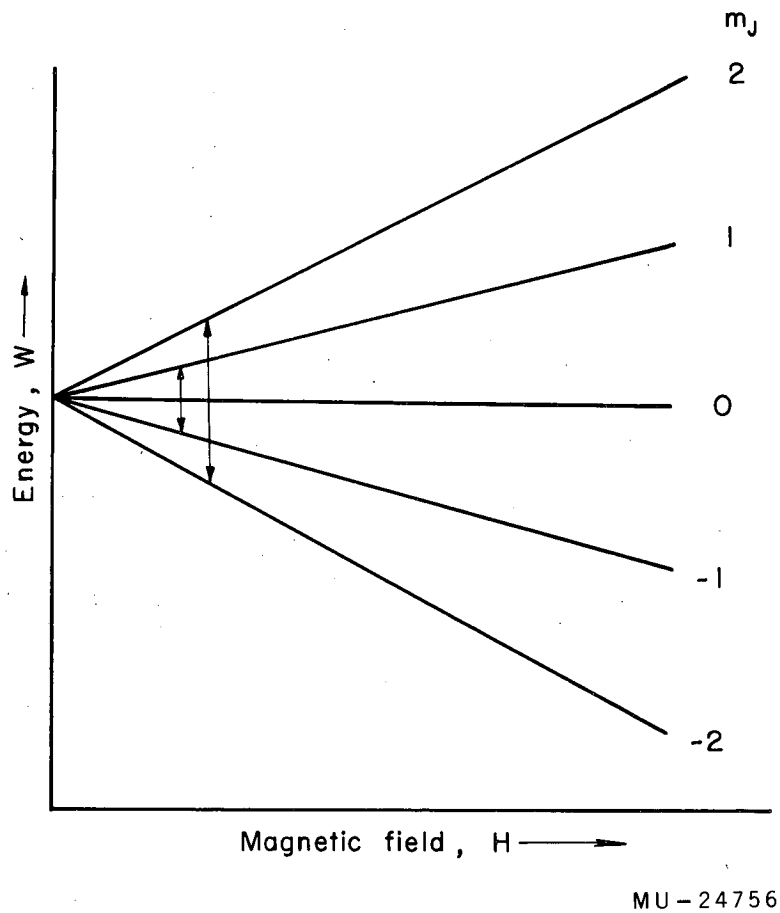


Fig. 15. Energy-level diagram for polonium-210 for $H < 500$ gauss. Energy levels are linear functions of the magnetic field, H. The double-headed arrows indicate observable transitions. Note the multiple quantum nature of such transitions.

The foregoing argument is strictly valid for those values of the applied magnetic field that are sufficiently small so that there is very little decoupling of the total angular momentum vector, $\vec{J}$, into its components, i.e., $\vec{L}$ and $\vec{S}$. For decoupling to occur, the magnitude of the decoupling term (80) should be comparable to the value of the fine-structure separation which for polonium is on the order of 10,000 $cm^{-1}$.[53] Corresponding to the value of the magnetic field of, say, 100 gauss, the gross value of the one-term Hamiltonian (80) is about $\mathcal{H} \approx 1 \times 10^{-8}$ $cm^{-1}$. Since there is a large factor here of about $10^{12}$ between the fine-structure effects and the applied magnetic field term, our previous argument is valid, and resonant frequencies will strictly be given by the linear Eq. (82).

The Russell-Saunders value for the $g_J$ factor is derived from the familiar spectroscopic relation

$$g_J = 1 + \frac{J(J+1) + S(S+1) - L(L+1)}{2J(J+1)} (g_s - 1), \tag{83}$$

where $g_s$ is the anomalous g factor for the electron, which is taken as $g_s = 2.00228$. Polonium has an electronic ground state $^3P_2$ which gives in conjunction with Eq. (83) the value of $g_J = 1.5011$. Here, in keeping with a somewhat confusing convention, $g_s$ and $g_J$ are given as positive numbers, whereas they are used in Eqs. (81), (82), and (83) as negative numbers.

## C. Method

The technique of this research was similar to that dealing with bismuth-210. The same apparatus, machine A, and the same oven design and oven-loader arrangement were used.

The method of production was simply waiting for the decay of $Bi^{210}$ in a given target sample. This period of waiting was taken as two or three half lives of bismuth-210, i.e., 10 to 15 days. The overall production scheme was

$$Bi^{209} \xrightarrow[\text{pile}]{+n} Bi^{210} \xrightarrow[\text{decay}]{-\beta} Po^{210}. \tag{84}$$

As can be readily seen, this is an extremely simple type of production.

After the Reaction (84) had gone to near completion the experiment was performed. Polonium-210 was detected by its decay via α-particles in going to lead-206. The β-type counters previously discussed also function efficiently as α counters. One of the resonance-frequency exposures was decayed for a period of about 70 days during which time efforts were made to keep the counters plateaued at the same high voltage level. A decay plot is shown in Fig. 16, where it is seen that the observed value for the half life is $\tau_{1/2} = 122 \pm 35$ days. The commonly accepted value of the half life of polonium-210 is 138.4 days.[54] Since the only possible nuclear species that could be present are $Bi^{209}$ (stable), $Bi^{210}$ (5.0-day), $Po^{210}$ (138.4-day), and $Pb^{206}$ (stable), and since the observed half life agrees with the commonly accepted value for the decay of $Po^{210}$, it was felt that positive species identification had been made.

## D. Results

Three distinct resonances were observed. One such resonance is shown in Fig. 17. These three resonances are listed in Table VI.

Table VI. Observed resonant frequencies in $Po^{210}$

| Magnetic field | $Po^{210}$ resonant frequency (Mc) | Compounded uncertainty, $\Delta\nu$ (Mc) | $g_J$ |
|---|---|---|---|
| 5.000 | 9.810 | 0.129 | 1.402 ± .018 |
| 15.123 | 29.525 | 0.127 | 1.395 ± .006 |
| 39.997 | 79.100 | 0.185 | 1.413 ± .003 |

The compounded uncertainty in the third column of Table VI was derived from Eq. (66). The last column in Table VI gives the value of $g_J$ calculated from the data. The average value of the observed $g_J$ and its standard deviation is seen to be

$$g_J = 1.403 \pm .006. \tag{85}$$

This is considerably different from the value calculated on the assumption of pure LS coupling, which is $g_J = 1.5011$.

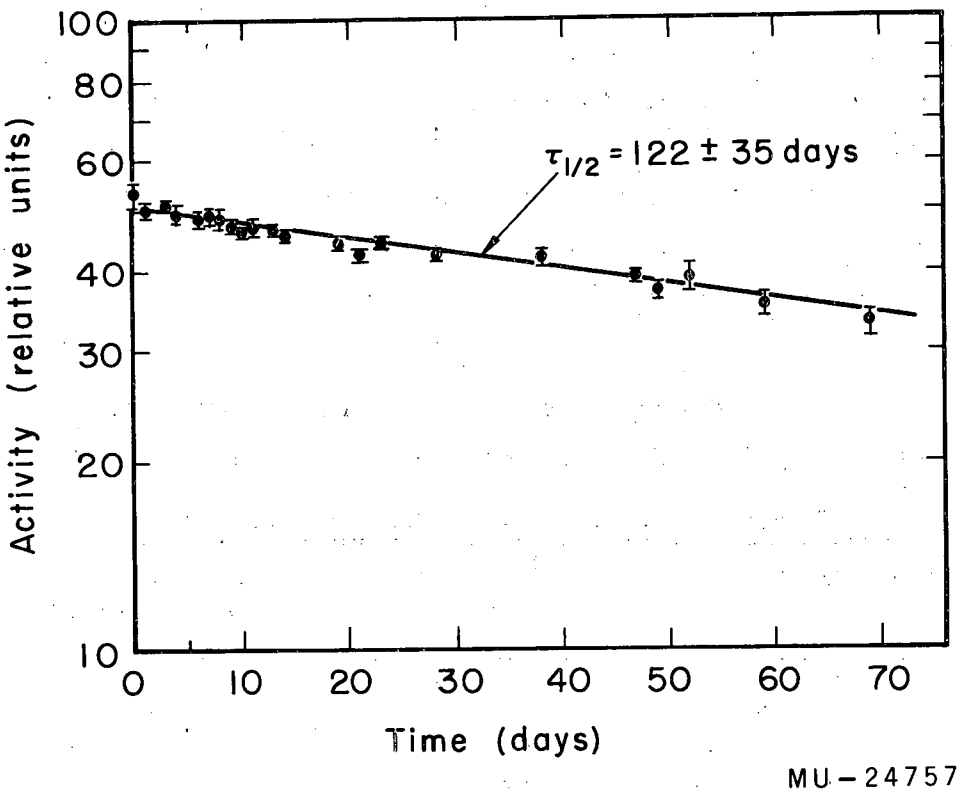


Fig. 16. Decay study of polonium-210 resonance button.
H = 15.00 gauss, $\nu$(Po) = 29.55 Mc.

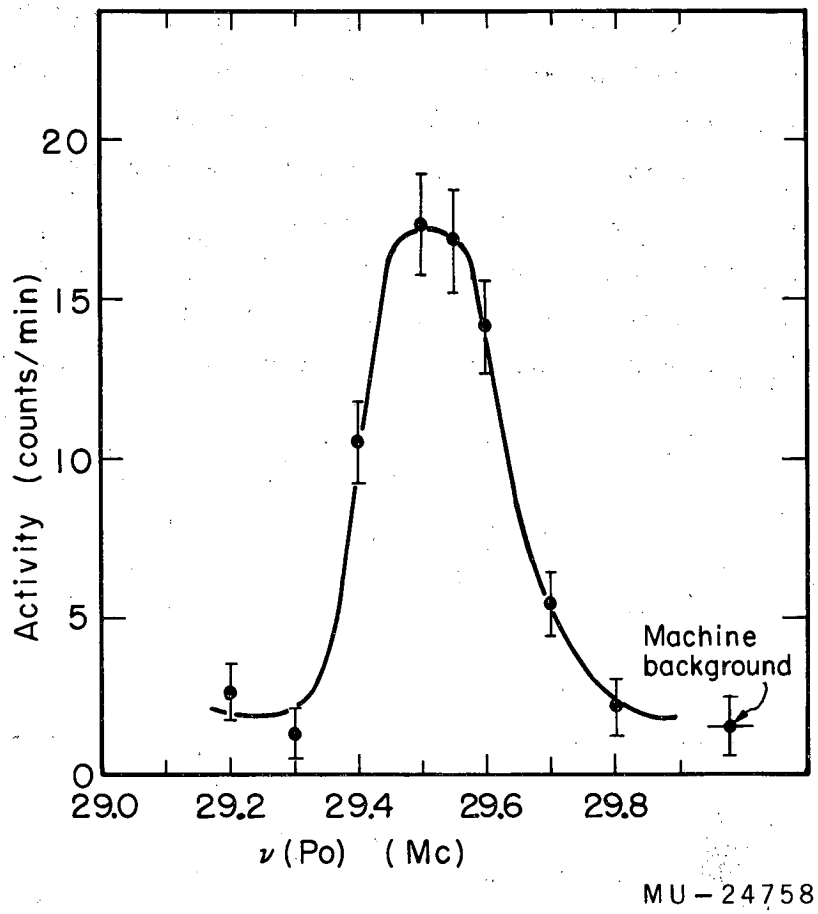


Fig. 17. A polonium-210 resonance. H = 15.00 gauss, $\nu$(Po) = 29.525 ± 0.128 Mc.

A plot of observed transition frequency vs magnetic field appears in Fig. 18. The linear dependency of the frequency on the magnetic field implies the validity of Eq. (82), which in turn is taken to mean I = 0 for polonium-210.

## E. Discussion

We have demonstrated that the spin of $Po^{210}$ is zero, as was to be expected for an even-even nucleus. We have also shown that there is a marked departure from pure LS coupling.

Condon and Shortley[2] have pointed out that the $6s^2 6p^4$ configuration can give rise to the levels $^3P_{2,1,0}$, $^1D_2$, and $^1S_0$. If we consider the departure from pure LS coupling to be caused by the mixing of states due to spin-orbit interaction of the form, $\sum_i \zeta_{n_i \ell_i} \vec{\ell}_i \cdot \vec{s}_i$, we may set up the energy matrix as

| | $^1D_2$ | $^3P_2$ | $^3P_1$ | $^3P_0$ | $^1S_0$ |
|---|---|---|---|---|---|
| $^1D_2$ | $6F_0 + F_2$ | $-\frac{\sqrt{2}}{2}\zeta$ | | | |
| $^3P_2$ | $-\frac{\sqrt{2}}{2}\zeta$ | $6F_0 - 5F_2 - \frac{1}{2}\zeta$ | | | |
| $^3P_1$ | | | $6F_0 - 5F_2 + \frac{1}{2}\zeta$ | | |
| $^3P_0$ | | | | $6F_0 - 5F_2 + \zeta$ | $\sqrt{2}\zeta$ |
| $^1S_0$ | | | | $\sqrt{2}\zeta$ | $6F_0 + 10F_2$ |

(86)

where Condon and Shortley's[2] notation is strictly adhered to. In the preceding matrix, $F_0$ and $F_2$ are matrix elements of the electrostatic interaction. For our purposes we will regard $F_0$ and $F_2$ as constant parameters. Since the term $6F_0$ appears in every diagonal term of

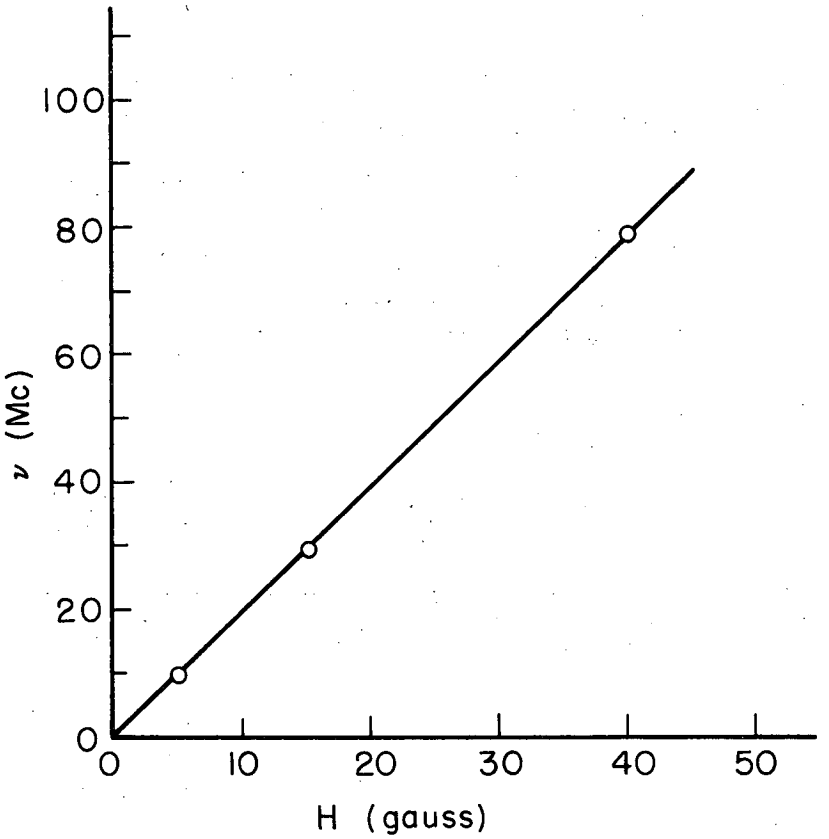


Fig. 18. Graph of observed transition frequency vs magnetic field for polonium-210. Note the linear dependency of frequency on field.

the Matrix (86), it can be neglected in the diagonalization of this matrix, since its only effect is to shift each energy level upwards by a fixed amount and does not at all affect the separations between the levels which are the physically observable quantities. In Matrix (86) $\zeta$ is taken to mean $\zeta_{6p}$, and is known as the spin-orbit splitting constant. We will also consider this to be a constant parameter.

The diagonalization of Matrix (86) gives

$$
\begin{aligned}
W(^1D_2) &= -2F_2 - \tfrac{1}{4}\zeta + \sqrt{9F_2^2 + \tfrac{3}{2}F_2\zeta + \tfrac{9}{16}\zeta^2} \\
W(^3P_2) &= -2F_2 - \tfrac{1}{4}\zeta - \sqrt{9F_2^2 + \tfrac{3}{2}F_2\zeta + \tfrac{9}{16}\zeta^2} \\
W(^3P_1) &= -5F_2 + \tfrac{1}{2}\zeta \\
W(^1S_0) &= 5/2\ F_2 + \tfrac{1}{2}\zeta + \sqrt{\tfrac{225}{4}F_2^2 - \tfrac{15}{2}F_2\zeta + \tfrac{9}{4}\zeta^2} \\
W(^3P_0) &= 5/2\ F_2 + \tfrac{1}{2}\zeta - \sqrt{\tfrac{225}{4}F_2^2 - \tfrac{15}{2}F_2\zeta + \tfrac{9}{4}\zeta^2}
\end{aligned}
\qquad (87)
$$

The observed energy separations between the energy levels given by Eqs. (87) are tabulated by Moore.[53] There are four energy separations between the levels given in Eqs. (87), whereas there are only two parameters to be fitted--namely $F_2$ and $\zeta$. This means that the results of any fit of $F_2$ and $\zeta$ should fit all the experimental spectroscopic data if these parameters are to be meaningful. The values arrived at for the parameters are

$$F_2 = 1105\ \text{cm}^{-1} \quad \text{and} \quad \zeta = 12{,}407\ \text{cm}^{-1}. \qquad (88)$$

When these values are substituted into Eqs. (87) and the separations relative to the $^3P_2$ level calculated, we get the results shown in Table VII.

Table VII. Comparison between calculated values of the energy separations relative to the $^3P_2$ level in polonium and the experimentally observed values. Values are calculated from the parameters $F_2 = 1105\ cm^{-1}$ and $\zeta = 12{,}407\ cm^{-1}$

| Level | Calculated separation from $^3P_2$ level ($cm^{-1}$) | Observed separation from $^3P_2$ level[56] ($cm^{-1}$) | Difference, obs-calc ($cm^{-1}$) |
|---|---|---|---|
| $^1S_0$ | 42,816 | 42,718 | -98 |
| $^1D_2$ | 21,738 | 21,679 | -59 |
| $^3P_1$ | 16,859 | 16,831 | -28 |
| $^3P_0$ | 7,477 | 7,514 | +37 |
| $^3P_2$ | 0 | 0 | 0 |

It is seen that the fit is good. The last column in Table VII shows the difference between the observed values of the energy separations and those calculated on the basis of the values (88). It seems likely that values of $F_2$ and $\zeta$ could be found such that the errors in the last column of Table VII would be minimized. Such a procedure will not be entered into, as we feel that sufficient accuracy in $F_2$ and $\zeta$ already exists.

We now wish to determine what the ground-level state is for polonium. Clearly it is not pure $^3P_2$ but must have an admixture of $^1D_2$. There is no other level that can be mixed in with the level $^3P_2$. Consider the $H_{J=2}$ matrix, which is

$$H_{J=2} \equiv \begin{array}{c|cc} & {}^1D_2 & {}^3P_2 \\ \hline {}^1D_2 & F_2 & -\frac{\sqrt{2}}{2}\zeta \\ {}^3P_2 & -\frac{\sqrt{2}}{2}\zeta & -5F_2 - 1/2\,\zeta \end{array} \qquad (89)$$

We must find the unitary transformation matrix, $\mathcal{B}$ such that we have

$$\mathcal{B} H_{J=2} \mathcal{B}^{-1} = W \text{ (diagonal)}, \tag{90}$$

or, completely written out,

$$\begin{pmatrix} b_{11} & b_{12} \\ b_{21} & b_{22} \end{pmatrix} \begin{pmatrix} F_2 & -\frac{\sqrt{2}}{2}\zeta \\ -\frac{\sqrt{2}}{2}\zeta & -5F_2 - \frac{1}{2}\zeta \end{pmatrix} = \begin{pmatrix} W(^1D_2) & 0 \\ 0 & W(^3P_2) \end{pmatrix} \begin{pmatrix} b_{11} & b_{12} \\ b_{21} & b_{22} \end{pmatrix}$$

Multiplying up; using the parameter values (88), using Eqs. (87) for $W(^1D_2)$ and $W(^3P_2)$, and equating gives, for the unitary matrix elements $b_{12}$ and $b_{22}$, the values

$$b_{21} = 0.453 \quad \text{and} \quad b_{22} = 0.892 . \tag{91}$$

Thus we see that the ground-state wave function for polonium is

$$\psi(J=2) = 0.453 \left| {}^1D_2 \right\rangle + 0.892 \left| {}^3P_2 \right\rangle . \tag{92}$$

Let us now consider the $g_J$ operator, which can be written as

$$(g_J)_{op} = \frac{g_S(\vec{J}^2 + \vec{S}^2 - \vec{L}^2) + g_L(\vec{J}^2 + \vec{L}^2 - \vec{S}^2)}{2\,\vec{J}^2} , \tag{93}$$

where $g_L = 1.00000$ and $g_S = 2.00228$. Clearly $(g_J)_{op}$ is diagonal in a system where L, S, J, and $M_J$ are good quantum numbers. Taking the expectation value of $(g_J)_{op}$ in an $LSJM_J$-representation using the wave function (92) therefore immediately gives

$$g_J = b_{21}^2\, g_J(^1D_2) + b_{22}^2\, g_J(^3P_2)$$

or

$$g_J = 0.2052\, g_J(^1D_2) + 0.7957\, g_J(^3P_2). \tag{94}$$

Using $g_J(^1D_2) = 1.000$ and $g_J(^3P_2) = 1.501$ gives a theoretical value for the intermediately coupled $g_J$ of

$$g_J = 1.400. \tag{95}$$

Our experimental value was $g_J = 1.403 \pm .006$, which agrees with value (95) to within the experimental error. This agreement is gratifying to the author.

The accuracy of the experimental determination of $g_J$ could be pushed much farther, but is has since come to the attention of the author that Olsmats et al. have accurately measured this constant in an atomic beam experiment on $Po^{205}$ and $Po^{207}$.[55] Their value is reported as $g_J = 1.3961(1)$, which is in agreement with our value.

# VI. IODINE-133

## A. Introduction

This paper reports the nuclear moments of iodine-133 as determined by the method of atomic beams. These results are of interest for several reasons. Firstly, this isotope occurs in a region of the periodic table where collective effects are not expected to predominate; thus the results can be interpreted in terms of the single-particle shell model. Secondly, much work has been done on many other isotopes of iodine.[19, 56, 57, 58] This research extends the totality of information concerning the moments of iodine isotopes and further adds to our understanding of the variation of nuclear quantities such as spin, moments, and hyperfine structure as a function of nuclear neutron number; i.e., it allows us a firmer experimental foundation for an understanding of the single-particle shell model.

## B. Method

The apparatus used in this experiment was machine A as described in previous parts of this thesis. The transitions observed were those labeled as $\alpha$ and $\beta$ in the schematic energy-level diagram (Fig. 19). These two transitions are the only two of the type $\Delta F = 0$, $\Delta M_F = \pm 1$ that are refocused by the "flop-in" type of atomic beam machine; that is, they are the only two $\Delta F = 0$ transitions that go from a level of one $M_J$ (in the strong field approximation) to a level of equal and opposite $M_J$ as required for refocusing by the atomic-beam flop-in apparatus. The $\alpha$ and $\beta$ resonances are transitions of the types

$$\alpha: \quad (F = 5,\ M_F = -3 \leftrightarrow F = 5,\ M_F = -4);$$

$$\beta: \quad (F = 4,\ M_F = -2 \leftrightarrow F = 4,\ M_F = -3).$$

These transitions were observed in magnetic fields ranging from 26 gauss to 300 gauss.

The magnetic field was determined by observing the resonant frequency of $K^{39}$ $(F = 2,\ M_F = -1 \leftrightarrow F = 2,\ M_F = -2)$ which was observed alternately with the resonant frequency of $I^{133}$.

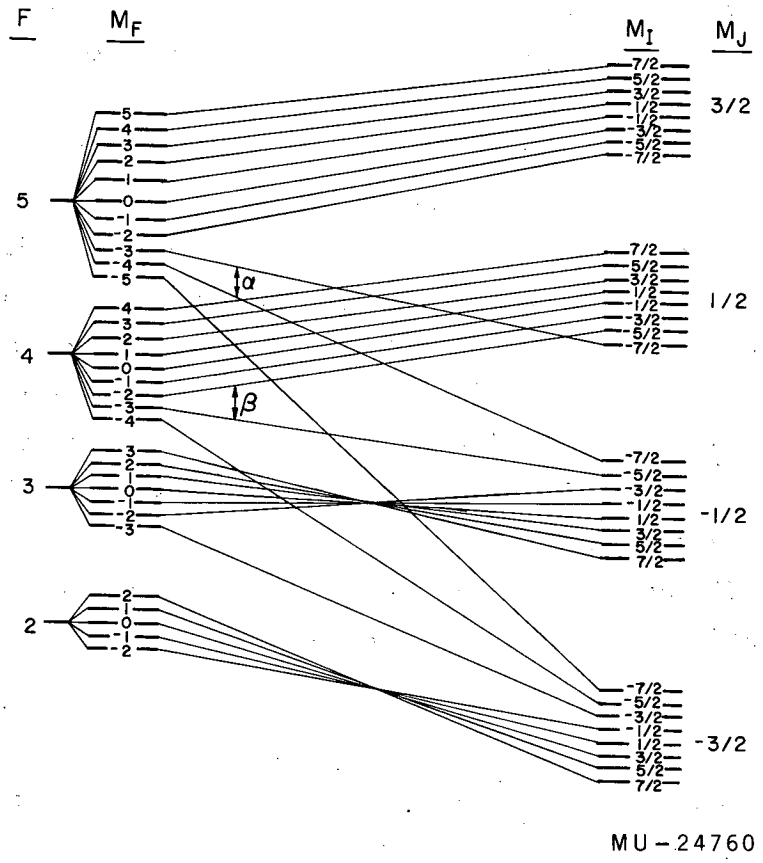


Fig. 19. Schematic energy-level diagram for $I^{133}$; J = 3/2 and I = 7/2.

The active sample was obtained in 100-Mc amounts as a fission product from the Brookhaven National Laboratory. Air freight was essential for transportation because of the 21-hour half life of the iodine-133. As received, the iodine was in aqueous solution as NaI. The solution was made slightly acidic with $H_2SO_4$ and then $NaNO_2$ was added to oxidize the ionic $I^{133}$ to its elemental form. Extraction was effected after the addition of suitable amounts of a nonactive carrier by $CS_2$, which was then evaporated off, leaving behind crystals of iodine. The crystals, which were formed in a special vial, were then attached directly to the atomic-beam machine. It was found that room temperatures were adequate to allow the iodine to diffuse through the source slit into the atomic beam machine at a reasonable rate. The specific activity was controlled by the amount of the carrier, i.e., nonactive iodine, that was added to the active sample. Dissociation was achieved by both discharge and thermal heating. The thermal heater was a simple snout arrangement (Fig. 20). The radio-frequency discharge system is shown in Fig. 21.

Exposures were made on silver-coated buttons. Counting was then performed in small-volume continuous-flow $\beta$ counters as previously described.

## C. Results

The spin of $I^{133}$ had previously been measured and found to be 7/2 by Garvin et al.[59] Furthermore, the electronic splitting factor, $g_J$, is accurately known by paramagnetic resonance experiments carried out on $I^{127}$ by Bowers et al.[60] This value is $g_J = 1.333977 \pm .000003$. With these parameters, the low-field search was undertaken.

A total of fourteen resonance frequencies was observed. Representative $\alpha$ and $\beta$ transitions are shown in Figs. 22 and 23. The tabulated results are shown in Table VIII.

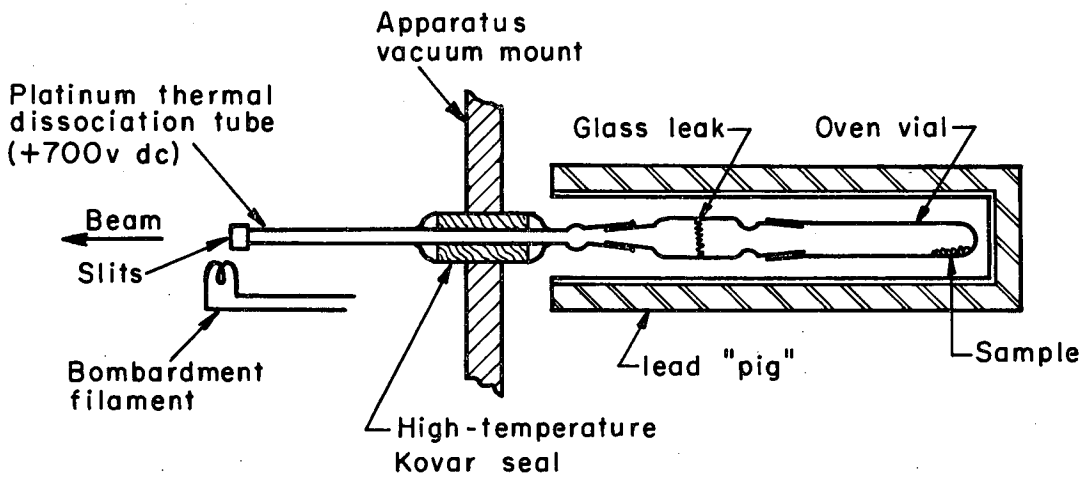


Fig. 20. Iodine beam source employing a thermal-dissociation snout.

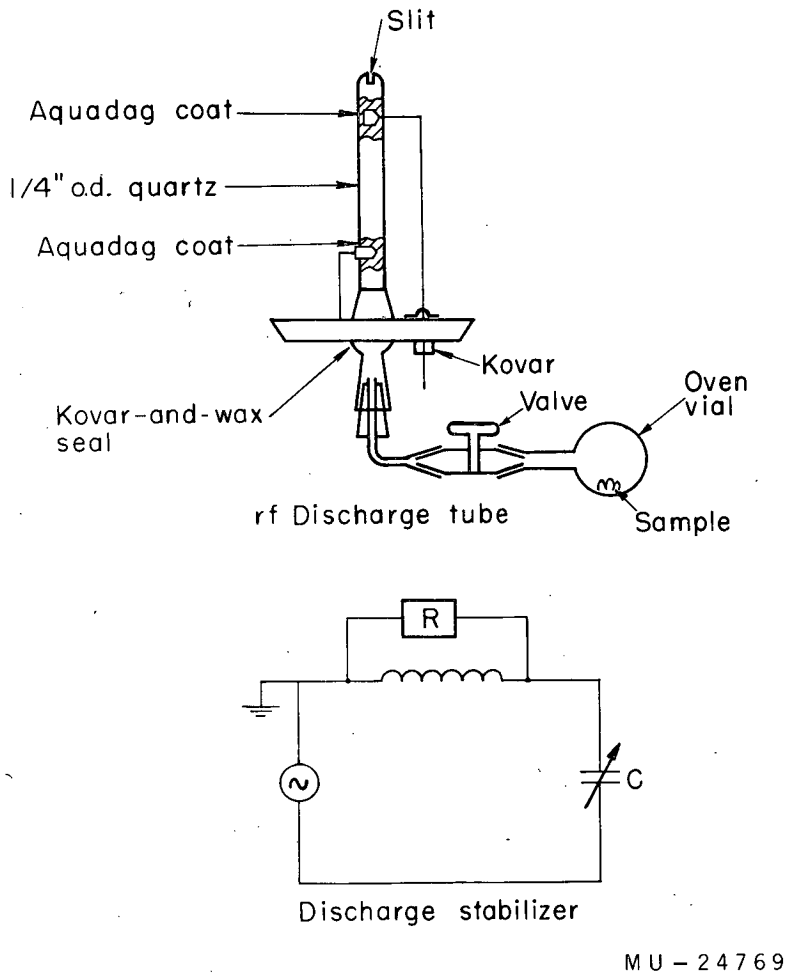


Fig. 21. Radio-frequency discharge tube and associated stabilizing circuit.

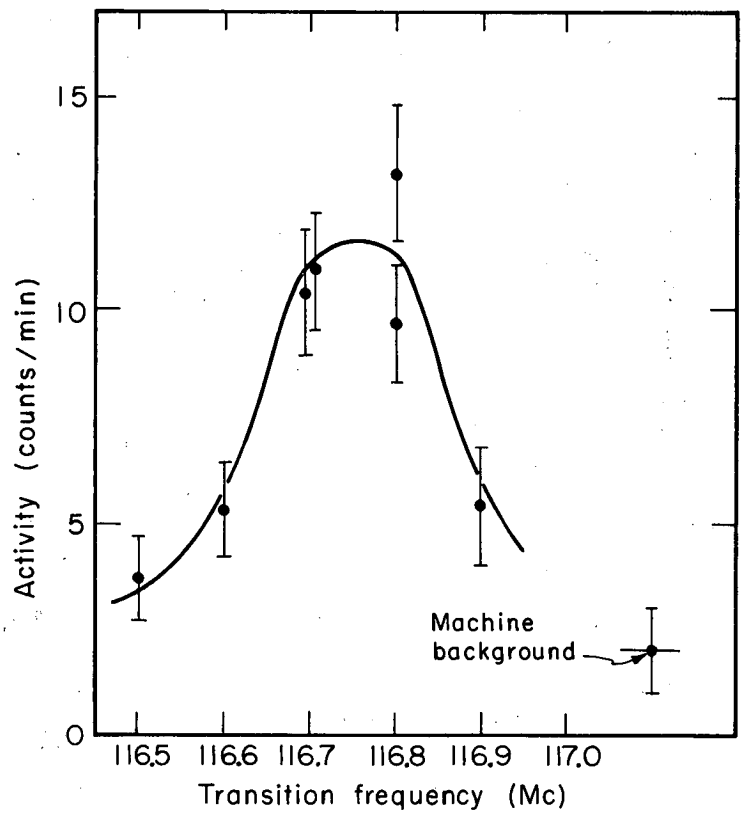


Fig. 22. An α resonance in iodine-133 ($F = 5$, $M_F = -3 \leftrightarrow F = 5$, $M_F = -4$). H = 196.28 gauss, $\nu(I^{133})$ = 116.75 Mc.

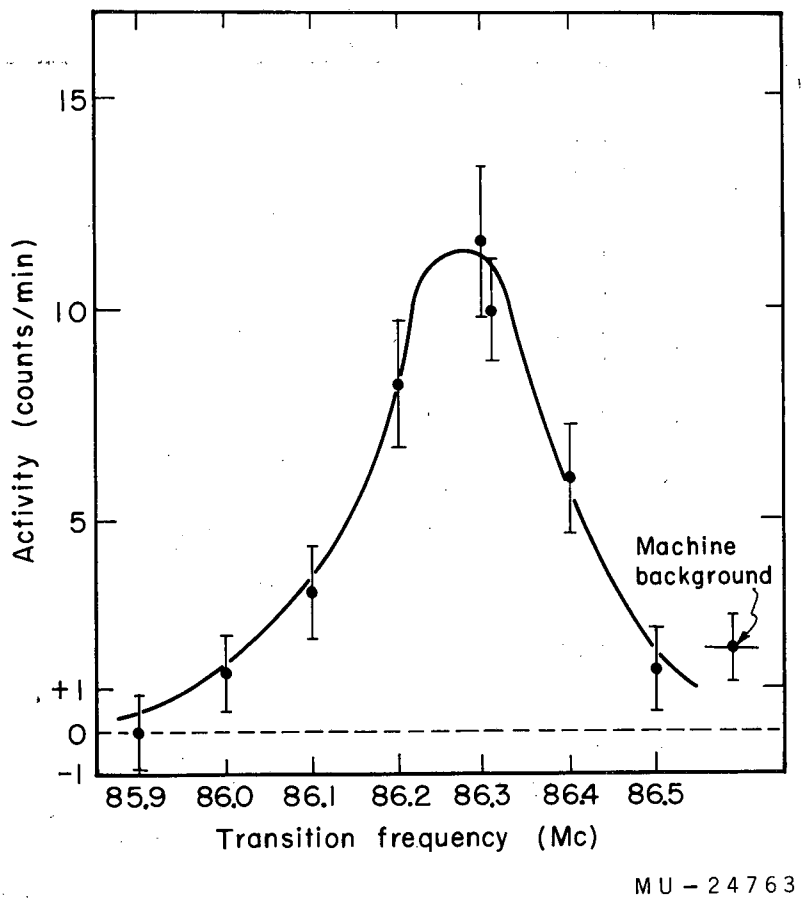


Fig. 23. A β resonance in iodine-133 ($F = 4$, $M_F = -2 \leftrightarrow F = 4$, $M_F = -3$). $H = 196.28$ gauss, $\nu(I^{133}) = 86.28$ Mc.

Table VIII. The observed resonance frequencies in $I^{133}$

| Number | Resonance type | Potassium frequency and uncertainty (Mc) | | Magnetic field and uncertainty (gauss) | | Observed $I^{133}$ frequency and uncertainty (Mc) | | Compounded uncertainty (Mc) |
|---|---|---|---|---|---|---|---|---|
| 1 | α | 21.000 | .022 | 26.517 | .025 | 14.960 | .040 | .042 |
| 2 | α | 40.000 | .024 | 46.077 | .023 | 26.100 | .040 | .044 |
| 3 | α | 80.000 | .028 | 79.132 | .020 | 45.400 | .040 | .042 |
| 4 | α | 160.000 | .028 | 128.875 | .015 | 75.000 | .040 | .041 |
| 5 | α | 300.000 | .052 | 196.278 | .023 | 116.750 | .040 | .043 |
| 6 | α | 554.430 | .080 | 300.103 | .031 | 184.200 | .100 | .102 |
| 7 | β | 16.000 | .021 | 20.755 | .025 | 7.900 | .040 | .041 |
| 8 | β | 21.000 | .022 | 26.517 | .025 | 10.100 | .040 | .041 |
| 9 | β | 30.000 | .023 | 36.199 | .024 | 13.900 | .040 | .041 |
| 10 | β | 40.000 | .024 | 46.077 | .023 | 17.900 | .040 | .041 |
| 11 | β | 80.000 | .028 | 79.132 | .020 | 31.600 | .040 | .041 |
| 12 | β | 160.000 | .037 | 128.875 | .020 | 53.600 | .040 | .041 |
| 13 | β | 300.000 | .052 | 196.279 | .023 | 86.280 | .050 | .051 |
| 14 | β | 554.430 | .080 | 300.103 | .031 | 143.000 | .080 | .082 |

The last column in Table VIII contains the compounded uncertainty in the ith resonance center. The compounded uncertainty is defined by Relation (66). We have taken the uncertainty in the $I^{133}$ and calibrating-isotope resonances as 1/5 of their observed line widths.

Positive identification of nuclear species was achieved by radioactive decay studies. A sampling of the full beam intensity was taken at the beginning of a run; this was presumably from 15 to 30 hours after the production of the $I^{133}$ fission product at Brookhaven. Observations of the radioactive decay of the full beam sample, using a locally fabricated automatic timer-printer device (nicknamed the "Pipper"), showed that initially there were two species present in the beam. At the start of the run 55% of the beam consisted of 21-hr $I^{133}$ and 45% of 8.14-day $I^{131}$ (see Fig. 24). A low-field resonance was taken immediately after the full-beam sample exposure. The resonance button decayed exponentially with a half life of 25 ± 3 hr, with not more than 10% of the activity being initially due to the 8.14-day $I^{133}$ (see Fig. 25). This fivefold diminution of the initial amounts of the 8.14-day activity along with the short half life observed on the resonance button was taken as sufficient evidence for positive identification.

The fourteen observed resonances listed in Table VIII were used as input data along with the accurately known value of $g_J$ for the least-squares fit program as mentioned in a previous section of this thesis. First $g_I$ was assumed positive and a convergence was obtained. The assumption was then made that $g_I$ was negative and the process was repeated. The results are shown in Table IX.

Table IX. Results of IBM program for $I^{133}$

| Assumption on sign of $g_I$ | Magnetic dipole interaction constant (Mc) | Electric quadrupole interaction constant (Mc) | $\chi^2$ |
|---|---|---|---|
| $g_I > 0$ | 597.0 ± 1.0 | 385.2 ± 7.4 | 9.54 |
| $g_I < 0$ | 606.8 ± 1.0 | 413.9 ± 7.7 | 34.69 |

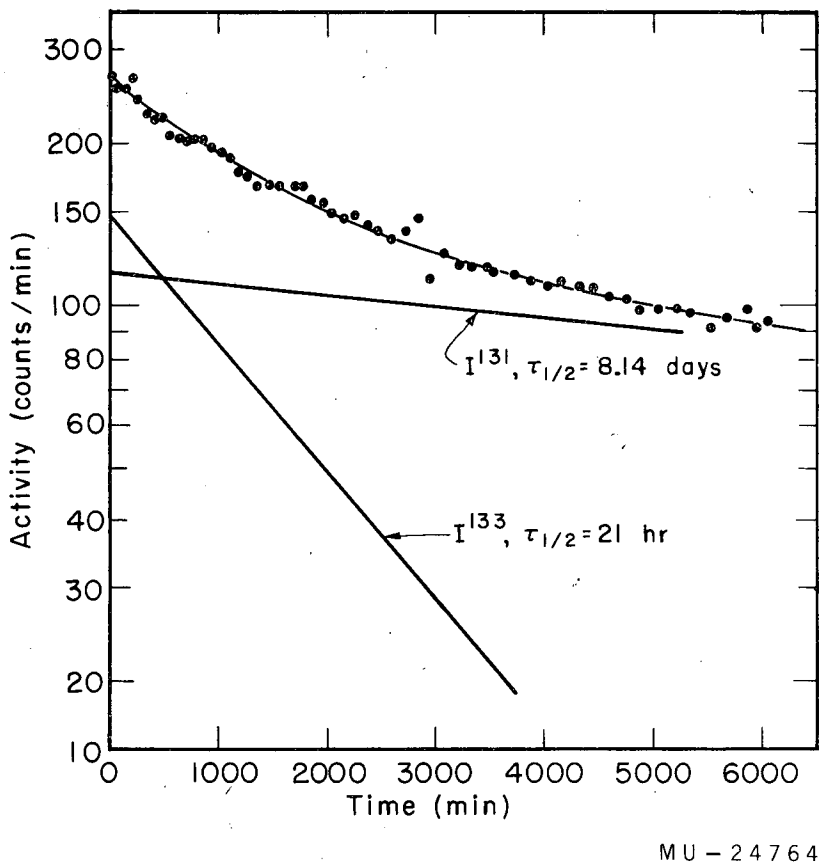


Fig. 24. Decay of representative full-beam sample taken during $I^{133}$ run. Experimentally determined decay curve at the top of the figure is the sum of the two exponentially decaying species, $I^{131}$ and $I^{133}$. Initially, $I^{133}$ is present in 55% amounts.

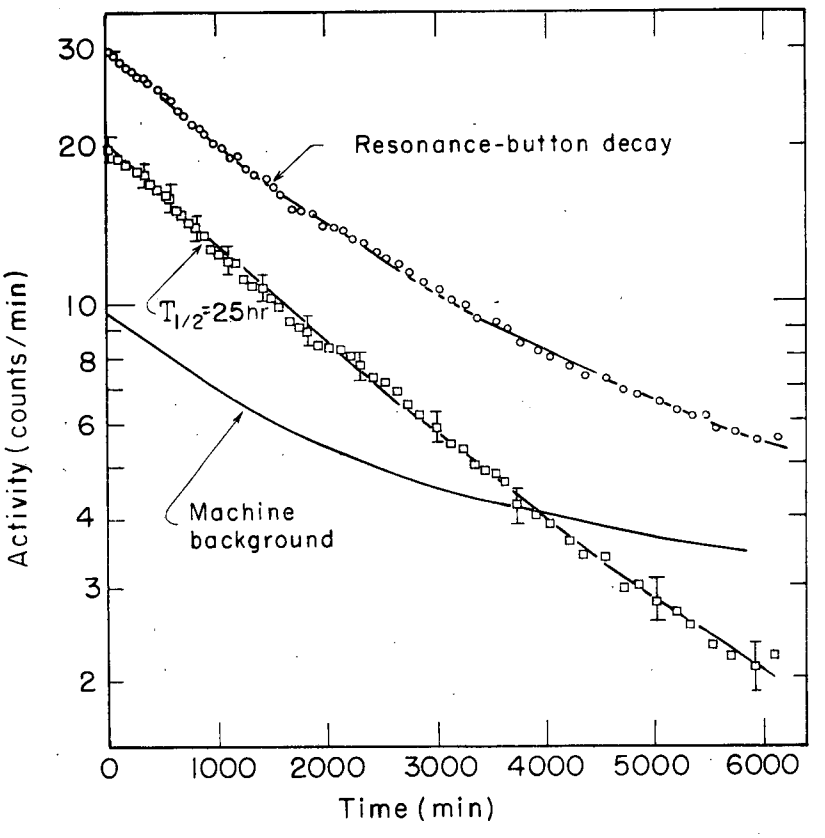


Fig. 25. Decay of a resonance exposure. The sample ($I^{133}$) used in this decay study was taken within minutes of that of Fig. 24. Since the machine background contributed 32 ± 5% of a resonance intensity, a curve with the decay characteristics of the full beam was subtracted from the observed resonance-button decay after initial normalization so that it originally was 32% of the observed curve. The resulting curve after subtraction of the background decay should be indicative of the nature of the deposited material.

The last column of Table IX shows the appropriate value of $\chi^2$, the "goodness of fit" parameter, which is defined as

$$\chi^2 = \sum_{i=1}^{14} (f_i^{obs} - f_i^{calc})^2 \omega_i, \tag{96}$$

where $f_i^{obs}$ is the observed frequency of the ith resonance, $f_i^{calc}$ is the associated resonance calculated by diagonalizing the Hamiltonian (64), and $\omega_i$ is a weighting factor which is taken as inversely proportional to the square of the compounded uncertainty as listed in Table VIII. Table IX shows that not only are the $\chi^2$'s significantly different under the assumption of $g_I > 0$ and $g_I < 0$ but also that the values of a and b lie outside the limits of error for these two assumptions.

The question arises as to which set of the results displayed in Table IX is the correct one. There is not an unambiguous answer to this question and no statement of certainty can be made. On the basis of statistical arguments, however, one can make certain probabilistic statements. From tabulated values of $\chi^2$ given by Fisher[26] it is seen that corresponding to a value of $\chi^2 = 9.54$ for the fourteen observed resonances of this experiment there is a probability, $P = 0.70$, that repetition of the entire experiment would give a larger value of $\chi^2$ by chance. For a value of $\chi^2 = 34.69$ there is less than a probability of $P = 0.01$ that repetition of the experiment would give a larger value of $\chi^2$ by chance. We interpret these values to mean that $g_I > 0$ is very much more probable. Under this interpretation we consider $g_I$ to be a positive quantity, keeping in mind the possibility that there is a small chance that we are mistaken in this interpretation. To take the compromising course and state the results of a and b to be halfway between the values determined for $g_I > 0$ and $g_I < 0$ and to increase the quoted errors in these quantities so as to include both sets of results would not be doing justice to the accuracy of the atomic-beam method and the author's faith in it.

## D. Magnetic Dipole Moment

The ground state of iodine is known to be $^2P_{3/2}$ with an electronic configuration of $5p^5$, i.e., a closed electronic shell less one. The magnetic dipole interaction constant a is related to the nuclear splitting factor $g_I$ by the relation

$$a = \frac{\mu_0^2}{h} g_I \mathcal{F} \frac{2L(L+1)}{J(J+1)} \left\langle 1/r^3 \right\rangle , \qquad (45)$$

where $\mathcal{F}$ is a relativistic correction factor close to unity and tabulated by Kopfermann.[16] The other symbols in Eq. (45) have their usual meanings. The nuclear splitting factor $g_I$ is related to the nuclear moment by the relation

$$g_I = \frac{m}{M} \frac{\mu}{I} , \qquad (96)$$

where m and M are the electron mass and the proton mass, respectively, and $\mu$ is expressed in nuclear magnetons.

The expectation value of the $1/r^3$ operator in Eq. (45) is not usually known accurately; hence, direct evaluation of $g_I$ from Eq. (45) is not generally feasible, at least for reasonable accuracy. Fortunately, the magnetic dipole interaction constant a has been determined for $I^{127}$ by the method of atomic beams by Jaccarino et al.;[61] the magnetic moment of $I^{127}$ has also been determined directly by Walchli et al.[62] in a nuclear induction experiment. Simple modification of Eq. (52) gives the relation

$$\left|\mu_{133}\right| = \left|\mu_{127} \frac{a_{133}}{a_{127}}\right| \frac{I_{133}}{I_{127}} . \qquad (97)$$

Equation (97) is written using absolute values because of the inherent difficulty in fixing the absolute signs of the interaction constants by the method of atomic beams. Perusal of Eq. (45) shows that a will have the same sign as $g_I$, which we have previously stated to be very likely positive. This would imply that $\mu_{133}$ is also positive.

Using $I_{127} = 5/2$, $I_{133} = 7/2$, $a_{127} = 827.265(3)$ Mc, as given by Jaccarino,[61] and $\mu_{127} = 2.7937(4)$ nm, which is the diamagnetically uncorrected value as taken from Walchli,[62] we evaluate the nuclear moment of $I^{133}$ by means of Eq. (97) and find it to be

$$\left|\mu_{133}\right| = 2.822 \pm .005 \text{ nm}. \tag{98}$$

This value is not diamagnetically corrected.

Since $^{80}_{53}I^{133}$ has a closed neutron shell less two neutrons, and since there are only three protons in excess of the magic number 50, it would seem that the single-particle model would adequately describe the properties of $I^{133}$. The single-particle model[50] predicts the odd proton to be in the $g_{7/2}$ configuration and predicts the nuclear magnetic moment to be $\mu = +1.717$ nm. Although the agreement as to the magnitudes of the moments is not extremely good, the single-particle model lends further support to the assumption that the nuclear moment of $I^{133}$ is a positive quantity.

## E. Electric Quadrupole Moment

The electric quadrupole interaction constant b is related to the nuclear quadrupole moment Q by the expression

$$b = -\frac{e^2}{h} Q\mathcal{R} \frac{2L}{2L+3} \left\langle 1/r^3 \right\rangle , \tag{46}$$

where $\mathcal{R}$ is a relativistic correction factor tabulated by Kopfermann,[16] and the other symbols have their usual meaning. Equation (46) is combined with Eqs. (45) and (96) to give the relation

$$Q = -\left(\frac{8}{3}\right)\left(\frac{\mu_0}{e}\right)^2 \left(\frac{m}{M}\right)\left(\frac{\mu}{I}\right)\left(\frac{\mathcal{F}}{\mathcal{R}}\right)\left(\frac{b}{a}\right). \tag{99}$$

Here the quantities $\mu$, I, and a refer to iodine-127; these values are noted in the previous section. From Kopfermann[16] we take the values $\mathcal{F} = 1.062$ and $\mathcal{R} = 1.128$. To the results of Eq. (99) we have applied the multiplicative correction factor C = 1.029 due to Sternheimer,[49] which has its basis in the deformation of the electronic charge distribution due to the nuclear core polarization. Our value of the

quadrupole moment thus derived is

$$Q = -0.27 \pm .01 \text{ barn.} \tag{100}$$

For an odd-proton nucleus, the single-particle model[50] predicts the quadrupole moment to have the value

$$Q = -\frac{2j - 1}{2(j + 1)} \left\langle r^2 \right\rangle, \tag{101}$$

where $j$ is the angular momentum of the odd proton and $\left\langle r^2 \right\rangle$ is the expectation value of the orbit of the odd proton taken over the nuclear wave function. This expectation value is taken to be $\frac{3}{5} R_0^2$, where $R_0$ is the nuclear radius of iodine-133. The single-particle model gives the value $Q = -0.20$ barn. This is in good agreement with the value in Eq. (100), both in magnitude and in sign.

There is much experimental evidence that nuclei with odd numbers of protons just in excess of a magic number have negative electric quadrupole moments. This further gives confidence that the sign assignment in Eq. (100) is correct.

## F. Hyperfine Separations

The solutions of Eq. (27) can be written in the form

$$\left.\begin{aligned} \Delta\nu_{5,4} &= 5a + 5/7\ b \\ \Delta\nu_{4,3} &= 4a - 2/7\ b \\ \Delta\nu_{3,2} &= 3a - 5/7\ b \end{aligned}\right\}, \tag{102}$$

where $\Delta\nu_{5,4}$ is the zero-field separation between the hyperfine levels of $F = 5$ and $F = 4$, and similarly for the other separations. Using the values of $a$ and $b$ as determined in this experiment, we arrive at the following values of the hyperfine separations as calculated from Eq. (102):

$$\left.\begin{aligned} \Delta\nu_{5,4} &= 3260.1 \pm 7.3 \text{ Mc} \\ \Delta\nu_{4,3} &= 2277.9 \pm 4.6 \text{ Mc} \\ \Delta\nu_{3,2} &= 1515.9 \pm 6.1 \text{ Mc} \end{aligned}\right\}. \tag{103}$$

# VII. NEODYMIUM

## A. Introduction

Neodymium-141 is an even-odd nucleus with 60 protons and 81 neutrons. Since the neutron number is one less than the magic number 82, the properties of the nucleus should be well described by the single-particle shell model, which predicts that the state of the eighty-second neutron is $d_{3/2}$. Hence the spin of $Nd^{141}$ should be 3/2 and the ground state should have even parity.

Evidence concerning the spin comes from the measurements by Polak et al.,[63] who have investigated the positron decay of $Nd^{141}$ and the associated gamma rays. The resulting spectrum is consistent with the assignment of 3/2 for the spin of $Nd^{141}$.

A prerequisite for the determination of the nuclear spin from hyperfine-structure measurements is the knowledge of the electronic structure. The ground-state configuration of neodymium is known to be $4f^4$, from the optical spectroscopic investigations by Schuurmans.[64] The atomic-beam work of Smith and Spaulding[65] has further established the ground state to be characterized by $^5I_4$ with $g_J = -0.6031$. This value is used throughout this work.

## B. Method

The apparatus used was machine B, as described previously. The oven-loader arrangement utilized was particularly convenient for handling materials with high radiation levels. This oven-loader arrangement is shown in Fig. 26. Beam was collected on freshly flamed platinum foils. The collection efficiency of platinum for neodymium is comparable to that of the other elements in the lanthanide and actinide series. After collection, the deposited neodymium was counted in methane counters.

For an odd-A isotope such as $Nd^{141}$ in an electronic state with $J = 4$, at least two transitions are observable in a flop-in apparatus. These transitions are between levels characterized by the quantum numbers

$$(F = I + 4,\ M_F = -I + 1 \leftrightarrow F = I + 4,\ M_F = -I - 1)$$

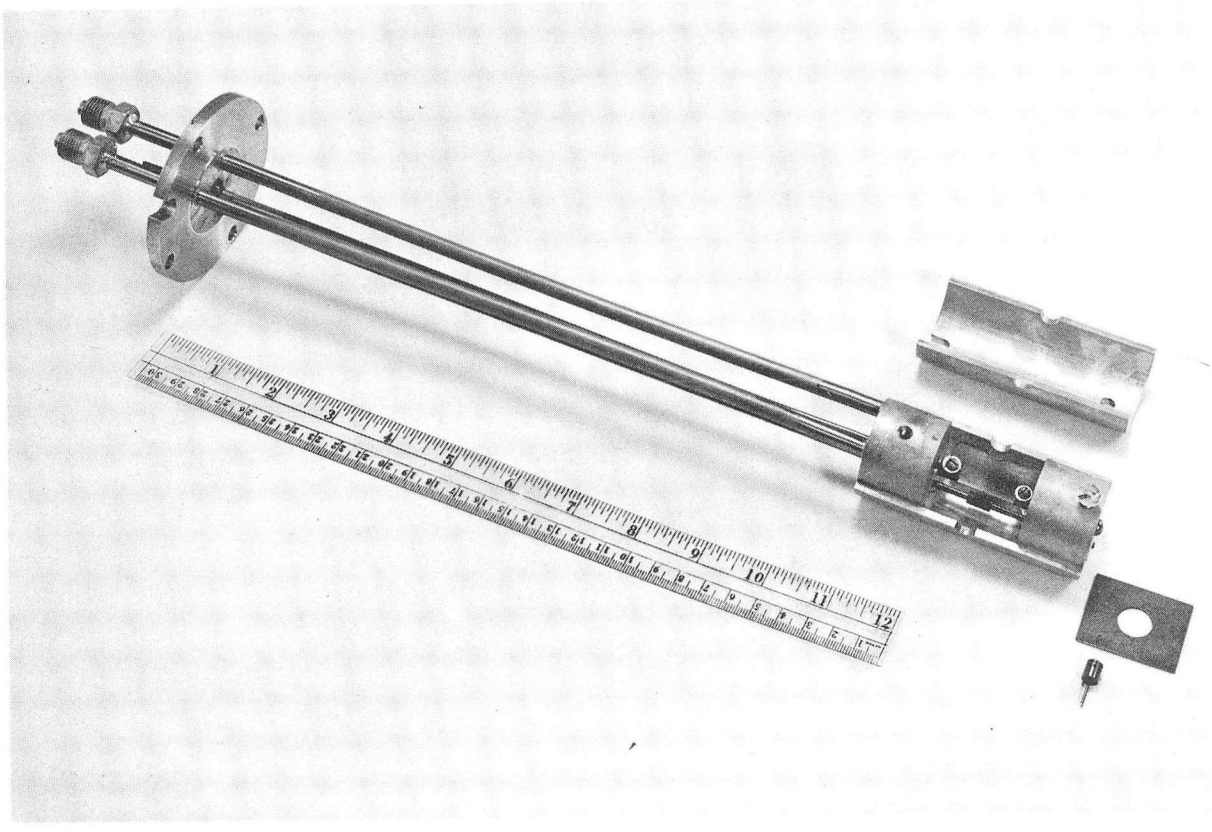

ZN-2453

Fig. 26. Oven loader, cover, heat shield, and oven for machine B. At left are fittings for water cooling.

and

$$(F = I + 3,\ M_F = -I + 2 \leftrightarrow F = I + 3,\ M_F = -I),$$

where $F$ is the total angular momentum, $M_F$ is the projection along the axis of quantization, and $I$ is the nuclear spin. Resonances arising from transitions in the state $F = I + 4$ will be denoted as $\alpha$ resonances, and those in the state $F = I + 3$ will be denoted as $\beta$ resonances. Both the above transitions are of a double-quantum nature, i.e., $\Delta M_F = \pm 2$. This is a consequence of an integral $J$ value and can best be seen from the schematic energy-level diagram of Fig. 27. Such transition types were first observed in $Pu^{239}$ by Hubbs et al.,[17] and, as we have already discussed, were definitely seen in $Bi^{210}$.

In the Zeeman region--i.e., in the weak-magnetic-field region--the frequency $\nu$ of an observable transition is given essentially by

$$\nu \approx -g_F \frac{\mu_0 H}{h}, \tag{37}$$

where

$$g_F \equiv \frac{F(F+1) + J(J+1) - I(I+1)}{2F(F+1)}\ g_J .$$

All the symbols above have previously been defined. Equation (37) is an approximation, since a small term involving the nuclear moment has been omitted. Using $g_J = -0.6031$ for the $J = 4$ state neodymium, one determines the transition frequencies for the $\alpha$- and $\beta$-type resonances to be

$$\nu \approx \frac{2.4124}{I + 4} \frac{\mu_0 H}{h} \quad (\alpha \text{ type}) \tag{104}$$

and

$$\nu \approx \frac{0.30155\ (3I + 16)}{(I + 4)\ (I + 3)} \frac{\mu_0 H}{h} \quad (\beta \text{ type}) .$$

These Eqs. (104) determine the nuclear spin from the resonant frequencies observed in weak magnetic fields.

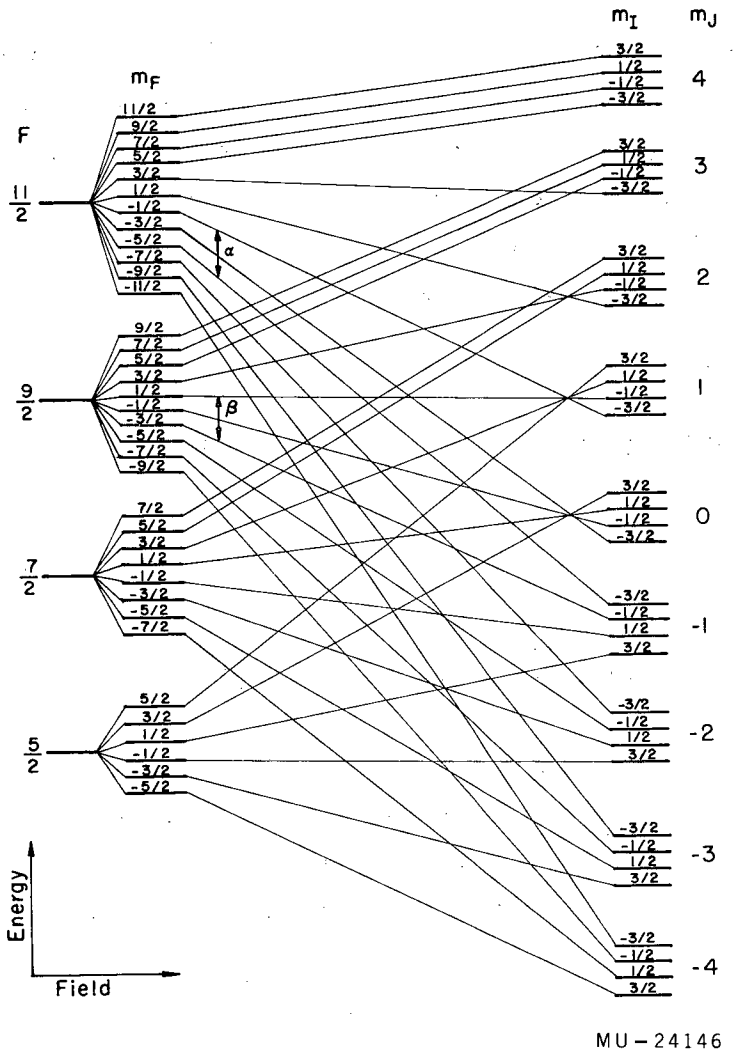


Fig. 27. Schematic energy-level diagram for isotope with J = 4 and I = 3/2, i.e. neodymium-141.

The experimental procedure consisted of searching for a signal from the isotope of unknown spin at the discrete frequencies given by Eqs. (104). This procedure was repeated at several magnetic fields.

## C. Sample Preparation

The radioactive sample was produced in the Berkeley 60-inch Crocker cyclotron by the reaction $Pr^{141}(p, n)Nd^{141}$. The target material, praseodymium, was machined into discs 0.025 in. thick and bombarded with 12-Mev protons for from 5 to 8 hr. The total integrated flux was generally about 175 μa-hr.

At the completion of a scheduled bombardment, the target material was immediately unloaded and placed in a sharp-lipped tantalum crucible which was in turn placed in a tantalum oven. This type of oven and crucible are shown in Fig. 28. The oven containing the target material was then introduced into the atomic beam machine. Optical line-up was effected and oven outgassing was carried out. Usually less than 2 hr elapsed between the completion of the cyclotron bombardment and the production of a stable beam. The duration of a run was ordinarily about 4 hr.

## D. Results

An initial search made at a low magnetic field at frequencies determined from Eqs. (104) for all likely half-integral spin values yielded the results shown in the graph of Fig. 29. It is seen from this figure that I = 3/2 is strongly indicated. The transitions observed were seen at several higher fields, and a linear relation between transition frequency and field established. Two resolved resonances are shown in Figs. 30 and 31 and the observations are summarized in Table X.

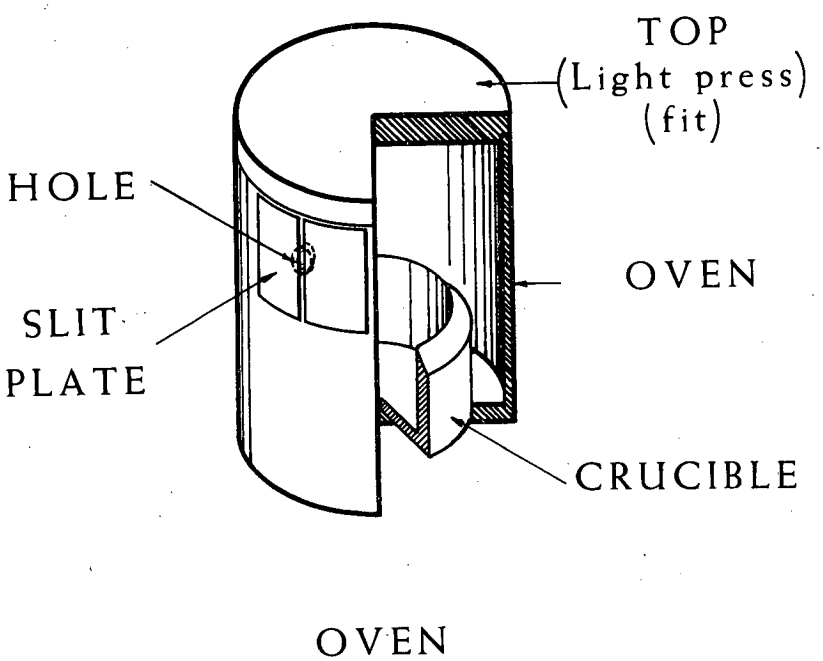


Fig. 28. Tantalum crucible and oven arrangement as used with $Nd^{141}$ and $Eu^{152}$.

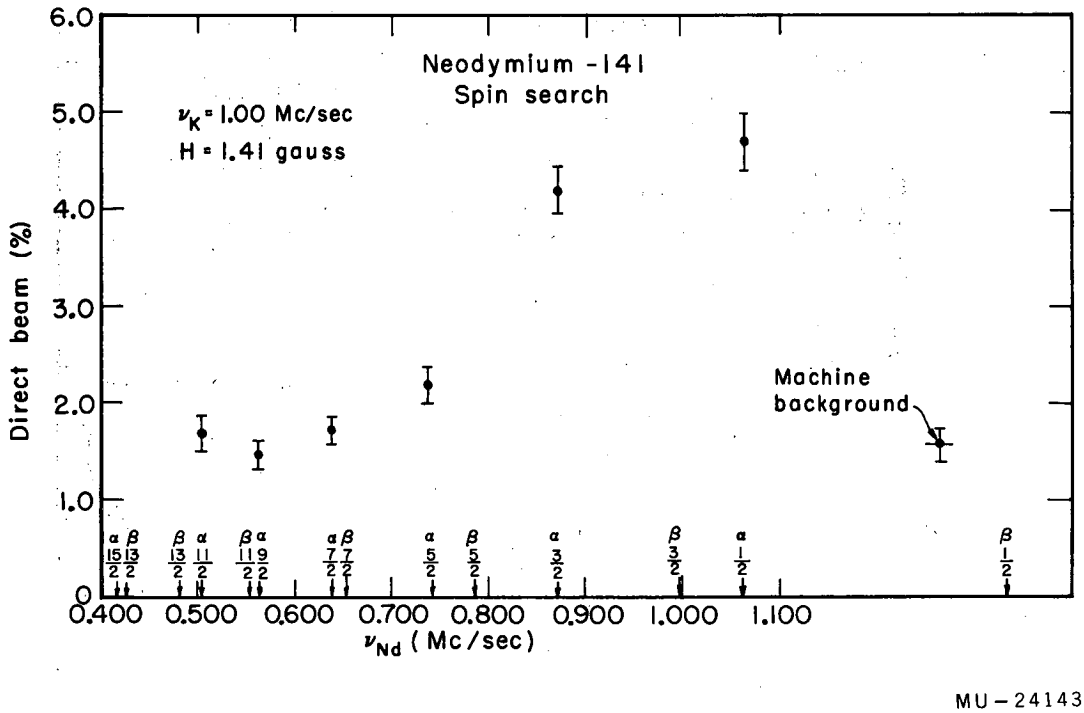


Fig. 29. Low-field spin search for neodymium-141.

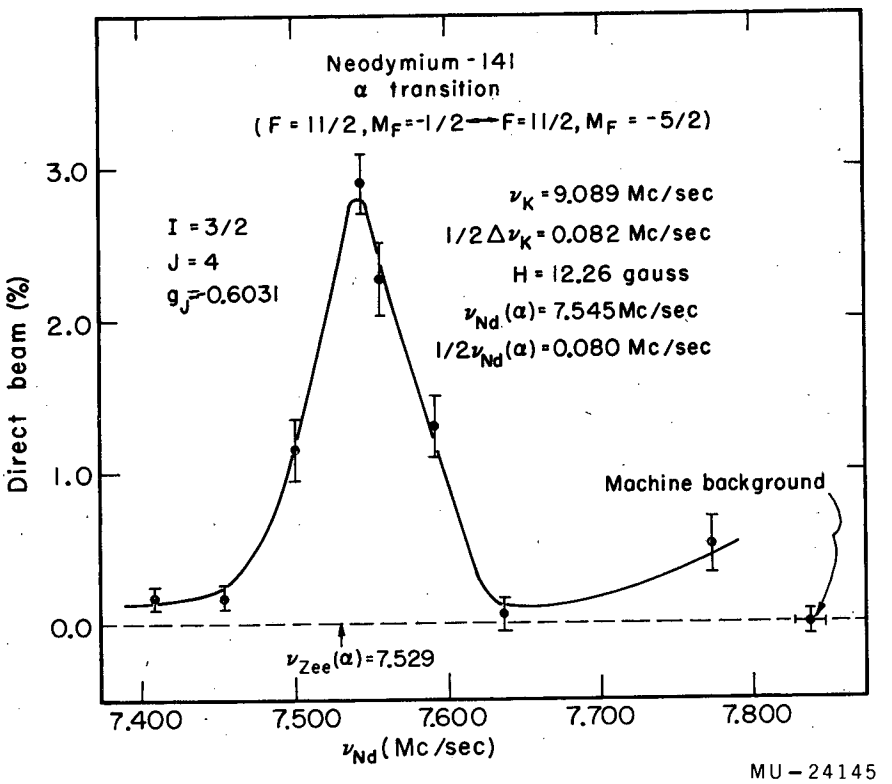


Fig. 30. An α resonance in neodymium-141.

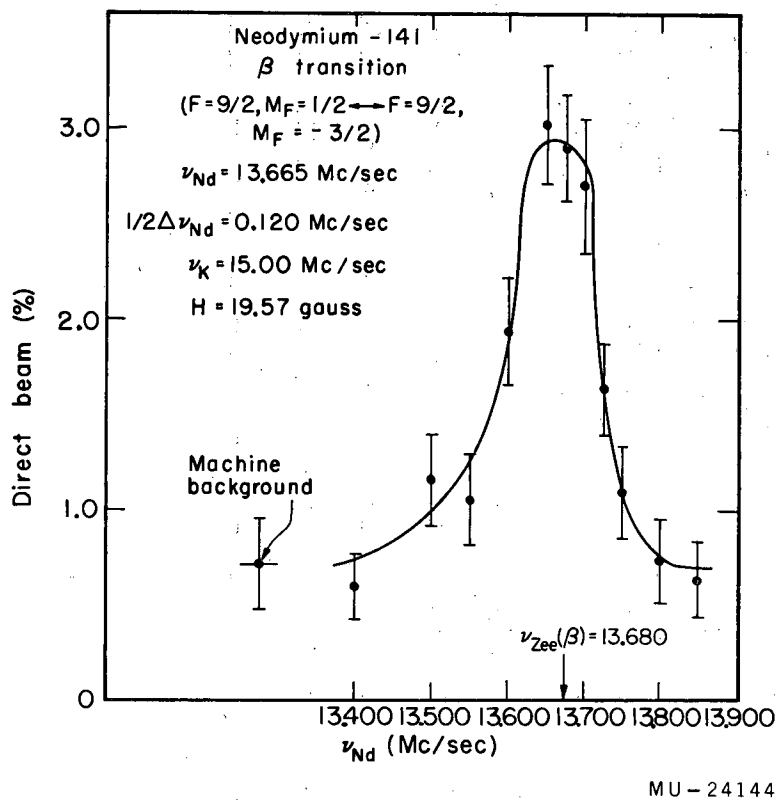


Fig. 31. A β resonance in neodymium-141.

Table X. Resolved resonances in $Nd^{141}$. The Zeeman frequency is calculated on the assumption of I = 3/2, J = 4, and $g_J = -0.6031$.

| No. | Resonance type | Potassium frequency and uncertainty (Mc) | | Magnetic field and uncertainty (gauss) | | Calculated Zeeman frequency (Mc) | Observed frequency and uncertainty (Mc) | | Compounded uncertainty (Mc) |
|---|---|---|---|---|---|---|---|---|---|
| 1 | α | 9.089 | .027 | 12.264 | .034 | 7.529 | 7.545 | .040 | 0.045 |
| 2 | α | 15.000 | .022 | 19.566 | .026 | 12.012 | 12.025 | .050 | 0.052 |
| 3 | α | 30.000 | .073 | 36.198 | .075 | 22.223 | 22.215 | .050 | 0.068 |
| 4 | β | 5.000 | .028 | 6.915 | .038 | 4.835 | 4.838 | .050 | 0.057 |
| 5 | β | 15.000 | .022 | 19.566 | .026 | 13.680 | 13.665 | .060 | 0.062 |
| 6 | β | 30.000 | .073 | 36.198 | .075 | 25.310 | 25.325 | .100 | 0.113 |

Identification of the observed material as $Nd^{141}$ is assured in several ways. The target material is known from spectrocopic analysis to be more than 99% $Pr^{141}$ by weight. The method of production, the observed $g_J$ value, the half-integral spin, and several decay studies all serve to establish unambiguously that the observed material is $Nd^{141}$. A decay study for a full-beam-intensity sample is shown in Fig. 32, and a similar such performed on a button exposed at a resonant frequency is shown in Fig. 33. That the statistics in the latter graph are poorer than in the former reflects the presence of less activity to decay.

## E. Conclusions

The measured spin of 3/2 is in agreement with the shell-model prediction and the work of Polak et al.[63] as noted in the introduction.

The observed data make possible the setting of a lower limit to the zero-field hyperfine-structure separation between the $F = 11/2$ and $F = 9/2$ states, $\Delta\nu_{11/2,\,9/2}$. From second-order perturbation theory the deviation of an $\alpha$ resonance from the Zeeman frequency $\delta_\alpha$ should be related to $\Delta\nu_{11/2,\,9/2}$ according to

$$\delta_\alpha = \frac{0.1190\,(g_J \frac{\mu_0}{h} H)^2}{\Delta\nu_{11/2,\,9/2}} \quad . \tag{105}$$

Assuming the value of $\delta_\alpha$ to be equal to or less than the compounded uncertainty at the highest observed field, we obtain

$$\Delta\nu_{11/2,\,9/2} \geq 1630 \text{ Mc}$$

as a lower limit to the hyperfine separation.

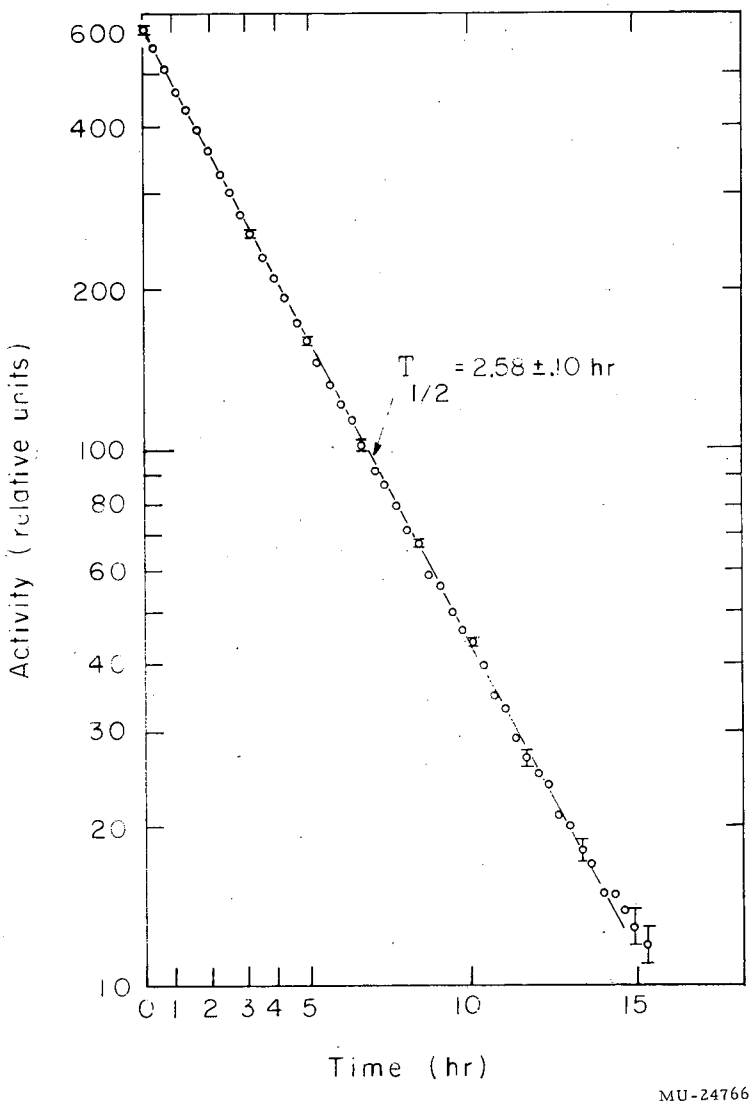


Fig. 32. Decay of full-beam sampling of cyclotron-produced $Nd^{141}$.

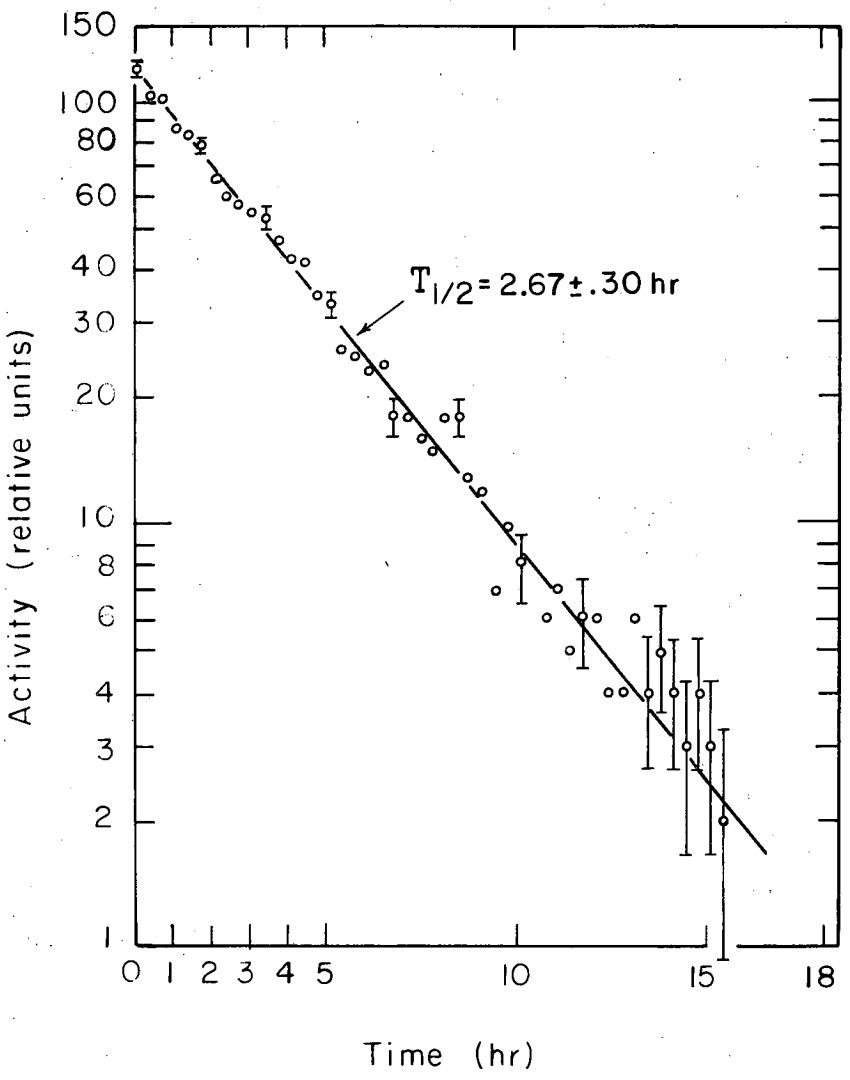


Fig. 33. Decay of resonant exposure, $Nd^{141}$.
H = 19.566 gauss, $\nu$(Nd) = 13.675 Mc.

# VIII. EUROPIUM

## A. Introduction

In recent years much work has been done on the isotopes of europium. Pichanik et al. directly determined the magnetic dipole moment of stable $Eu^{153}$ in a triple-resonance atomic beam experiment.[66] Sandars and Woodgate, also using the atomic-beam method and mass-spectrographic detection, determined the interaction constants for the stable europium isotopes.[67] With the results of these experiments, it becomes possible by means of comparison to determine the nuclear magnetic dipole moment for all the other europium isotopes for which the interaction constants can be measured in the free atom.

Since there are sixteen isotopes of europium with atomic weights in the range 144 to 159, it would seem that the validity of the collective model that is generally taken to hold in the region $150 < A < 190$ could be checked or modified with knowledge of the nuclear moments of many of the isotopes of europium. Also the transition from the shell model to the collective model could be better understood if the moments of the neutron-deficient europium isotopes were known.

Abraham et al., working with crystalline-bound divalent europium ions, have performed paramagnetic resonance experiments on $Eu^{151}$, $Eu^{152}$, $Eu^{153}$, and $Eu^{154}$.[68] When these results are compared with the results of atomic beams, significant differences are seen in the interaction constants. This, when subjected to theoretical analysis, may furnish useful information about the electronic wave function of europium.

## B. Method

Atomic beam apparatus B was used in this experiment. The salient points of the general method have been described earlier.

In this experiment the source material, 13-year $Eu^{152}$, was produced by irradiation with thermal neutrons. The target material, natural metallic europium, was put into a nuclear pile operating at a high flux of $9 \times 10^{13}$ neutrons/$cm^2$ sec for 96 hr. As a result of the

large thermal neutron cross section of 7200 barns for the reaction $Eu^{151}(n, \gamma)Eu^{152}$ (13-year), it was possible to produce reasonable specific activities of the 13-year $Eu^{152}$, on the order of 15.0 mC/mg. Before beginning a run, at least a full week was allowed to elapse after removal from the pile so that all the 9.2-hr $Eu^{152}$, which is also produced by an (n, $\gamma$) reaction, could decay away.

The decay scheme of 13-year $Eu^{152}$ is known and has been summarized by Strominger et al.[54] A diagram of the decay scheme is shown in Fig. 34. The active isotope decays both with K-electron capture (approx 80%) and $\beta$ decay (approx 20%). It is known that the former process gives rise to several strong $\gamma$ rays with energies between 0.9 and 1.5 Mev.[54] For this reason, heavy lead shielding was required and loading procedures were carried out remotely as much as possible.

In the first few attempts at beam production, the sample was introduced into a sharp-lipped tantalum crucible which was then put into a tantalum oven (Fig. 28). Slow heating by electron bombardment was effected. At temperatures of about 1200°K there was a marked burst of activity after which little activity remained in the oven. This behavior is thought to be a result of the existence of a thin film of high-melting $Eu_2O_3$ which breaks and allows the volatile europium metal to escape quickly. This problem was surmounted by introducing the active sample into a carbon crucible half-filled with fine carbon powder. The oven was heated slowly. At temperatures on the order of 2000°K, a stable beam was produced. It is thought that the carbide of europium is formed at low temperatures and then is dissociated at the higher operational temperature. Beam stability was adequate, with intensity falling off uniformly at a rate of a factor of about two every hour.

Beam collection was tested on cold, clean surfaces of sulfur, silver, and freshly flamed platinum. All these materials showed comparable collection efficiencies. Platinum foils were used throughout the experiment for collection purposes. Counting was done in small-volume methane counters.

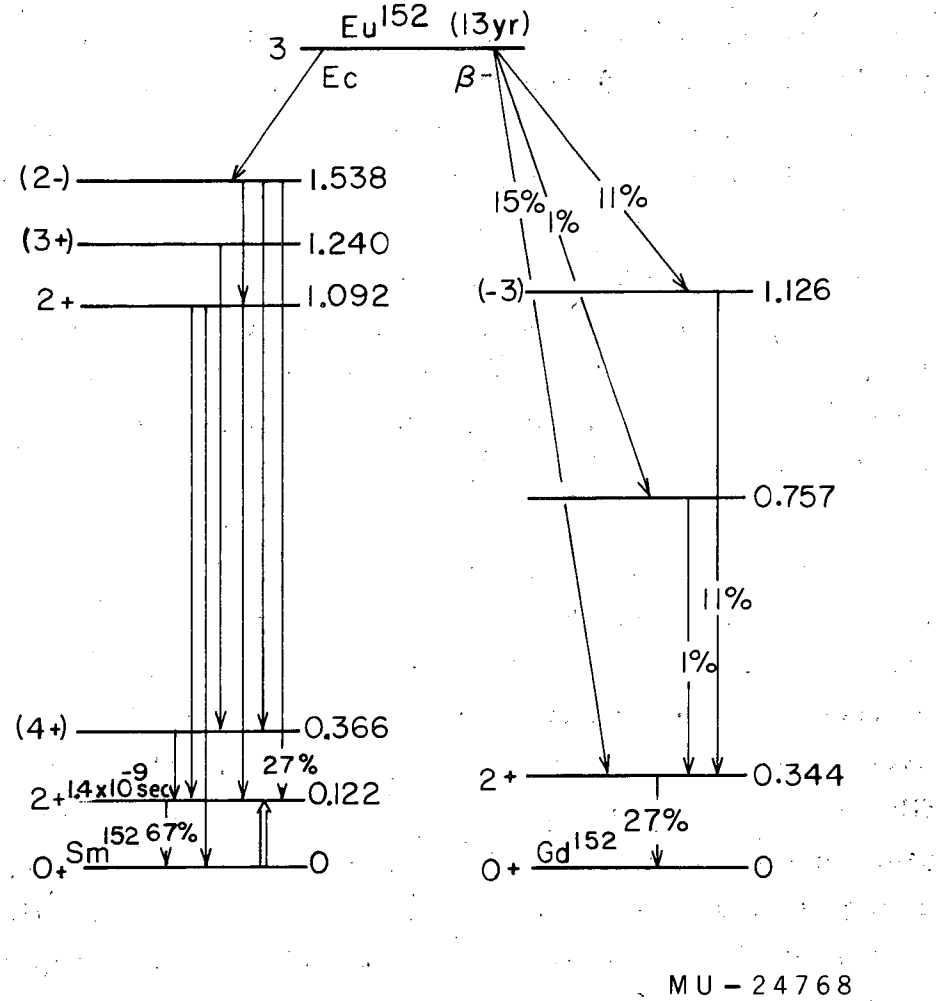


Fig. 34. Decay scheme for $Eu^{152}$ (13-yr) as taken from Strominger et al.[53] Horizontal lines represent energy levels. At right of energy-level lines are given energy values in Mev and at left are given spins and parities. Parentheses indicate no direct verification of spin values.

The beam intensity was measured after each resonance exposure for purposes of normalization. This was done by taking a short exposure with all beam barriers, i.e., stopwires, removed but with the magnetic fields still on. It was noted by this method that the beam consisted of about 95% atoms. This is believed to result from the stability of the electronic configuration of europium, which which is $4f^7 6s^2$. The s subshell is completely filled and the f subshell is exactly half filled.

## C. Results

A total of eleven resolved resonances was observed, representing eight different types of transitions. The results are displayed in Table XI.

Under the heading "transition type" in Table XI there appear the subheadings $F_1, M_1$ and $F_2, M_2$, which indicate the levels between which the observed transition occurs. The next-to-the-last column in Table XI gives the difference between the observed transition frequency and the frequency calculated from the diagonalization of the Hamiltonian (64) using the values of a and b resulting from the best fit of the data; we call this difference the residual of a resonance. The last column in Table XI is the now familiar compounded uncertainty, $\Delta\nu_i$, in the position of the ith resonance center obtained from the relation (66), where we have taken the uncertainty in the $Eu^{152}$ resonances as 1/2 their width and the uncertainty in the calibrating $K^{39}$ resonances as 1/3 their width.

The eleven observed resonances listed in Table XI were used as input data along with the accurately known value of $g_J$ for a least-squares-fit program, as was indicated in a previous section of this paper. First $g_I$ was assumed positive and a convergence was obtained. The assumption was then made that $g_I$ was negative and the process repeated. The results are shown in Table XII.

Table XI. Observed resolved resonances in $Eu^{152}$; I = 3, J = 7/2.

| No. | Transition type $F_1$ | $M_1$ | $F_2$ | $M_2$ | Potassium frequency and uncertainty (Mc) | | Magnetic field and uncertainty (gauss) | | Observed resonance frequency and uncertainty (Mc) | | $(f_{obs} - f_{calc})$ (Mc) | Compounded uncertainty (Mc) |
|---|---|---|---|---|---|---|---|---|---|---|---|---|
| 1 | 13/2 | -5/2 | 11/2 | -5/2 | .704 | .020 | 1.000 | .028 | 59.950 | .075 | +0.006 | 0.075 |
| 2 | 11/2 | -3/2 | 9/2 | -3/2 | .704 | .020 | 1.000 | .028 | 51.325 | .035 | -0.002 | 0.035 |
| 3 | 9/2 | -1/2 | 7/2 | -1/2 | .704 | .026 | 1.000 | .036 | 42.350 | .063 | +0.005 | 0.063 |
| 4 | 7/2 | 5/2 | 5/2 | 3/2 | 7.334 | .027 | 10.001 | .035 | 49.400 | .150 | +0.051 | 0.175 |
| 5 | 7/2 | 3/2 | 7/2 | 5/2 | 7.334 | .027 | 10.001 | .035 | 48.350 | .175 | -0.107 | 0.214 |
| 6 | | | α | | 6.000 | .028 | 8.248 | .037 | 13.570 | .050 | +0.035 | 0.083 |
| 7 | | | α | | 12.065 | .017 | 16.001 | .021 | 28.485 | .240 | -0.079 | 0.244 |
| 8 | | | α | | 20.542 | .050 | 26.001 | .056 | 51.360 | .125 | +0.074 | 0.185 |
| 9 | | | α | | 35.777 | .037 | 42.007 | .036 | 92.430 | .150 | +0.003 | 0.179 |
| 10 | | | β | | 6.000 | .028 | 8.248 | .037 | 14.400 | .130 | +0.008 | 0.150 |
| 11 | | | γ | | 26.006 | .059 | 32.004 | .063 | 83.875 | .163 | +0.139 | 0.239 |

The symbols α, β, and γ denote the transitions of the type

α: ($F = 13/2,\ M_F = -5/2 \leftrightarrow F = 13/2,\ M_F = -7/2$)

β: ($F = 11/2,\ M_F = -3/2 \leftrightarrow F = 11/2,\ M_F = -5/2$)

γ: ($F = 9/2,\ M_F = -1/2 \leftrightarrow F = 9/2,\ M_F = -3/2$)

Table XII. Results of the IBM program using $g_J = 1.9935(3)$ (from Ref. 67), I = 3, and J = 7/2.

| Assumption on sign of $g_I$ | Magnetic dipole interaction constant (Mc) | Electric quadrupole interaction constant (MC) | $\chi^2$ |
|---|---|---|---|
| $g_I > 0$ | 9.345 ± 0.004 | -1.930 ± 0.117 | 1.29 |
| $g_I < 0$ | 9.345 ± 0.004 | -1.930 ± 0.117 | 1.14 |

It is readily seen from Table XII that the assumption of both positive and negative values of $g_I$ does not affect the resulting values of a and b. It is also seen that there is no significant difference in the $\chi^2$'s resulting from either sign assignment. Because there is no significant difference between the values of $\chi^2$ for the assumption of both $g_I > 0$ and $g_I < 0$, no statement concerning the sign of $g_I$ is warranted.[26]

Positive identification is assured in several ways. Bombarding natural europium with neutrons gives rise to isotopes of europium other than $Eu^{152}$. Simple analysis shows that the only other isotope that can possibly be confused with $Eu^{152}$ is $Eu^{154}$, and that this isotope is produced in small amounts. The ratio of produced $Eu^{152}$ to $Eu^{154}$ is 21:1. Since the noise level is usually about 1/10 of a resonance maximum, any effects due to $Eu^{154}$ will not be seen. Comparison of the ratio of the magnetic-dipole interaction constants for $Eu^{152}$ as determined in this experiment to the value determined by Sandars and Woodgate[67] for $Eu^{151}$ gives the same results as found in a paramagnetic resonance experiment by Abraham et al.[69] This is discussed in a later section. Our identification is consistent with the results found by these other researchers. Lastly, use of a RCL 256-channel analyzer showed eight definite peaks in the γ-ray spectrum, all of which agreed within 1% with the known γ-ray energies of $Eu^{152}$ as listed by Strominger et al.[54] No peak was observed that could not be identified as a definite member of the $Eu^{152}$ spectrum. All these means of identification give unambiguous evidence that $Eu^{152}$ was the isotope studied in this experiment.

## D. Magnetic Dipole Moment

The magnetic moment of stable $Eu^{151}$ was measured directly by Pichanick et al. by means of a triple-resonance atomic beam method.[66] The diamagnetically corrected value that these researchers found for the moment of $Eu^{151}$ was $\mu_{151} = 3.419(4)$ nuclear magnetons. The nuclear magnetic dipole moment of $Eu^{152}$ is related to that of $Eu^{151}$ by the relation

$$\left|\mu_I^{152}\right| = \left|\frac{a^{152}}{a^{151}}\right| \left|\mu_I^{151}\right| \frac{I^{152}}{I^{151}} , \qquad (67)$$

where the superscripts indicate to which nuclear species the symbol refers and the symbols themselves have already been defined. The absolute values are taken in Eq. (67) because of the inherent difficulty of the atomic-beam method in determining the absolute sign of the interaction constants. The value of the magnetic-dipole interaction constant for $Eu^{151}$, $a^{151}$, has been determined by Sandars and Woodgate[67] to be $a^{151} = -20.0523(3)$ Mc. Using the appropriate values in Eq. (67), we determine the value

$$\left|\mu_I^{152}\right| = 1.912 \pm 0.003 \text{ nuclear magnetons.} \qquad (106)$$

(diamagnetically corrected)

Since comparison is made to a diamagnetically corrected moment, the value (106) can be considered as diamagnetically corrected.

Because of possible changes in diamagnetic shielding theories, it is often prudent to quote experimental values without the application of diamagnetic corrections. The diamagnetically uncorrected value for the moment of $Eu^{151}$ was originally found by Pichanick et al.[66] to be $\mu = 3.395(4)$ nuclear magnetons. Using this value in Eq. (67) in place of the previously corrected value, we get

$$\left|\mu^{152}\right| = 1.896 \pm .003 \text{ nuclear magnetons.}$$

This value is diamagnetically uncorrected.

It is known that the individual-particle model is invalid in the region $150 < A < 190$, where large nuclear deformations are known to occur. It is in this region that the collective model has its greatest utilization.[70,71] In $Eu^{152}$, with $Z = 63$ and $N = 89$, we are dealing with an odd-odd nucleus subject to the coupling rules proposed by Gallagher and Moszkowski.[72] These rules state that in strongly deformed nuclei described by the asymptotic quantum numbers $N$, $n_z$, $\Lambda$, and $\Sigma$ stated in the order $(N, n_z, \Lambda, \Sigma)$ where $N$ is the total harmonic oscillator quantum number, $n_z$ is the number of oscillator quanta along a spatial axis, $\Lambda$ is the projected orbital angular momentum of the odd nucleon along the axis of nuclear symmetry, and $\Sigma$ is the projected spin angular momentum of the odd nucleon along the axis of nuclear symmetry, we have the relations

$$\left.\begin{aligned} I &= \Omega_P + \Omega_N \text{ if } \Omega_P = \Lambda_P \pm 1/2 \text{ and } \Omega_N = \Lambda_N \pm 1/2 \\ I &= \left| \Omega_P - \Omega_N \right| \text{ if } \Omega_P = \Lambda_P \pm 1/2 \text{ and } \Omega_N = \Lambda_N \mp 1/2 \end{aligned}\right\} . \qquad (107)$$

Here $\Omega = \Lambda + \Sigma$ and is the total angular momentum of an odd nucleon along the axis of nuclear symmetry; the subscripts $P$ and $N$ refer to the odd proton or neutron, respectively. Using the collective model,[70,71] Gallagher and Moszkowski[72] have assumed a configuration of $[411+]$ for the proton part and either $[521+]$ or $[651+]$ for the neutron part. This configuration assignment is consistent with the first of the two rules stated above, i.e., $I = \Lambda_P + \Sigma_P + \Lambda_N + \Sigma_N = 1 + 1/2 + 1 + 1/2 = 3$, which was experimentally observed. Gallagher and Moszkowski further state the relation derived from the collective model

$$\mu = \frac{I}{I+1} \left[ \pm (\Lambda_P + 5.6\, \Sigma_P) \mp 3.8\, \Sigma_N + \frac{Z}{A} \right] , \qquad (108)$$

where the signs of the two terms of the expression are the same as the signs of $\Omega_P$ and $\Omega_N$ appearing in the coupling rules (107). Using Expression (108), which makes use of the Schmidt values for the gyromagnetic ratios of the odd nuclei, i.e., no quenching, one derives the

value for the moment as

$$\mu_I{}^{152}(\text{calc}) = 1.73 \text{ nm.} \tag{109}$$

This value compares favorably in magnitude to the experimentally observed value of $|\mu_I{}^{152}(\text{exp})| = 1.912(3)$ nm. This seems to imply that the asymptotic quantum-number nuclear configuration has been correctly made, and gives further support to the collective model in this region.

## E. Electric Quadrupole Moment

The electric quadrupole interaction constant b is related to the quadrupole moment by the expression

$$hb = -e^2 Q \left\langle 1/r^3 \right\rangle \left\langle LSJJ \left| 3\cos^2\theta - 1 \right| LSJJ \right\rangle . \tag{50}$$

This cannot be evaluated directly because the ground-state electronic wave function is not known for europium. Admixture of small amounts of the level $^6P_{7/2}$ has been hypothesized by Sandars and Woodgate[67] to explain the deviation of the observed $g_J = -1.9953(3)$ from the pure LS-coupled value of the Hund's rule ground level of $^8S_{7/2}$, which should be $g_J = -2.0023$. This admixture is not adequate to explain the existence of hyperfine effects in europium, and it is further hypothesized by Sandars and Woodgate that there is also admixture of a $^6D_{7/2}$ level in the ground state. Clearly, further theoretical analysis is required before Eq. (50) can be evaluated directly.

Although the quadrupole moment cannot currently be calculated, it is known that for the same electronic wave function--i.e., the same chemical substance--the relation

$$\left| \frac{Q_1}{Q_2} \right| = \left| \frac{b_1}{b_2} \right| , \tag{52}$$

where the subscripts are used to indicate different nuclei, holds for various isotopes. Absolute values are taken for the reason indicated previously.

Using Eq. (52) and the results of Sandars and Woodgate,[67] we find

$$\left|\frac{Q^{152}}{Q^{151}}\right| = 2.75 \pm .17 \quad \text{and} \quad \left|\frac{Q^{152}}{Q^{153}}\right| = 1.08 \pm .07 \,. \tag{110}$$

Although the atomic-beam method is ill suited to the absolute determination of the signs of the interaction constants, the relative signs of the interaction constants can readily be determined; hence, we display our results with those of Sandars and Woodgate,[67]

$$\begin{aligned} &Eu^{151};\ b/a = +0.03497(18), \\ &Eu^{152};\ b/a = -0.207(12), \\ &Eu^{153};\ b/a = +0.2016(4). \end{aligned} \tag{111}$$

## F. Hyperfine-Structure Separations

Solution of Eq. (27) gives the zero-field separation in energy levels characterized by different F values. These values are

$$\begin{aligned} \Delta\nu_{13/2,\,11/2} &= 59.848 \pm .060 \text{ Mc}, \\ \Delta\nu_{11/2,\,9/2} &= 51.246 \pm .022 \text{ Mc}, \\ \Delta\nu_{9/2,\,7/2} &= 42.343 \pm .025 \text{ Mc}, \\ \Delta\nu_{7/2,\,5/2} &= 33.191 \pm .032 \text{ Mc}, \end{aligned} \tag{112}$$

where $\Delta\nu_{13/2,\,11/2}$ is the zero-field separation between the F = 13/2 and F = 11/2 levels, and similarly for the other separations.

## G. Discussion

An interesting feature results from the comparison of the measured values of the magnetic-dipole interaction constant determined by both the atomic-beam and paramagnetic-resonance techniques. The atomic-beam technique is based on the nuclear interaction with the electronic charge in the free atom, whereas the paramagnetic-resonance technique is based on nuclear interaction with electronic charge in the $Eu^{++}$ ion bound in a KCl crystal. Abraham, Kedzie, and Jeffries[68] measured the spin of $Eu^{152}$ and $Eu^{154}$ in a paramagnetic resonance experiment, and also the magnetic dipole interaction constants of $Eu^{151}$, $Eu^{152}$, and $Eu^{153}$ in the doubly ionized form bound in a crystal of KCl. These results, converted to units of Mc, are indicated in Table XIII along with our results and those of Sandars and Woodgate.[67]

Table XIII. Values of the magnetic dipole interaction constant.

| Isotope | Value from paramagnetic resonance $\lvert a_{PR} \rvert$ (Mc) | Value from atomic beams $\lvert a_{AB} \rvert$ (Mc) | Ratio of paramag. resonance value to atomic beam value $\lvert a_{PR}/a_{AB} \rvert$ |
|---|---|---|---|
| $Eu^{152}$ | 97.61(18) | 20.0523(2) | 4.868(9) |
| $Eu^{153}$ | 45.33(4) | 9.345(4) | 4.851(5) |
| $Eu^{154}$ | 43.11(9) | 8.8532(2) | 4.869(9) |

It is seen that the magnetic dipole interaction constant is 4.86 times as large in the crystal-bound $Eu^{++}$ ion as in the free atom.

The magnetic dipole interaction constant is defined as

$$a = \left\langle II \left| \vec{\mu} \right| II \right\rangle \left\langle JJ \left| \vec{N} \right| JJ \right\rangle \frac{1}{IJ} \quad , \tag{113}$$

where the first set of brackets indicates the expectation value of the magnetic moment operator, $\vec{\mu}$, for nuclear states with $M_I = I$, and the second set of brackets indicates the expectation value of the magnetic

field operator, $\vec{N}$, for electronic states with $M_J = J$. The magnetic field operator $\vec{N}$ is defined as

$$\vec{N} = 2\mu_0\mu_{nm}\gamma\left[\sum_k\left\{\frac{(\vec{\ell}_k - \vec{s}_k)}{r_k^3} + \frac{3(\vec{r}_k\cdot\vec{s}_k)\vec{r}_k}{r_k^5}\right\} + \frac{8\pi\delta(\vec{r}_k)}{3}\vec{s}_k\right], \tag{114}$$

where $\mu_0$ is the Bohr magneton, $\mu_{nm}$ is the nuclear magneton, and $\gamma$ is the gyromagnetic ratio. The subscript k refers to the kth electron of the system; $\vec{\ell}_k$, $\vec{s}_k$, and $\vec{r}_k$ denote the orbital angular momentum, spin angular momentum, and position of the kth electron, respectively. The first term in the braces in Eq. (114) corresponds to classical dipole-dipole interaction. The second term, first hypothesized by Fermi,[14] denotes the anomalous interaction of the s electrons with the nuclear spin.

The theoretical explanation for the large difference in the expectation value of the operator $\vec{N}$ of Eq. (114) is not readily apparent. Neglecting small effects from the crystalline field, one might at first assume that the removal of two 6s electrons in the divalent ion would have little, if any, effect on the magnetic field at the nucleus, since the total electron-spin density of these two electrons taken together is zero and hence the Fermi term in Eq. (114) would make no contribution to the field. Work of Heine has indicated, however, that there is an s-electron effect even when there are no unpaired s electrons.[69] His explanation for this is based on electron exchange between the s-electrons and electrons from other subshells, resulting in a net polarization of the s electron and thus making possible a contribution from the Fermi term in Eq. (114). Abragam et al.[73] have hypothesized s-electron promotion in ions to explain effects such as seen in this experiment. By "promotion" is meant admixture to the ground ionic electronic state, assumed in $Eu^{++}$ to be $4f^7 6s^2$, of electron configurations of the type $4f^7 ns\ r\ s$, where $n \leqslant 6$ and $r \geqslant 7$. Such a mechanism might possibly allow for effects as seen in this experiment. Unfortunately calculations based on this mechanism are prohibitively complex and impracticable.

## ACKNOWLEDGMENTS

It has been my pleasure to have worked with many worth-while people during the performance of this research project. I would like to express my indebtedness to many, including the following.

Professor William A. Nierenberg for his encouragement and support.

Professor Edgar Lipworth for his patience and enthusiasm as well as for his generously given knowledge and advice.

Dr. Richard Marrus, Professor Howard Shugart, and Professor K. F. Smith for their sincerely appreciated help during many different phases of the experimental work.

Mathew B. White and Burton Budick for their able assistance during the runs.

Dr. Amado G. G. Cabezas for many stimulating discussions.

Homer H. Adams, Kaye Voice, Robert McCracken, and the LRL Health Chemistry Department for their efficient handling and scheduling of the radioactive targets.

Douglas B. MacDonald for his help and advice relating to problems of machine design.

G. G. Young and his shop staff for their able and agreeable fabrication of necessary parts.

Milton Firth and Marion L. Davis for their help with the electronic systems.

An lastly, I would like to express my deepest gratitude to my soon-to-be wife, Miss Elizabeth Hurwitz, for her encouragement, enthusiasm, faith, and understanding.

This work was performed under the auspices of the U. S. Atomic Energy Commission and was supported in part by the U. S. Air Force Office of Scientific Research.

# APPENDICES

## A. The 6-j Symbol

### 1. Definition

The 6-j symbol was first expressed by Racah[9] in 1942 and is associated with the unitary transformation connecting systems coupled by three angular momenta. We quote the definition given by Judd,[10]

$$\begin{Bmatrix} j_1 & j_2 & j_3 \\ \ell_1 & \ell_2 & \ell_3 \end{Bmatrix} = \Delta(j_1 j_2 j_3)\,\Delta(j_1 \ell_2 \ell_3)\,\Delta(\ell_1 j_2 \ell_3)\,\Delta(\ell_1 \ell_2 j_3)$$

$$\times \sum_z \frac{(-1)^z (z+1)!}{[(z-j_1-j_2-j_3)!\,(z-j_1-\ell_2-\ell_3)!\,(z-\ell_1-j_2-\ell_3)!\,(z-\ell_1-\ell_2-j_3)!}$$

$$\times \frac{}{(j_1+j_2+\ell_1+\ell_2-z)!\,(j_2+j_3+\ell_2+\ell_3-z)!\,(j_3+j_1+\ell_3+\ell_1-z)!\,]} \tag{115}$$

where the summation over $z$ in Eq. (115) extends only until one of the factors in the denominator becomes $0!$ and where

$$\Delta(abc) = \sqrt{\frac{(a+b-c)!\,(a-b+c)!\,(-a+b+c)!}{(a+b+c+1)!}}\,.$$

2. Evaluation of $\begin{Bmatrix} I+J & J & I \\ k & I & J \end{Bmatrix}$

Edmonds[12] has considered the special case of the 6-j symbol of the form $\begin{Bmatrix} j_1 & j_2 & \ell_1+\ell_2 \\ \ell_1 & \ell_2 & \ell_3 \end{Bmatrix}$. He states that the following holds:

$$\begin{Bmatrix} j_1 & j_2 & \ell_1+\ell_2 \\ \ell_1 & \ell_2 & \ell_3 \end{Bmatrix} = (-1)^{j_1+j_2+\ell_1+\ell_2}$$

$$\times \left[ \frac{(2\ell_1)!\ (2\ell_2)!\ (j_1+j_2+\ell_1+\ell_2+1)!\ (j_1+\ell_1+\ell_2-j_2)!\ (j_2+\ell_1+\ell_2-j_1)!}{(2\ell_1+2\ell_2+1)!\ (j_1+j_2-\ell_1-\ell_2)!\ (j_1+\ell_2-\ell_3)!\ (\ell_2+\ell_3-j_1)!\ (j_1+\ell_2+\ell_3+1)!} \right.$$

$$\left. \frac{(j_1+\ell_3-\ell_2)!\ (j_2+\ell_3-\ell_1)!}{(\ell_1+j_2-\ell_3)!\ (\ell_1+\ell_3-j_2)!\ (\ell_1+j_2+\ell_3+1)!} \right] \qquad (116)$$

Since the 6-j symbol is invariant to the interchange of any two columns, we get $\begin{Bmatrix} I+J & J & I \\ k & I & J \end{Bmatrix} = \begin{Bmatrix} J & I & I+J \\ I & J & k \end{Bmatrix}$. To evaluate $\begin{Bmatrix} J & I & I+J \\ I & J & k \end{Bmatrix}$, we resort to Eq. (116) with the substitutions $j_1 \to J$, $j_2 \to I$, $\ell_1 \to I$, $\ell_2 \to J$, $\ell_3 \to k$. This immediately gives, after simplification,

$$\begin{Bmatrix} J & I & I+J \\ I & J & k \end{Bmatrix} = (-1)^{2(I+J)} \quad \frac{(2I)!\ (2J)!}{[\,(2J-k)!\ (2I-k)!\ (2J+k+1)!\ (2I+k+1)!\,]} \,. \qquad (117)$$

3. A General Expression for M(I, J; F; k)

Referrring back to Eq. (19), we have the relation

$$W_{F, M_F}(k) = (-1)^{I+J-F} W(I\,J\,I\,J; Fk) \left\langle I \left|\left| T^{(k)}(n) \right|\right| I \right\rangle \left\langle J \left|\left| T^{(k)}(e) \right|\right| J \right\rangle , \tag{118}$$

where we have replaced the 6-j symbol in Eq. (19) with the appropriate Racah W coefficient. We have also defined

$$W_{F, M_F}(k) = A_k M(I, J; F; k) .$$

Equating and introducing the expression for $A_k$ as given in Eq. (23) gives

$$(-1)^{I+J-F} W(I\,J\,I\,J; Fk) = \frac{(2J)!\ (2I)!\ M(I, J; F; k)}{\left[ (2J-k)!\ (2J+k+1)!\ (2I-k)!\ (2I+k+1)! \right]^{1/2}} . \tag{119}$$

One form of the definition of the Racah W coefficient is

$$W(I\,J\,I\,J; Fk) = \frac{(I+J-F)!\ (I+F-J)!\ (J+F-1)!\ (k!)^2}{(I+J+F+1)!}$$

$$\times \left[ \frac{(2I-k)!\ (2J-k)!}{(2I+k+1)!\ (2J+k+1)!} \right]^{1/2}$$

$$\times \sum_z \frac{(-1)\ (2I+2J+1-z)!}{z!\ \left[ (I+J-F-z)!\ (F+k-I-J+z)! \right]^2\ (2I-k-z)!\ (2J-k-z)!} . \tag{120}$$

Substitution of Eq. (120) into Eq. (119) gives, after simplification,

$$M(I, J; F; k) = \frac{(2I-k)!\ (2J-k)!}{(2I)!\ (2J)!}$$

$$\times \frac{(I+J-F)!\ (J-I+F)!\ (I-J+F)!\ (k!)^2}{(I+J+F+1)!}$$

$$\times \sum_z \frac{(-1)^{z+I+J-F}\ (2I+2J+1-z)!}{z!\ (2I-k-z)!\ (2J-k-z)!\ [(1+J-F-z)!\ (k+F-I-J+z)!]^2}\ , \qquad (121)$$

where the phase factor $(-1)^{I+J-F}$ is placed under the summation sign.

## B. The 3-j Symbol

Consider the system of any two angular momenta, I and J, coupled together to form a third angular momentum, F. The ket $|\gamma IJFF_z\rangle$ may be expanded in terms of the kets $|\gamma I I_z J J_z\rangle$, where $\gamma$ represents any other pertinent set of quantum numbers of the system. This expansion is

$$|\gamma IJFF_z\rangle = \sum_z \langle IJFF_z | I I_z J J_z\rangle\ |\gamma I I_z J J_z\rangle\ , \qquad (122)$$

where the scalar products appearing in Eq. (122) above are the Clebsch-Gordan coefficients. The 3-j symbol is related to a Clebsch-Gordan coefficient by

$$\begin{pmatrix} I & J & F \\ I_z & J_z & F_z \end{pmatrix} = (-1)^{I-J-F_z}\ (2F+1)^{-1/2}\ \langle IJ-F_z | I I_z J J_z\rangle, \qquad (123)$$

where

$$\left\langle IJF\text{-}F_z \middle| II_z JJ_z \right\rangle = \delta(I_z + J_z, -F_z) \sqrt{\frac{(2F+1)!\,(I+J-F)!\,(I-J+F)!\,(-I+J+F)!}{(I+J+F+1)!}}$$

$$\times \sqrt{(I+I_z)!\,(I-I_z)!\,(J+J_z)!\,(J-J_z)!\,(F-F_z)!\,(F+F_z)!}$$

$$\times \sum_y (-1)^y \frac{1}{y!\,(I+J-F-y)!\,(I-I_z-y)!\,(J+J_z-y)!\,(F-J+I_z+y)!\,(F-I-J_z+y)!} \,. \tag{124}$$

The $\delta$ function occurring in Eq. (124) is equivalent to noting that the bottom row of the 3-j symbol must add algebraically to zero if it is not to vanish.

## REFERENCES


1. There have been many descriptions in the literature of the effect first discovered by P. Zeeman in 1896. A treatment of both the normal and the anomalous atomic Zeeman effect will be found in M. Born, Atomic Physics, 5th Ed. (Hafner Publishing Co., New York 1951), p. 120 ff.
2. E. U. Condon and G. H. Shortley, Theory of Atomic Spectra (Cambridge University Press, London, 1935).
3. L. H. Thomas, Proc. Cambridge Phil. Soc. 23, 542 (1927).
4. E. Fermi, Z. Physik 48, 73 (1928).
5. L. I. Schiff, Quantum Mechanics (McGraw-Hill Book Co., Inc., New York, 1955).
6. V. Bush and S. H. Caldwell, Phys. Rev. 38, 1898 (1931).
7. C. Schwartz, Phys. Rev. 97, 380 (1955).
8. N. F. Ramsey, Molecular Beams (Oxford University Press, London, 1956).
9. G. Racah, Phys. Rev. 62, 438 (1942).
10. Brain R. Judd, Berkeley Notes (unpublished), University of California, 1960.
11. M. E. Rose, Elementary Theory of Angular Momentum (John Wiley and Sons, Inc., New York, 1957).
12. A. R. Edmonds, Angular Momentum in Quantum Mechanics (Princeton University Press, Princeton, N. J., 1957).
13. J. M. Blatt and V. F. Weisskopf Theoretical Nuclear Physics (John Wiley and Sons, Inc., N. Y., 1952).
14. E. Fermi, Z. Physik 60, 320 (1930).
15. L. Davis, B. T. Feld, C. W. Zabel, and J. R. Zacharias, Phys. Rev. 76, 1076 (1949).
16. H. Kopfermann, Nuclear Moments (Academic Press, New York, 1958).
17. J. C. Hubbs, R. Marrus, W. A. Nierenberg, and J. L. Worcester, Phys. Rev. 109, 390 (1958).

18. William A. Nierenberg (University of California), private communication.
19. H. L. Garvin, T. M. Green, and E. Lipworth, Phys. Rev. 111, 534 (1958).
20. Hugh Leslie Garvin, Nuclear Spin and Hyperfine Structure Measurements on the Radioactive Iodine and Astatine Isotopes (Thesis), Lawrence Radiation Laboratory Report UCRL-8860, Aug. 1959.
21. G. O. Brink, J. C. Hubbs, W. A. Nierenberg, and J. L. Worcester, Phys. Rev. 107, 189 (1957).
22. Gilbert O. Brink, Nuclear Spins of Thallium-197, Thallium-199, and Thallium-204 (Thesis), University of California Radiation Laboratory Report UCRL-3642, June 1957.
23. G. Breit and I. I. Rabi, Phys. Rev. 38, 2082 (1931).
24. P. G. H. Sandars, Investigations of Hyperfine Structure by the Method of Magnetic Resonance in Atomic Beams (Thesis), Balliol College, Oxford, October 1959.
25. Amado Y. Cabezas, Electronic and Nuclear Properties of Some Radioactive Rare-Earth Elements, (Thesis), Lawrence Radiation Laboratory Report UCRL-9346, August 1960.
26. For a discussion of this significance test, see R. A. Fisher, Statistical Methods for Research Workers (Oliver and Boyd, London, 1948).
27. H. L. Garvin, T. M. Green, E. Lipworth, and W. A. Nierenberg, Phys. Rev. 116, 393 (1959).
28. R. Marrus, W. A. Nierenberg, and J. Winocur, Phys. Rev. 120, 1429 (1960).
29. A. G. Petschek and R. E. Marshak, Phys. Rev. 85, 698 (1952).
30. M. Yamada, Progr. Theoret. Phys. (Kyoto) 10, 253 (1953).
31. The nuclear spin of RaE was measured at Cambridge University, England, by R. S. Title and K. F. Smith and first reported at the Second Brookhaven Conference on Atomic Beams, 1957.
32. E. A. Plassmann and L. M. Langer, Phys. Rev. 96, 1593 (1954).

33. C. S. Wu, in Proceedings of the International Glasgow Conference on Nuclear and Meson Physics, 1954 (Pergamon Press, Ltd., London, 1955), p. 177.
34. P. R. Lewis, Phys. Rev. 108, 904 (1957).
35. J. Fujita, M. Yamada, Z. Matumoto, and S. Nakamura, Phys. Rev. 108, 1104 (1957).
36. A. Bincer, E. Church, and J. Weneser, Phys. Rev. Letters 1, 95 (1958).
37. A. I. Alikhanov, G. P. Eliseev, and V. A. Liubimov, Soviet Physics--JETP 8, 740 (1959).
38. B. V. Geskenbein, S. A. Nemirovskaya, and A. P. Rudik, Nuclear Phys. 13, 60 (1959).
39. M. Fred, F. Tomkins, and R. Barnes, Phys. Rev. 92, 1324 (1953).
40. G. E. Lee-Whiting, Phys. Rev. 97, 463 (1955).
41. I. Lindgren and C. M. Johansson, Arkiv Fysik 15, 445 (1959).
42. R. G. Blin-Stoyle and M. A. Perks, Proc. Phys. Soc. (London) 67, 885 (1954).
43. R. S. Title and K. F. Smith, Phil. Mag. 5, 1281 (1960).
44. W. G. Procter and F. C. Yu, Phys. Rev. 78, 471 (1950).
45. H. E. Walchli, A Table of Nuclear Moments, Oak Ridge National Laboratory Report ORNL-1469, Suppl II, Feb. 1955 (unpublished).
46. D. B. Inglis and M. H. Johnson, Jr., Phys. Rev. 38, 1642 (1931).
47. H. Schüler and T. Schmidt, Z. Physik 99, 717 (1936).
48. G. Breit and L. A. Wills, Phys. Rev. 44, 470 (1933).
49. R. M. Sternheimer, Phys. Rev. 86, 316 (1952) and 95, 736 (1954).
50. R. J. Blin-Stoyle, Revs. Modern Phys. 28, 75 (1956).
51. N. Newby and E. J. Konopinski, Phys. Rev. 115, 434 (1959).
52. M. Rotenberg, R. Bivens, N. Metropolis, and J. K. Wooten, Jr., The 3-j and 6-j Symbol, Technology Press, MIT, Cambridge, Mass., 1959.
53. C. E. Moore, Atomic Energy Levels, Vol 3, Circular of the National Bureau of Standards 467, May 1958.

54. D. Strominger, J. M. Hollander, and G. T. Seaborg, Rev. Mod. Phys. 30, 582 (1958).
55. C. M. Olsmats, S. Axensten, and G. Liljegren, Arkiv för Fysik 19, 469 (1961).
56. H. L. Garvin and E. Lipworth, Bull. Am. Phys. Soc. 2, 316 (1957).
57. E. Lipworth, H. L. Garvin, and W. A. Nierenberg, Bull. Am. Phys. Soc. 4, 353 (1959).
58. Hugh Leslie Garvin, Nuclear Spin and Hyperfine Structure Measurements on the Radioactive Iodine and Astatine Isotopes, (Thesis), Lawrence Radiation Laboratory Report UCRL-8860, August 1959.
59. H. L. Garvin and E. Lipworth, Bull. Am. Phys. Soc. 4, 353 (1959).
60. K. D. Bowers, R. A. Kamper, and C. D. Lustig, Proc. Phys. Soc. (London) B, 70, 1176 (1957).
61. V. Jaccarino, J. G. King, R. A. Satten, and H. H. Stroke, Phys. Rev. 94, 1798 (1954).
62. H. Walchli, R. Livingston, and G. Hebert, Phys. Rev. 82, 97 (1951).
63. H. L. Polak, W. Schoo, B. L. Scram, R. K. Girgis, and R. VanLieshout, Nuclear Phys. 5, 271 (1958).
64. Ph. Schuurmans, Physica 11, 419 (1946).
65. K. F. Smith and Spalding (Cavendish Laboratories, Cambridge, England), private communication.
66. F. M. Pichanik, P. G. H. Sandars, and G. K. Woodgate, Proc. Roy. Soc. (London) A 257, 277 (1960).
67. P. G. H. Sandars and G. K. Woodgate, Proc. Roy. Soc. (London) A 257, 269 (1960).
68. M. Abraham, R. Kedzie, and C. D. Jeffries, Phys. Rev. 108, 58 (1957).
69. V. Heine, Phys. Rev. 107, 1002 (1957).
70. S. G. Nilsson, Kgl. Danske Videnskab. Selskab Mat. -fys. Medd. 29, No. 16 (1955).

71. B. R. Mottelson and S. G. Nilsson, Kgl. Danske Videnskab. Selskab Mat.-fys. Skr. 1, No. 8 (1959).

72. C. J. Gallagher, Jr., and S. A. Moszkowski, Phys. Rev. 111, 1282 (1958).

73. A. Abraham, J. Horowitz, and M. H. L. Pryce, Proc. Roy. Soc. (London) A 230, 169 (1955).